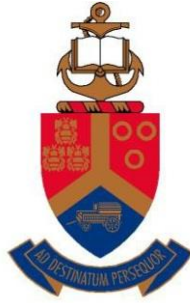


FTire model parameterization and validation of an all-terrain SUV tyre



UNIVERSITEIT VAN PRETORIA
UNIVERSITY OF PRETORIA
YUNIBESITHI YA PRETORIA

This thesis is submitted in partial fulfilment of the requirements for
the degree

Master of Mechanical Engineering

Department of Mechanical and Aeronautical Engineering
Faculty of Engineering, Built Environment and Information
Technology
University of Pretoria

by

Hans-Rudolf Björn Bosch

Abstract

Tyre modelling has been a focal point of vehicle dynamics modelling since the beginning of vehicle dynamics research. Many tyre models are based on single point contact models which utilize some form of the Pacejka Magic Formula curve fit. The Pacejka Magic Formula approach was formulated in the 1980s and has certain advantages such as high computational efficiency and easily obtainable parameterization data. However, the Pacejka Magic Formula is limited to function on smooth roads and a finite number of well defined, long wavelength discrete obstacles.

A high fidelity approach in the form of Cosin's FTire tyre model was developed, in which the tyre is modelled as a three dimensional object populated with bending, tangential, lateral and radial stiffnesses as well as damping. The tyre is numerically approximated with a predetermined number of elements. The disadvantages of using FTire include its low computational efficiency and the large number of parameters prescribed to parameterize the tyre model. However, FTire is claimed to be capable of accurately predicting the forces and moments generated by the tyre on smooth as well as uneven road surfaces for on-road tyres.

The focus of this study lies on parameterizing and validating an FTire model of an all-terrain SUV tyre. The aim is to verify whether a parameterized FTire model is able to predict the tyre behaviour of an all-terrain SUV tyre for lateral and longitudinal forces on smooth road surfaces and vertical forces on uneven but hard terrain.

Static laboratory and dynamic field tests are conducted to acquire parameterization and validation test data to parameterize the FTire model. An Adams model of the tyre testing equipment is implemented to simulate the FTire model and validate it against dynamic validation test results.

It is found that the FTire model is able to predict the lateral tyre behaviour well on a smooth road surface. The longitudinal tyre behaviour on a smooth road surface and vertical tyre behaviour on an uneven road surface are predicted very well by the parameterized FTire model.



Acknowledgements

The author would like to thank the following people who have contributed to this project in various ways:

- Prof. P.S. Els for his guidance.
- Mr C. M. Becker and Mr H. A. Hamersma for their help with the experimental testing.
- Mr M. J. Stallmann for his help with the Cosin FTire software.
- My fellow students Michael Kapp, Glenn Guthrie, Wietsche Penny, Torsten Löwe and Brett Kent for their help, support and friendship.
- All members of the Vehicle Dynamics Group of the University of Pretoria for the help and support provided throughout the project.
- My parents for their encouragement throughout the project.
- My grandparents for the interest shown in my studies.
- Our heavenly father for enabling me to do this project.

Without these people the project would have been a much more difficult task.



Table of contents

Abstract.....	i
Acknowledgements.....	ii
Table of contents.....	iii
List of Figures.....	v
List of tables.....	viii
Nomenclature.....	ix
English symbols.....	ix
Greek symbols.....	x
Abbreviations.....	x
1 Introduction.....	1
2 Literature survey.....	2
2.1 Pneumatic tyres.....	2
2.1.1 Tyre axis system.....	3
2.1.2 Tyre handling properties.....	4
2.1.2.1 Slip angle.....	4
2.1.2.2 Camber angle.....	5
2.1.3 Tyre traction properties.....	6
2.1.3.1 Longitudinal slip.....	6
2.2 Tyre modelling.....	6
2.2.1 Tyre models.....	7
2.2.2 The FTire model.....	10
2.2.2.1 Structure model.....	12
2.2.2.2 Tread model.....	13
2.2.2.3 Thermal model.....	14
2.2.2.4 Data parameterization.....	14
2.3 Tyre testing.....	14
2.3.1 Indoor tyre testing equipment.....	15
2.3.2 Outdoor tyre testing equipment.....	16
2.4 Chapter summary.....	17
2.5 Problem statement.....	18
2.6 Thesis outline.....	18
3 Parameterization and validation data acquisition.....	19
3.1 Introduction.....	19
3.2 FTire model parameterization procedure.....	19



3.3	Tyres	20
3.4	Static parameterization tests.....	20
3.4.1	Footprints and vertical tyre stiffness	21
3.4.2	Static cleat tests.....	23
3.4.3	Static in-plane and out-of-plane tyre stiffness tests	25
3.4.4	Modal analysis	28
3.5	Dynamic parameterization and validation tests	31
3.5.1	Vertical field tests	34
3.5.1.1	Dynamic parameterization tests	34
3.5.1.2	Validation tests.....	35
3.5.2	Handling validation tests.....	36
3.5.3	Traction validation tests	38
3.6	Chapter summary	42
4	Parameterization of the FTire model	43
4.1	Introduction.....	43
4.2	Preparation phase	44
4.3	Identification/validation phase	46
4.4	Finishing phase	52
4.5	Chapter summary	52
5	Validation.....	53
5.1	Introduction.....	53
5.2	Adams modelling	54
5.2.1	Experimental determination of moments of inertia of the tyre testing rig	55
5.2.1.1	Determination of the position of the centre of gravity of the tyre testing rig.....	55
5.2.1.1.1	In-plane position of the centre of gravity of the tyre testing rig.....	55
5.2.1.1.2	Vertical position of the centre of gravity	55
5.2.1.2	Determination of the moments of inertia of the tyre testing rig	57
5.2.1.2.1	Pitch moment of inertia of the tyre testing rig	57
5.2.1.2.2	Roll moment of inertia of the tyre testing rig.....	59
5.2.2	Simulation velocity input	61
5.2.3	Handling simulation inputs	61
5.2.4	Traction simulation inputs	62
5.2.5	Vertical simulation inputs	63
5.3	Lateral tyre properties validation	64
5.3.1	Lateral force vs. slip angle validation	64

5.3.2	Self-aligning moment.....	67
5.4	Longitudinal tyre properties validation.....	68
5.4.1	Longitudinal force.....	68
5.4.2	Braking moment.....	70
5.5	Vertical tyre properties validation.....	71
5.5.1	Discrete obstacles.....	71
5.5.2	Rough terrain	73
5.5.2.1	Belgian paving	76
5.5.2.2	Fatigue track.....	77
5.6	Chapter summary	78
6	Conclusion and recommendations	79
6.1	Conclusion	79
6.2	Recommendations.....	80
7	References.....	81
A.	Appendix – Measurement and simulation results	84
Vertical tests.....		84
Traction tests.....		91
Handling tests.....		92

List of Figures

Figure 2-1: The SAE coordinate system (Gillespie, 1992).....	3
Figure 2-2: Lateral Force vs. slip angle characteristics of two tyres (Optimum, 2014).....	4
Figure 2-3: Lateral force and aligning moment generation due to slip angle (Gillespie, 1992)	5
Figure 2-4: Camber thrust and aligning moment generation due to camber angle (Blundell et al., 2004)	5
Figure 2-5: Longitudinal force vs. slip characteristics (Gillespie, 1992).....	6
Figure 2-6: Contact models used for various tyre models (Zegelaar, 1998).....	7
Figure 2-7: Tyre model accuracy vs. required data (Oosten, 2011).....	9
Figure 2-8: FTire tyre model negotiating a large, sharp-edged obstacle (MSC Software, 2013)	10
Figure 2-9: FTire belt element stiffnesses (Gipser, 2013)	12
Figure 2-10: Belt segment degrees of freedom. From left to right: translational, torsional and bending (Gipser, 2013)	12
Figure 2-11: FTire structural force elements, Gipser (2013)	13
Figure 2-12: FTire thermal model (Gipser, 2013)	14
Figure 2-13: Left: Drum tyre testing equipment Right: Flat belt tyre testing equipment (Rill, 2006)..	16
Figure 2-14: Tyre testing rig with mounted motorcycle tower (TNO, 2014)	16
Figure 2-15: Tyre testing rig during outdoor tyre testing procedure.....	17
Figure 3-1: Michelin LTX LT235/85R16 AT ² all-terrain tyre (Michelin, 2013) and tyre tread pattern	20

Figure 3-2: Flat plate experimental setup	21
Figure 3-3: Experimental results for flat plate static test at 0 degrees camber and 1 bar inflation pressure	22
Figure 3-4: Footprint experimental setup at a camber angle of 5 degrees	22
Figure 3-5: Left: Footprint captured by the stereo-vision camera system. Right: Footprint bitmap image.....	23
Figure 3-6: Static cleat test experimental setup for 2 bar inflation bar at 3° camber angle	24
Figure 3-7: Static 25x25mm oblique cleat test at 1 bar inflation pressure.....	24
Figure 3-8: 25x25mm static cleat test experimental results at 0 degrees camber and 1 bar inflation pressure	25
Figure 3-9: In-plane experimental setup in the longitudinal direction.....	26
Figure 3-10: In-plane lateral force experimental results at 7000N vertical load and 2 bar inflation pressure	26
Figure 3-11: In-plane longitudinal force experimental results at 8000N vertical load and 2 bar inflation pressure.....	27
Figure 3-12: Schematic representation of determining the angular position of the steel plate	27
Figure 3-13: In-plane torsional moment experimental results at 7680N vertical load.....	28
Figure 3-14: First six vibrational modes of an unloaded tyre with a fixed rim (Gipser, 2013)	28
Figure 3-15: Left: Experimental setup of the modal analysis from the top. Right: Tyre, as captured by the Polytec PSV – 400 (Polytec, 2014) scanning laser vibrometer from the top.....	29
Figure 3-16: Left: Experimental setup of the modal analysis from the front. Right: Tyre, as captured by the Polytec PSV – 400 (Polytec, 2014) scanning laser vibrometer from the front	29
Figure 3-17: Torsional modal analysis experimental setup	30
Figure 3-18: Outdoor tyre testing equipment load cell orientation.....	31
Figure 3-19: Outdoor tyre testing equipment stabilisation system	32
Figure 3-20: Tyre testing rig offset position	34
Figure 3-21: Dynamic cleat test (LC0)	35
Figure 3-22: 50x50mm dynamic cleat test result.....	35
Figure 3-23: Dynamic validation test conducted on the Belgian paving	36
Figure 3-24: Handling validation test (LC3) at 2 bar inflation pressure.....	36
Figure 3-25: Handling validation test results (LC3) at 0° camber angle.....	37
Figure 3-26: Varying slip angle during a handling validation test (LC1) at 0° camber.....	37
Figure 3-27: Varying lateral force during a handling validation test (LC1) at 0° camber	38
Figure 3-28: Lateral force vs. slip angle relationship during handling validation test (LC1) at 0° camber.....	38
Figure 3-29: Traction validation test (LC1) at 2 bar inflation pressure	39
Figure 3-30: Traction validation test results (LC1).....	39
Figure 3-31: Velocity during a dynamic traction validation test (LC1).....	40
Figure 3-32: Angular velocity of the wheel during a dynamic traction validation test (LC1).....	40
Figure 3-33: Longitudinal slip of the wheel during a dynamic traction validation test (LC1)	40
Figure 3-34: Longitudinal force during a dynamic traction validation test (LC1).....	41
Figure 3-35: Longitudinal force vs. slip relationship for a dynamic traction validation test (LC1)	41
Figure 4-1: FTire parameterization procedure (Gipser, 2002).....	43
Figure 4-2: Section of the cleat definition file	44
Figure 4-3: FTire generation file window.....	45
Figure 4-4: Footprint at 1 bar inflation pressure, 0 degrees camber and 3496N vertical load.....	46



Figure 4-5: Footprint images at 2 bar inflation pressure. Left: 8123N vertical load (3° camber). Right: 1845N vertical load (5° camber angle)..... 47

Figure 4-6: Vertical stiffness on a flat plate at 1 bar inflation pressure and 0 degrees camber 47

Figure 4-7: Vertical stiffness on a flat plate at 2 bar inflation pressure and 6 degrees camber 48

Figure 4-8: Vertical tyre stiffness on a 25x25mm transversal cleat at 0 degrees camber and 1 bar inflation pressure..... 48

Figure 4-9: Vertical tyre stiffness on a 32x32mm transversal cleat at 0 degrees camber and 2 bar inflation pressure..... 49

Figure 4-10: Longitudinal tyre stiffness at 1 bar inflation pressure, 0 degrees camber and 8.61 kN vertical load..... 49

Figure 4-11: Lateral tyre stiffness at 1 bar inflation pressure, 0 degrees camber and 3.61 kN vertical load..... 50

Figure 4-12: Torsional tyre stiffness at 1 bar inflation pressure, 0 degrees camber and 5 kN vertical load..... 50

Figure 4-13: 50x50mm cleat test damping correlation at 3.5 m/s..... 51

Figure 5-1: MSC Adams (2013) model of the outdoor tyre testing equipment 54

Figure 5-2: Experimental setup to determine the vertical position of the C. O. G. with pneumatic brake system 56

Figure 5-3: Locating the vertical position of C. O. G. without pneumatic brake system 57

Figure 5-4: Schematic representation of the rotation of a rigid body (Uys et al., 2006)..... 57

Figure 5-5: Measurement equipment setup to determine the pitch moment of inertia 58

Figure 5-6: Pitch moment of inertia experimental results..... 58

Figure 5-7: Measurement equipment setup to determine the roll moment of inertia..... 60

Figure 5-8: Handling test simulation inputs..... 61

Figure 5-9: Longitudinal test simulation inputs..... 62

Figure 5-10: Left: Profiled Belgian paving, Right: Profiled Fatigue track (right) (Becker, 2008) 63

Figure 5-11: First gear simulation speed input for vertical test simulations..... 64

Figure 5-12: Second gear simulation speed input for vertical test simulations 64

Figure 5-13: Lateral force vs. slip angle (LC1) at 0 degrees camber angle 65

Figure 5-14: Validation method in the lateral direction..... 66

Figure 5-15: Self-aligning moment vs. slip angle (LC1) at 0 degrees camber angle..... 67

Figure 5-16: Longitudinal force (LC0) at 2 bar inflation pressure 69

Figure 5-17: Braking moment (LC0) at 2 bar inflation pressure 70

Figure 5-18: Vertical validation phases for a 50x50mm cleat test (LC0) at 6m/s Green: Impact phase. Red: After impact phase..... 71

Figure 5-19: Measured and simulated 50x50mm cleat test (LC0) at 6m/s 72

Figure 5-20: Measured and simulated results of the Belgian paving (LC0) at 3.5 m/s..... 74

Figure 5-21: Measured and simulated results of the Fatigue track (LC0) at 3.5 m/s..... 74

Figure 5-22: Gaussian (normal) distribution example (Distributions, 2014)..... 75

Figure 5-23: Normal distribution curve fit to vertical validation test data on the Belgian paving at 3.5 m/s..... 76

Figure 5-24: Normal distribution of the vertical load (LC0) over the Belgian paving at 3.5 m/s..... 76

Figure 5-25: Normal distribution of the vertical load (LC0) over the Fatigue track at 3.5 m/s..... 77

Figure A-1: 50x50mm cleat (LC0) at 6 m/s and 2 bar inflation pressure 84

Figure A-2: 50x50mm cleat (LC0) at 3.5 m/s and 2 bar inflation pressure 84

Figure A-3: 32x32mm cleat (LC0) at 6 m/s and 2 bar inflation pressure 85

Figure A-4: 32x32mm cleat (LC0) at 3.5 m/s and 2 bar inflation pressure 85



Figure A-5: 25x25mm cleat (LC0) at 6 m/s and 2 bar inflation pressure 86
 Figure A-6: 25x25mm cleat (LC0) at 3.5 m/s and 2 bar inflation pressure 86
 Figure A-7: Belgian paving track (LC0) at 6 m/s and 2 bar inflation pressure..... 87
 Figure A-8: Belgian paving track (LC0) at 6 m/s and 2 bar inflation pressure validation..... 87
 Figure A-9: Belgian paving track (LC0) at 3.5 m/s and 2 bar inflation pressure..... 88
 Figure A-10: Belgian paving track (LC0) at 3.5 m/s and 2 bar inflation pressure validation..... 88
 Figure A-11: Fatigue track (LC0) at 6 m/s and 2 bar inflation pressure 89
 Figure A-12: Fatigue track (LC0) at 6 m/s and 2 bar inflation pressure validation 89
 Figure A-13: Fatigue track (LC0) at 3.5 m/s and 2 bar inflation pressure 90
 Figure A-14: Fatigue track (LC0) at 3.5 m/s and 2 bar inflation pressure validation 90
 Figure A-15: Longitudinal force (LC3) at 2 bar inflation pressure 91
 Figure A-16: Longitudinal force (LC1) at 2 bar inflation pressure 91
 Figure A-17: Longitudinal force (LC0) at 2 bar inflation pressure 92
 Figure A-18: Lateral force vs. slip angle (LC1) at 0° camber angle and 2 bar inflation pressure..... 92
 Figure A-19: Lateral force vs. slip angle (LC1) at 2° camber angle and 2 bar inflation pressure..... 93
 Figure A-20: Lateral force vs. slip angle (LC1) at -2° camber angle and 2 bar inflation pressure 93
 Figure A-21: Lateral force vs. slip angle (LC3) at 0° camber angle and 2 bar inflation pressure..... 94
 Figure A-22: Lateral force vs. slip angle (LC3) at 2° camber angle and 2 bar inflation pressure..... 94
 Figure A-23: Lateral force vs. slip angle (LC3) at -2° camber angle and 2 bar inflation pressure 95

List of tables

Table 2-1: Adams tyre model application selection chart (MSC Adams, 2013) 9
 Table 3-1: Modal analysis results 31
 Table 3-2: Three load cases considered during validation field tests (As measured by the WFT)..... 34
 Table 5-1: Results of pitch moment of inertia 59
 Table 5-2: Results of roll moment of inertia..... 60
 Table 5-3: Validation results for lateral force vs. slip angle for three load cases and camber angles .. 66
 Table 5-4: Validation results for self-aligning moment vs. slip angle for three load cases and camber angles 68
 Table 5-5: Validation results of longitudinal force for three load cases 69
 Table 5-6: Validation results of the braking moment for three load cases 70
 Table 5-7: Cleat test validation results for 3.5 m/s test for LC0 at 2 bar inflation pressure 72
 Table 5-8: Cleat test validation results for 6 m/s test for LC0 at 2 bar inflation pressure 73
 Table 5-9: Validation results for the Belgian paving..... 77
 Table 5-10: Validation results for the Fatigue track 78

Nomenclature

English symbols

A	Distance from Laser 1 to side post	(m)
B	Distance from Laser 2 to side post	(m)
b	Longitudinal distance from C.O.G to pivoting point	(m)
CG_x	Position of the centre of gravity in the longitudinal direction	(m)
CG_y	Position of the centre of gravity in the lateral direction	(m)
F	Force	(N)
F_{spring}	Spring force	(N)
g	Gravitational acceleration	(m/s ²)
GR	Gear Ratio	
h	Height of C.O.G	(m)
H	Vertical distance between pivoting point and force application point	(m)
I_o	Moment of inertia about pivoting point	(kgm ²)
$I_{pitch,CG}$	Pitch moment of inertia about the C.O.G	(kgm ²)
$I_{roll,CG}$	Roll moment of inertia about the C.O.G	(kgm ²)
i	Index of Summation	
k	Spring stiffness	(N/m)
l	Distance between lasers 1 and 2	(m)
L	Length	(m)
L_{force}	Distance between spring and pivoting point	(m)
L_x	Distance between pivoting point and C.O.G in the longitudinal direction	(m)
L_y	Distance between pivoting point and C.O.G in the lateral direction	(m)
L_z	Distance between pivoting point and C.O.G in the vertical direction	(m)
m	Mass	(kg)
n	Number of points in data set	
p	Measured data points	
p_a	Normal pressure	(Pa)
\bar{r}	Distance from predefined point to centre of gravity	(m)
r_i	Inner radius	(m)
r_o	Outer radius	(m)
R	Contact point with the ground	
s	Simulated data points	
T_{brake}	Torque	(Nm)
x_1 and x_2	displacement amplitudes of consecutive oscillations	(m)

Greek symbols

α	Slip angle	(degrees)
δ	Logarithmic decrement	
γ	Camber angle	(degrees)
σ	Standard Deviation	
σ^2	Variance	
μ	Mean	
μ_f	Coefficient of friction	
τ	Natural period of oscillating spring	(s)
τ_d	Damped period of oscillating spring	(s)
θ	Angular displacement	(degrees)
$\theta_2 - \theta_1$	Annular brake pad side	(degrees)
ζ	Damping ratio	

Abbreviations

BRIT	Brush and Ring Tyre Model
C.O.G	Centre of gravity
CRG	Curved Regular Grid
DNS-Tire	Dynamic Nonlinear Spatial Tire Model
FEM	Finite Element Model
FRF	Frequency Response Function
FTire	Flexible Structure Tire Model
GPS	Global Positioning System
KMT	Krauss Messtechnik und Telemetrie
LC0	Load Case with zero added 200kg steel plates
LC1	Load Case with one added 200kg steel plate
LC3	Load Case with three added 200kg steel plates
LDVT	Linear Variable Displacement Transducer
m%RE ^m	Modified percentage relative error defined by the mean of the %REs
m%RE ^s	Modified percentage relative error divided by a specified percentage relative error
RMS	Root Mean Square
SAE	Society of Automotive Engineers
SUV	Sports Utility Vehicle
TYDEX	Tyre Data Exchange
VDG	Vehicle Dynamics Group
WFT	Wheel Force Transducer
%RE	Percentage relative error



1 Introduction

Vehicle design and development has seen a large paradigm shift in the last few decades. Previously, vehicle design and development have been strongly dependent on accurate prototype models which were implemented in testing procedures and data collection for further development of vehicle components.

However, in recent times increasing emphasis has been placed on accurately predicting vehicle performance in a simulated environment. To simulate vehicle dynamics in a realistic manner, complex multi-body dynamics models must be developed and implemented in the simulation environment. Not only vehicle dynamics, but also the interaction between the vehicle, driver and passengers as well as the environment in which the vehicle operates have to be accurately modelled and simulated.

Therefore, complex mathematical and empirical models are designed and implemented in the simulation environment in order to simulate vehicle performance accurately. These models must be implemented with adequate accuracy to ensure that the simulation results have sufficient validity.

While prototype testing gives realistic results for vehicle tests being conducted, it is an onerous and costly testing method. Vehicle simulation is considered a simplification and idealization of the real-world scenario and is widely replacing prototype testing methods worldwide. Vehicle components are modelled and simulated during the procedure and it is of utmost importance that the modelling of each of these vehicle components is of sufficient accuracy to achieve acceptable results during the simulation.

The external forces experienced by a vehicle may be categorised as aerodynamic forces and tyre-road interaction forces. Thus, it may be said that all forces experienced by a vehicle occur between its tyres and the road surface when the vehicle is travelling at speeds for which aerodynamic forces can be neglected. Aerodynamic forces only play a major role when the vehicle is travelling at a high velocity since aerodynamic forces are strongly velocity dependent.

The SUV has become very popular and high in demand worldwide. South Africa has a large number of SUVs on its roads and it is thus of utmost importance that the safety of these vehicles is ensured in all circumstances under on-road as well as off-road conditions.

Since all-terrain tyres and on-road tyres differ substantially in design and construction it is important to characterise and parameterize all-terrain tyres used on SUVs to ensure the knowledge of the types of forces that act between the tyre and the road. Information required to parameterize tyre models is not readily available. Parameterization and modelling of all-terrain tyres has largely been neglected in research and should, therefore, be investigated such that the tyre-road interaction is understood thoroughly for future vehicle design and development.



2 Literature survey

The pneumatic tyre forms a complex component in vehicle design and the handling and traction characteristics of tyres play a key role in vehicle design. Therefore, it is imperative to understand the mechanics of tyre-road interactions.

The parameterization and modelling of pneumatic tyres on smooth road surfaces has been studied extensively over time. However, recent tyre research efforts have been focussed on tyre modelling on uneven road surfaces and off-road terrain. The development of tyre models which can predict tyre behaviour over uneven road surfaces has become an important aspect in vehicle design.

2.1 Pneumatic tyres

Pneumatic tyres form one of the most important components in automotive design. Not only do tyres form the contact between the road surface and the vehicle, but they also transmit all forces, except for aerodynamic forces, to the vehicle. According to Zegelaar (1998), the forces and moments generated by the tyre are the result of the interaction between the tyre's contact patch and the road surface it is travelling on.

The pneumatic tyre serves three main functions, namely supporting the vehicle's weight in the vertical direction, generating lateral forces allowing a vehicle to corner and, finally, to generate longitudinal forces for a vehicle to both accelerate and decelerate. Vibrations due to road undulations as well as steering and vertical vibrations have a large influence on the longitudinal, lateral and vertical forces generated by the tyre. Therefore, a thorough understanding of the behaviour of pneumatic tyres on various terrain surfaces is an important aspect of vehicle dynamics.

The complex construction of pneumatic tyres plays a major role in tyre behaviour under driving conditions. According to Barbosa et al. (2015), not only the rubber compounds used in the construction of the tyre but also the tread pattern as well as the nature and condition of road surfaces greatly affect tyre performance and characteristics.

On-road and all-terrain tyres differ significantly in design with the most prominent difference being the difference in tread design. While on-road tyres generally have a shallow tread, all-terrain tyres have a deep tread depth and larger spaced tread blocks to provide traction on off-road conditions. All-terrain tyre tread design allows for traction on smooth road surfaces as well as on off-road terrain. As stated by Nakajima (2003), the interlocking tread elements of all-terrain tyres provide for good traction properties on dry snow, mud, sand and gravel as well as paved surfaces. It is found, however, that all-terrain tyres experience higher wear on paved road surfaces due to the higher friction generated by the tyre tread elements on these surfaces.

The tyre tread compounds of all-terrain tyres generally differ to on-road tyre tread compounds. On-road tyre treads generally incorporate "softer" compounds which enable better traction properties on paved roads due to hysteresis and adhesion between the tread elements and the road surface.

All-terrain tyres, however, incorporate a “harder” rubber compound to reduce wear while still having good traction properties on paved road surfaces. As stated by Zebala et al. (2007), the tread design and compound composition of tyres greatly influence the tractive and handling behaviour of vehicles.

All-terrain tyres generally have a larger aspect ratio than on-road tyres. According to Byoung et al. (2007) the larger aspect ratio allows greater deformation of the tyre when encountering obstacles on off-road terrain. This, in turn, allows for better tractive properties in off-road conditions of the all-terrain tyre. However, due to the construction of the carcass of all-terrain tyres the handling characteristics are found to be poor as compared to on-road tyres.

2.1.1 Tyre axis system

The SAE tyre axis system (SAE International, 2014), indicated in Figure 2-1, is often used when analysing the forces and moments acting on a tyre. The vertical forces experienced by a tyre are in line with the vertical z-axis, where the z-axis is perpendicular to the road plane with a positive direction downward as stated by Gillespie (1992). The x-axis is the intersection of the wheel plane and the road plane with the positive direction forward. The longitudinal or tractive force acts in the direction of the x-axis which is the direction in which the tyre is orientated. The y-axis is the road plane, its direction being chosen to make the axis system orthogonal and right-hand. The lateral force acts in the direction of the y-axis, which is perpendicular to the direction the tyre is pointed at. It should be noted, however, that the origin of the SAE coordinate system lies in the centre of the tyre’s contact patch.

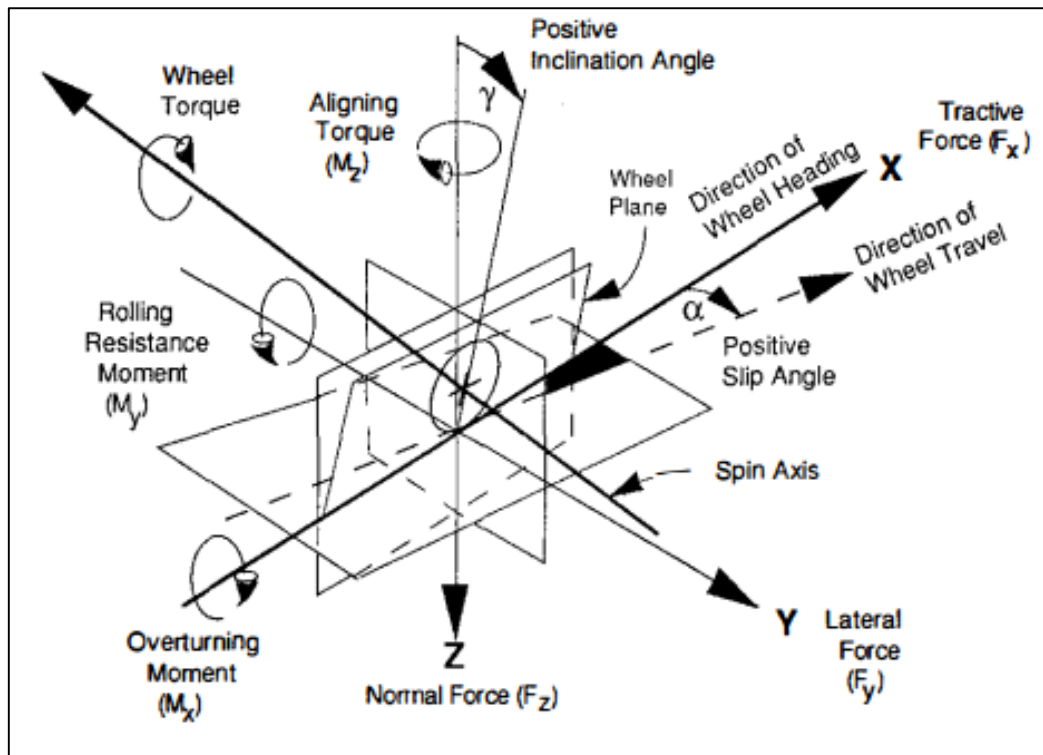


Figure 2-1: The SAE coordinate system (Gillespie, 1992)

2.1.2 Tyre handling properties

The lateral tyre performance is often related to the handling characteristics of vehicles. According to Kim (2009) the lateral tyre performance is governed predominantly by the lateral force vs. slip angle, α , characteristics of a tyre but is also influenced by the camber angle, γ , of the tyre during cornering.

2.1.2.1 Slip angle

According to Hajjahmad et al. (2014), when a vehicle is turning its tyres experience side slip. The side slip is determined predominantly by the slip angle and lateral forces experienced by the tyre. The slip angle of the tyre is defined as the angle between the heading of the tyre and the direction the tyre is moving.

When a tyre is pointing in the direction it is travelling in (slip angle, α , equals 0) the tyre does not generate any lateral force at a zero camber angle. The lateral forces on a tyre increase steeply and linearly with the first few degrees of slip angle. Depending on the tyre being analysed and the properties it exhibits, the lateral force generally peaks at between 4 to 10 degrees of slip angle. Figure 2-2 shows the lateral force generation for two different tyres at different vertical loads while Figure 2-3 depicts the mechanics of lateral force generation due to slip angle input.

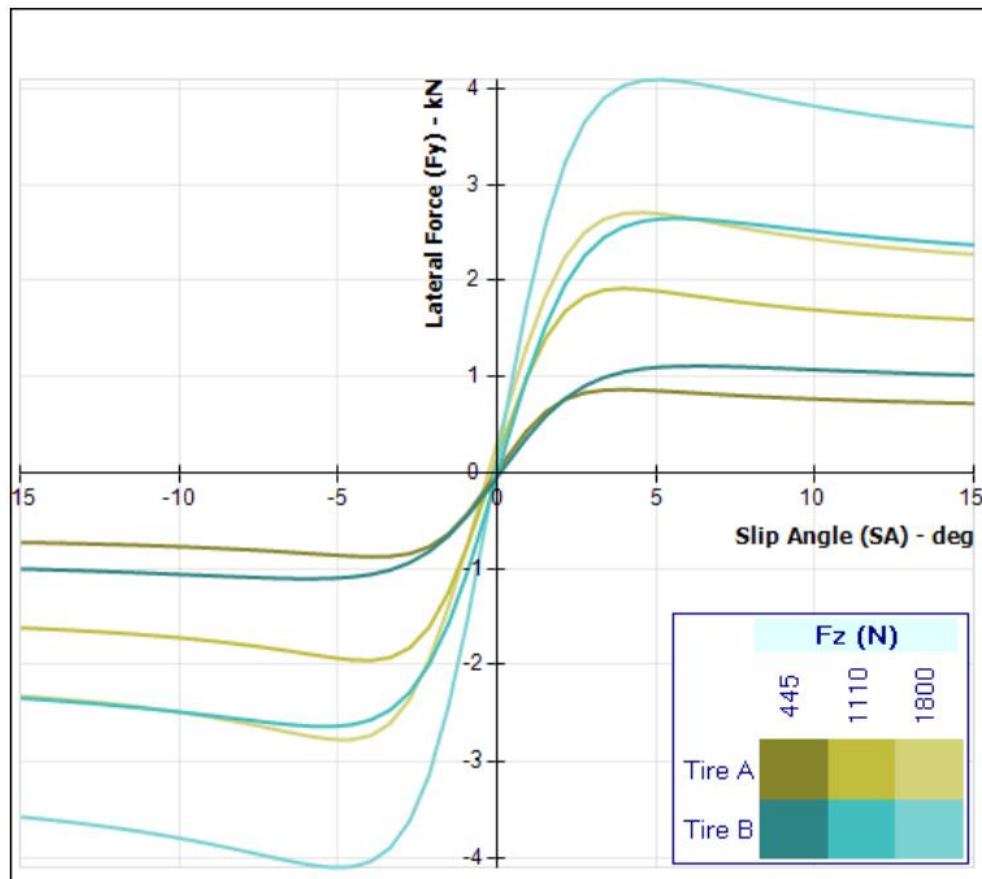


Figure 2-2: Lateral Force vs. slip angle characteristics of two tyres (Optimum, 2014)

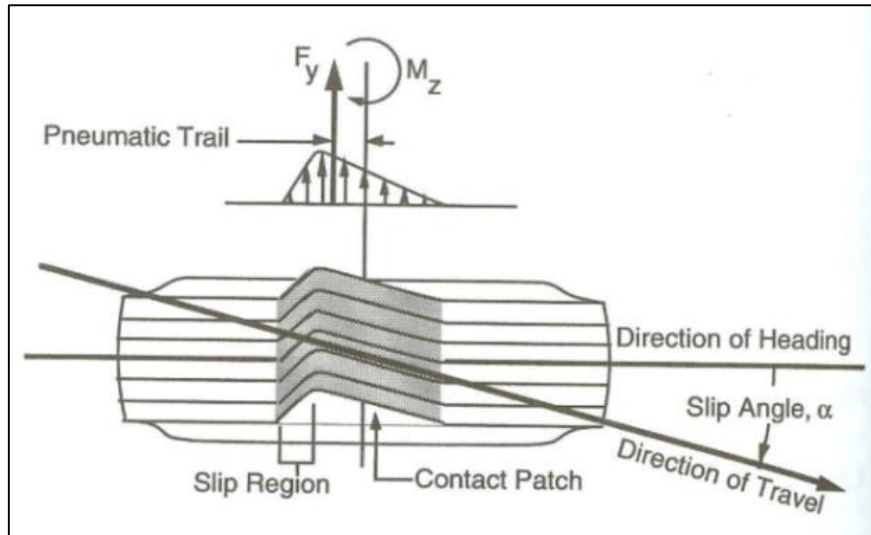


Figure 2-3: Lateral force and aligning moment generation due to slip angle (Gillespie, 1992)

From Figure 2-3 it can be seen that the lateral force does not act in the centre of the contact patch. Therefore, a moment is created about the z axis, which is located at the centre of the contact patch. This moment is commonly referred to as the self-aligning moment. According to Hajiahmad et al. (2014), the aligning moment has a stabilizing or centring effect on the wheel.

2.1.2.2 Camber angle

A tyre not only generates lateral forces due to slip angle (α), but also due to camber angle (γ). According to Lamy et al. (2010) camber is defined as the angle between the central plane of the wheel and a plane which is perpendicular to the road. When a tyre experiences a camber angle a lateral force is generated, which is referred to as camber thrust. The camber thrust force mechanism acts in front of the centre of the contact patch due to the conditions in the contact patch. This mechanism generates a moment, which is denoted as the camber torque. Figure 2-4 shows how camber thrust and torque are generated due to camber angle.

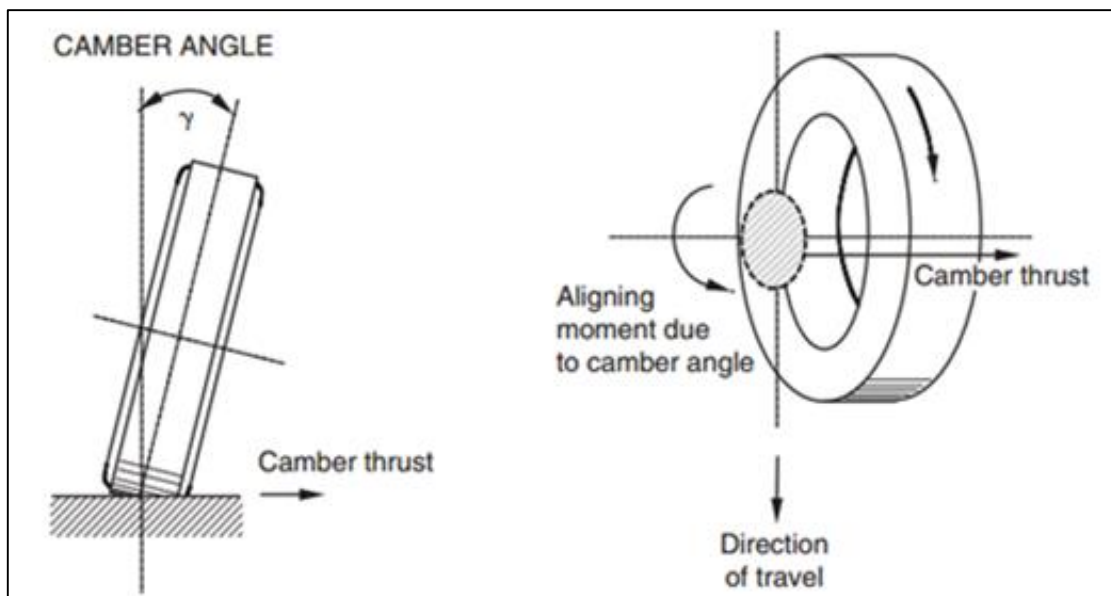


Figure 2-4: Camber thrust and aligning moment generation due to camber angle (Blundell et al., 2004)

2.1.3 Tyre traction properties

Longitudinal forces are generated by the tyres when a vehicle either accelerates or decelerates and longitudinal slip is induced by the deformation of the tyre's tread elements as these deflect to develop and sustain the frictional forces.

2.1.3.1 Longitudinal slip

When generating longitudinal force, tyres are observed to experience additional slip due to the tyre tread elements deforming to withstand the frictional forces developed between the road surface and the tyre itself. When a vehicle accelerates, the rolling velocity of the tyre minutely exceeds the velocity of the vehicle itself. Therefore, slip occurs between the tyre and the road surface. A force is developed between the road surface and the tyre termed the frictional force since it opposes the direction of the tyre's angular motion, as stated by Cho et al. (2006).

Similarly, when a vehicle experiences deceleration or braking, the angular velocity of the tyre decreases. This, in turn causes the tyre's rolling velocity to be minutely less than the vehicle's velocity which causes slip between the tyre and the road surface thus facilitating braking force.

The longitudinal force generated by a tyre on a road surface will generally differ with slip, depending on the coefficient of friction between the tyre and the road surface. The longitudinal force is seen to increase with slip until a maximum longitudinal force peak is reached after which the longitudinal force decreases as slip increases to 100%, as seen in Figure 2-5.

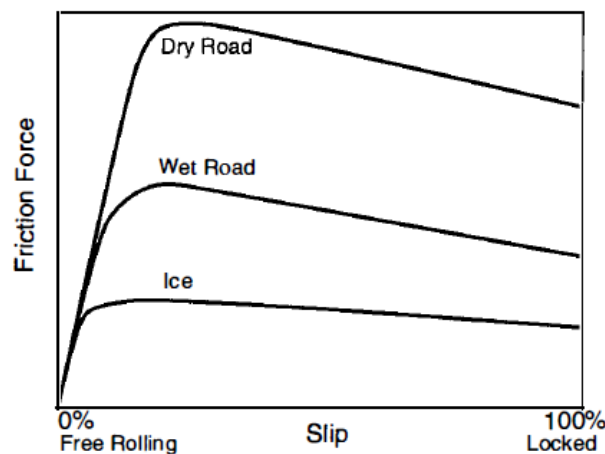


Figure 2-5: Longitudinal force vs. slip characteristics (Gillespie, 1992)

2.2 Tyre modelling

A vehicle handling simulation outcome is highly dependent on the accuracy of the tyre-road interaction prediction. Therefore, creating a sufficiently accurate tyre and road model in a vehicle simulation model should be emphasised.

While mathematical tyre and tyre contact models, such as Pacejka 89 and Pacejka 94 tyre models, are computationally efficient and give good handling simulation results on smooth road surfaces these are generally not able to accurately predict tyre behaviour over uneven terrain, as stated by Cabrera et al. (2004).

According to Zegelaar (1998), a number of physics based tyre models, such as the FTire tyre model, which are able to capture high frequency tyre responses and predict tyre behaviour over uneven road surfaces, exist. However, these tyre models are usually computationally inefficient and a large amount of parameterization data is required to parameterize these tyre models.

Empirical tyre models, such as the Pacejka 2002 tyre model, which require less parameterization data and are computationally more efficient than physics based tyre models, have been developed to predict tyre behaviour over uneven road surfaces. However, according to Frey (2009) empirical tyre models are generally not able to capture complex tyre behaviour.

2.2.1 Tyre models

Many tyre models have been developed to predict and model the tyre-road interaction. Most existing tyre models that have been developed to analyse tyre handling and traction characteristics on smooth road surfaces are efficient, readily available and are based on the Pacejka Magic Formula curve fit.

Tyre models which predict and model tyre behaviour over certain discrete and long-wavelength undulations and obstacles on smooth road surfaces are widely used. According to Cabrera et al. (2004), a number of tyre and tyre contact models have been developed in the past to simulate handling manoeuvres over smooth, manmade road surfaces. Mathematical tyre models are frequently implemented in simulation software to predict passenger vehicle handling performance.

However, there is a great need for modelling tyre behaviour over irregular and short-wavelength (shorter than the wheel circumference) undulations on uneven road surfaces or off-road conditions, as stated by Zegelaar (1998). The vertical tyre behaviour and its corresponding vibrational response become significant when considering the modelling of vehicle ride comfort and handling characteristics over uneven road surfaces.

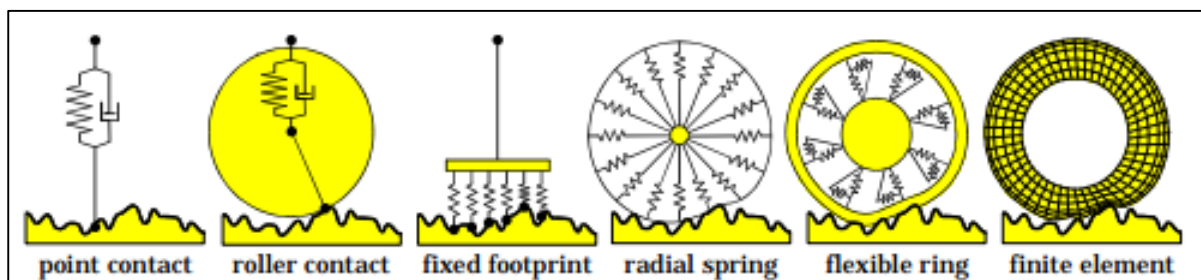


Figure 2-6: Contact models used for various tyre models (Zegelaar, 1998)

To predict tyre behaviour over uneven road surface several tyre contact models, depicted in Figure 2-6, and road contact models have been developed and implemented. These contact models attempt to model the tyre contact patch interaction with the road surface. Identifying and understanding the application capabilities of each of these models is vital to successfully simulate tyre behaviour over uneven terrain.



The point contact model is the most widely used contact model. The tyre contact patch is approximated as a single point on the road surface while the tyre is represented by a parallel single spring-damper system. As stated by Zegelaar (1998), the point contact model is valid for obstacles longer than 3 metres which have a slope of less than 5 degrees.

The roller contact model models the tyre as a rigid disk with a parallel spring and damper system rolling over undulations and obstacles on the road surface while the contact patch of the tyre is approximated as a single point. The contact point is not limited to lie below the axis of rotation of the wheel. This allows for small undulations and obstacles on the road surface to be filtered, as stated by Zegelaar (1998).

The fixed footprint model approximates the tyre contact patch as a series of point contacts with springs and damper systems. Road surface undulations and obstacles are averaged by the contact model which results in a smoother road excitation, as stated by Zegelaar (1998). Therefore, the fixed footprint model displays a more realistic representation of the tyre than the point contact model.

The radial spring model, which is an improvement of the roller contact model, approximates the tyre contact patch as a radially deforming ring. Springs, which originate from the spin axis of the wheel, are connected to the outer ring's circumference radially and allow for slight deformations of the contact patch. According to Zegelaar (1998), the radial spring contact model is able to approximate undulations and obstacles, such as cleats, on the road surface when implementing non-linear digressive radial springs within the model.

According to Zegelaar (1998), the flexible ring model consists of a deformable circular ring representing the tyre tread band. The centre of the spin axis is connected to the outer tread band by radially and tangentially connected springs which model tyre sidewalls and inflation pressure of the tyre.

The flexible ring model is most suitable for the modelling of high frequency tyre dynamics over short-wavelength undulations and obstacles on the road surface but is also used to calculate and determine tyre deformations. As stated by Kisilowski et al. (1986), the flexible ring model is often referred to as the adaptive footprint model since the deflection of the tread band and flexible carcass provides the model with an adaptive footprint.

The finite element model (FEM) is based on a detailed description of the tyre structure and is very powerful as it can be used to calculate dynamic tyre forces of the tyre rolling over undulations and obstacles on the road surface at high velocities, as stated by Zegelaar (1998).

In the simulation environment, compromises often have to be made concerning available resources. Time, financial, computational and equipment resources, as well as the level of accuracy which is required for the simulation, are factors when choosing the tyre model to be used for a simulation.

An important resource to be taken into account is the amount of parameterization data required to define or parameterize the tyre model. Figure 2-7 depicts the relationship between tyre model accuracy and required parameterization data for the given tyre models which may be implemented in MSC Adams (2013).

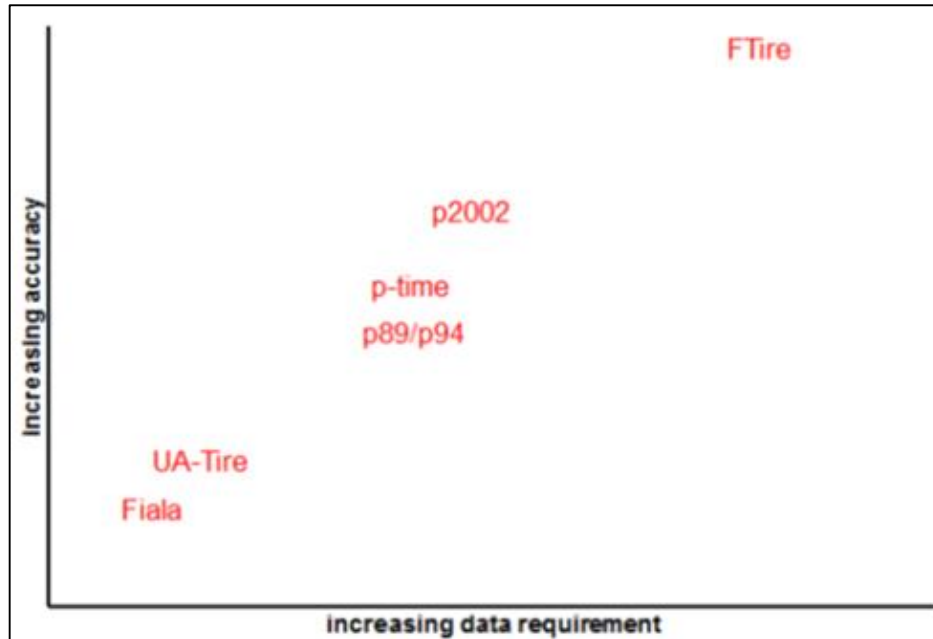


Figure 2-7: Tyre model accuracy vs. required data (Oosten, 2011)

Table 2-1 shows the level of accuracy provided by each tyre model for certain events or manoeuvres in MSC Adams (2013). Based on the information tabulated an informed decision can be made by the user as to which tyre model can provide the required accuracy for the application within the simulation.

Table 2-1: Adams tyre model application selection chart (MSC Adams, 2013)

MD Adams	Event / Maneuver	ADAMS/ Handling Tire							Specific Models	
		PAC2002 ¹	PAC-TIME ¹	PAC89 ¹	PAC94 ¹	FIALA ¹	5.2.1. ¹	UA Tire ¹	PAC-MC ¹	FTire
Handling	Stand still and start	+	o/+	o/+	o/+	o/+	o/+	o/+	o/+	+
	Parking (standing steering effort)	+	-	-	-	-	-	-	-	+
	Standing on tilt table	+	+	+	+	+	+	+	+	+
	Steady state cornering	+	+	o/+	+	o	o	o/+	+	o/+
	Lane change	+	+	o/+	+	o	o	o/+	+	o/+
	ABS braking distance	+	o/+	o/+	o/+	o	o	o/+	o/+	+
	Braking/power-off in a turn	+	+	o	o	o	o	o	+	o/+
	Vehicle Roll-over	+	o	o	o	o	o	o	o	+
Ride	On-line scaling tire properties	+	-	-	-	-	-	-	-	o
	Cornering over uneven roads *	o/+	o	o	o	o	o	o	o	o/+
	Braking on uneven road *	o/+	o	o	o	o	o	o	o	+
	Crossing cleats / obstacles	-	-	-	-	-	-	-	-	+
	Driving over uneven road	-	-	-	-	-	-	-	-	+
Chassis Control	4 post rig (A/Ride)	+	o/+	o/+	o/+	o/+	o/+	o/+	o/+	o/+
	ABS braking control	o/+	o	o	o	o	o	o	o	+
	Shimmy ²	o/+	o	o	o	o	o	o	o	+
	Steering system vibrations	o/+	o	o	o	o	o	o	o	+
	Real-time	+	-	-	-	-	-	-	-	-
	Chassis control systems > 8 Hz	o/+	-	-	-	-	-	-	-	+
Durability	Chassis control with ride	-	-	-	-	-	-	-	-	+
	Driving over curb	-	-	-	-	-	o	o	-	o/+
	Driving over curb with rim impact	o	-	-	-	-	o	o	-	o/+
	Passing pothole	-	-	-	-	-	o	o	-	o/+
	Load cases	-	-	-	-	-	o	o	-	o/+

-	Not possible/Not realistic
o	Possible
o/+	Better
+	Best to use

* wavelength road obstacles > tire diameter

¹ use_mode on transient and combined slip

² wheel yawing vibration due to suspension flexibility and tire dynamic response

From Table 2-1 it can be seen that FTire has the greatest ability to predict tyre behaviour in MSC Adams (2013) for the given events and manoeuvres from all the tyre models listed. The FTire model is the only tyre model that is able to predict handling as well as ride events and manoeuvres which makes the model useable in vehicle simulations for both on- and off-road conditions. Therefore, it is decided to focus this study on the parameterization of the FTire model.

2.2.2 The FTire model

The FTire (Flexible Structure Tire Model) model is classified as one of the strictly mechanics-based tyre models and is suitable to be used in vehicle dynamics simulations. According to Gipser et al. (2013), FTire is a fully three dimensional in- and out-of-plane tyre model.

According to Gipser (2007), FTire is a physics based, highly nonlinear and dynamic tyre model for simulations and optimization modelling. The tyre dynamics over large, sharp-edged obstacles can be simulated by the FTire, tyre model, as is depicted in Figure 2-8. FTire is designed for use in multi-body dynamics simulation models such as ride comfort and handling simulations as well as road load prediction models for durability applications on road irregularities even with very short wavelengths.

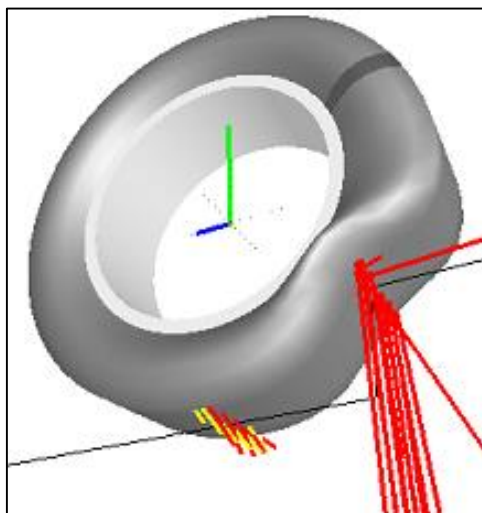


Figure 2-8: FTire tyre model negotiating a large, sharp-edged obstacle (MSC Software, 2013)

As reported by Gipser (2007), the development of FTire started in 1998 and used some of the numerical concepts and ideas of the so-called coarse-mesh finite element DNS-Tire (Dynamic Nonlinear Spatial Tire Model) model and the nonlinear rigid-ring BRIT (Brush and Ring Tire Model) model.

Based on the findings of Gipser et al. (2013) and Pacejka (2012), FTire is able to return reasonable dynamic tyre forces caused by road profile height and deformation, friction variations, suspension vibration, torque due to acceleration and braking, tyre imbalances and non-uniformities, variations in temperature and pressure as well as misuse events.

It should be noted that, according to Gipser (2007), although FTire simulations take about 5-20 times real time, all tyres can be simulated simultaneously at equal computation speeds during vehicle simulations. This is due to the fact that the FTire model allows the implementation of a multicore support.

Parameterized data, required by FTire, may be obtained from tyre data, provided by the manufacturer of the tyre, from laboratory measurement results, from similarity considerations, or from a combination of these sources and methods, as stated by Gipser (2002).

The key features of the FTire tyre model may be summarized as stated by Gipser et al. (2013).

- Structural dynamics based full 3-dimensional nonlinear in-plane and out-of-plane tyre model for simulation of belt dynamics, local contact patch pressure distribution, rolling resistance, side-wall contact, large camber angles and misuse scenarios.
- Suitable for a frequency range up to 200 Hz, excited by short surface wavelengths, mass imbalance, non-uniformity of tyre and/or rim, air cavity vibrations, or irregular tread patterns.
- Very fast and flexible, up to real-time capability. Orders of magnitude faster than explicit finite element models.
- Simulation of imbalances by inhomogeneous mass and stiffness distribution, radius variation, and local tread wear.
- Belt temperature distribution model.
- Air volume vibration model.
- Capability of tire slipping on rim for very large drive or brake torques.
- Integrated flexible and/or viscoplastic rim model.
- Support for user-defined wear, temperature distribution, and rim flexibility models.
- Full integration of cosin/road digital road library with support for complex rigid time-invariant and time-variant road surfaces.
- Full integration of cosin/soil digital road library with support for flexible and deformable road surfaces.
- Advanced online animation with belt deformation animation, pressure distribution plots, road surface visualization and movie export.
- Robust, multi-core system enabled solver engine.
- Parameter editing and validation tools.
- Tailored parameter fitting tool available (FTire/fit).
- Very good correlation to measurements.

Based on the findings of Stallmann (2014), it is found that a parameterized FTire model is able to predict the vertical tyre response of a large off-road tyre over uneven road surfaces more accurately than other tyre models. Other tyre models included one point contact, 3D Equivalent Volume Contact and 3D Enveloping Contact models. The correlation of FTire model simulated results to measured data results was found to be very good.

2.2.2.1 Structure model

FTire fundamentally consists of three components. The first component is the structural model of the tyre, which describes the tyre's structural stiffness, damping, as well as inertia properties.

According to Cosin (2014), the structure model of the tyre is based on a set of rings which are commonly referred to as belt segments, and are FTire's image of the actual tyre's belt layer structure. Thus, the structural model may be described as an extensible and flexible set of rings. These flexible rings each consist of a finite number of elements, each of which is connected to its direct neighbouring elements by means of springs.

These degrees of freedom of the tyre model elements thus allow for in-plane and out-of-plane motions. The belt element stiffnesses are shown illustratively in Figure 2-9 which depicts (from left to right) the in-plane bending stiffness, the out-of-plane bending stiffness, the belt circumferential torsion (red) and twist (blue) stiffnesses, and the lateral bending stiffness, respectively.

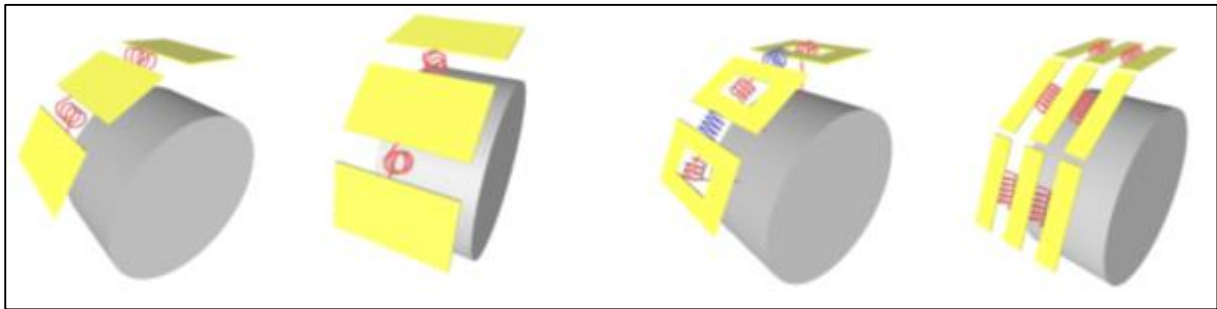


Figure 2-9: FTire belt element stiffnesses (Gipser, 2013)

In order to accurately compute the tyre dynamics with the FTire tyre model, each of the elements has $4+x$ dynamic degrees of freedom, which are described below, as given by Pacejka (2012), and may be seen in Figure 2-10.

- Longitudinal, lateral and vertical displacement of the centre point
- Rotational angle of the circumferential axis
- Flexible bending in lateral direction, described by x -independent shape functions.

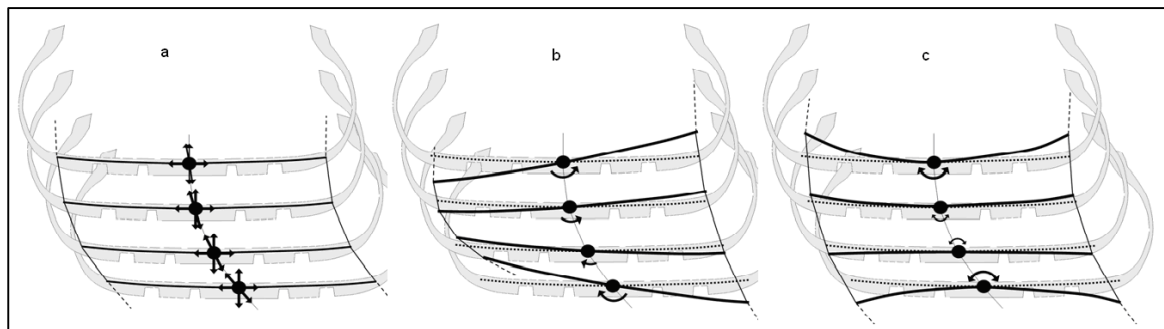


Figure 2-10: Belt segment degrees of freedom. From left to right: translational, torsional and bending (Gipser, 2013)

As stated by Pacejka (2012), the belt segments, as well as each of their internal degrees of freedom, which are assumed to be stiff, elastic or visco-elastic segments, are interconnected by nonlinear, inflation-pressure dependent force elements. These force elements consist of nonlinear translational and rotational stiffnesses, bending stiffnesses along all three axes, respective damping elements, which are assumed to be linearly viscous, as well as certain spring-damper and hysteresis elements. Furthermore, these belt segments are subjected to inflation pressure forces in the radial direction, as well as to forces and moments by the tread model. This may be seen in Figure 2-11.

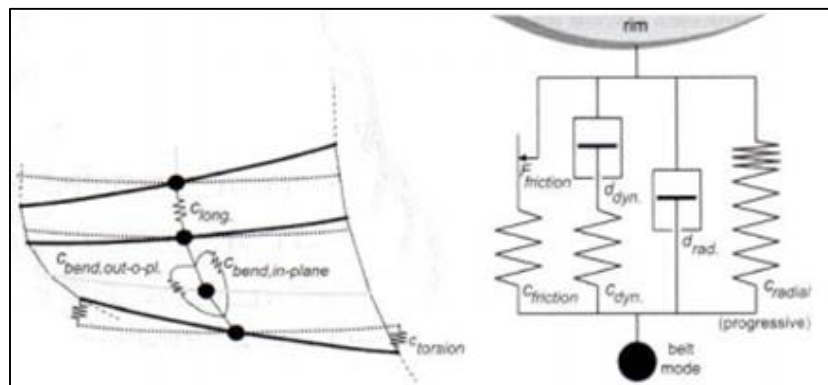


Figure 2-11: FTire structural force elements, Gipser (2013)

2.2.2.2 Tread model

FTire's second component is classified as the tread model of the tyre. The tread model consists of the estimation of the height, the compliance, the road surface friction coefficient and a computation of the resulting ground pressure and shear stresses within the contact patch, as found by Gipser (2002) and Pacejka (2012).

According to Cosin (2014), several massless contact and friction elements are located between each of the model's belt segments. The number of elements between segments depends on the desired road surface height resolution while the tread model is made up of contact elements. If the tread pattern is available in a black and white bitmap file, then the contact element lengths are determined by FTire itself, according to the pattern provided by the user.

Pacejka (2012), states that the tangential road surface plane is computed for each contact element by assessing the road surface height at three different locations close to each contact element. This is required in order to compute road undulations which are much smaller than the contact patch length of the tyre. In the case where the road surface changes with time both normal and tangential surface velocities are taken into consideration, as discussed by Gipser (2013).

The normal force of each contact element is commonly a nonlinear function of radial deflection as well as of deflection velocity. This describes the tread rubber stiffness and damping characteristics when experiencing a vertical load. The normal force, the tangential sliding velocity and the local friction coefficient are implemented to compute the tangential friction forces and, therefore, the shear stress in the tyre-road contact patch, as discussed by Pacejka (2012). The local friction coefficients are, therefore, a function of position, ground pressure, and sliding velocity as well as tread temperature, as discussed by Gipser (1999).

2.2.2.3 Thermal model

Based on the findings of Gipser (2013), the third component of the FTire model is an optional thermal model of the tyre. This model consists of a thermodynamic computation of the tyre's inflation pressure, a heat generation and transfer model as well as a tread temperature model. The heat generation and transfer model approximates the tyre to consist of three separated regions having defined thermal properties.

These regions are termed the tyre structure (which includes the sidewall, the belt and the air volume of the tyre), the tread (which is not in contact with the ground) and the contact patch. The thermal model is shown schematically in Figure 2-12.

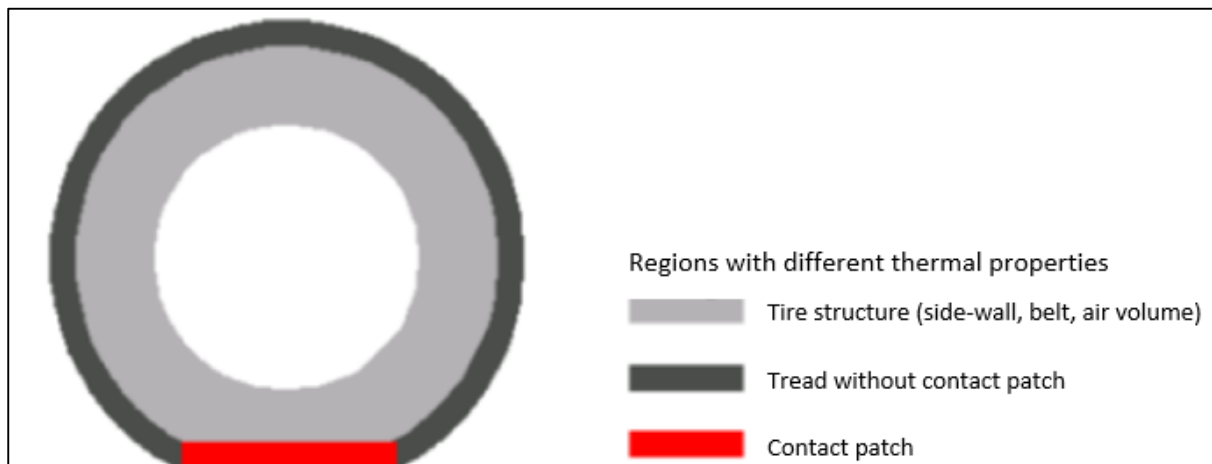


Figure 2-12: FTire thermal model (Gipser, 2013)

2.2.2.4 Data parameterization

Cosin (2014) emphasises that there is a difference between data, used in the FTire tyre model equations (pre-processed data), and data which is to be supplied by the user to FTire (basic data).

Recommendations are made that the user only supplies basic data, which may be obtained by conducting static and dynamic parameterization tests. The static tests conducted to obtain the basic data should, preferably, be repeatable in a reliable manner. The parameterization data provided should contain sufficient information to clearly and unambiguously determine all internal pre-processed tyre data and should be clearly and discretely defined. The dynamic parameterization tests should provide smooth and clearly defined data, as stated by Pacejka (2012).

2.3 Tyre testing

A large variety of tyre testing equipment is available, including indoor and outdoor tyre testing equipment which is implemented in the automotive industry, as well as universities and technical institutes to investigate static and dynamic properties of various types of tyres. According to Frey (2009), tyre testing equipment is utilized to obtain tyre test data which includes the determination of forces and moments generated by the tyres.

2.3.1 Indoor tyre testing equipment

Indoor tyre testing equipment is widely used due to the fact that the tyre testing data and results are obtained under controlled circumstances and are generally easily repeatable. Furthermore, tests conducted on indoor tyre testing equipment are not weather dependent which is advantageous in areas where extreme weather conditions prevail. However, certain problems with indoor tyre testing equipment exist. These problems include artificial road surfaces and unrealistic contact regions between the tyre and the artificial road surface.

The tyre drum testing equipment, as depicted in Figure 2-13 is used to obtain tyre test data by either placing the tyre inside the drum or outside the drum. Placing the tyre on the inside of the drum results in a tyre contact patch that is larger than that on a flat road while placing the tyre on the outside of the drum results in a tyre contact patch that is smaller than that on a flat road surface.

The inability of the tyre drum testing equipment to accurately capture the tyre contact patch leads to variations in forces and moments generated by the tyre. However, due to its simple and robust design the drum tyre testing equipment is widely used in industry.

Drum tyre testing equipment is generally capable of testing tyres at speeds ranging from 0-250 km/h. However, the maximum speed of the drum tyre testing rig depends on the design and electric motor specifications, as stated by FKA (2013). The drum tyre testing rig is used to measure both static and dynamic tyre properties. The drum surface, on which the tyre is being tested, is usually coated with an abrasive safety walk coating to which cleats and other obstacles can be bolted onto to conduct dynamic ride comfort tests of the tyre.

An adjustable hub, which is adjusted dynamically, may be implemented to investigate the tractive and handling properties of a tyre. Furthermore, the vertical wheel load may be varied by means of an air spring or hydraulic or pneumatic actuators such that a constant vertical force is applied during tyre testing procedures, as described by FKA (2013). Tyre forces and moments are measured by making use of load cells or strain gauges attached to the wheel hub. Tyre drum test equipment is often used to obtain static and dynamic parameterization data for tyre models.

As reported by Gipser (2007), tyre model parameterization software developers are working on tyre model analysis software which may be used to account for the curvature nature of the drum test rig and the resulting tyre test data.

According to MTS (2013), the flat belt tyre testing equipment, as depicted in Figure 2-13, gives more realistic tyre data results due to the fact that the tyre contact patch is replicated on a flat belt section. The belt, on which the tyre is being tested, is usually coated with an abrasive safety walk coating simulating smooth road surfaces.

Similar to the drum tyre testing rig, an adjustable hub allows the tractive and handling properties of the tyre to be investigated. According to MTS (2013), the speed rating of flat belt tyre testing rigs is generally very similar to that of drum tyre testing rigs.

Flat belt tyre testing rigs are used to test tyres under dynamic conditions. In order to account for vertical forces being applied to the tyre, the tyre load is supported by an air bearing or a water bearing. Air bearings are commonly used when passenger vehicle loads are applied to the tyre, while water bearings are implemented when higher loads are applied to the tyre during testing.

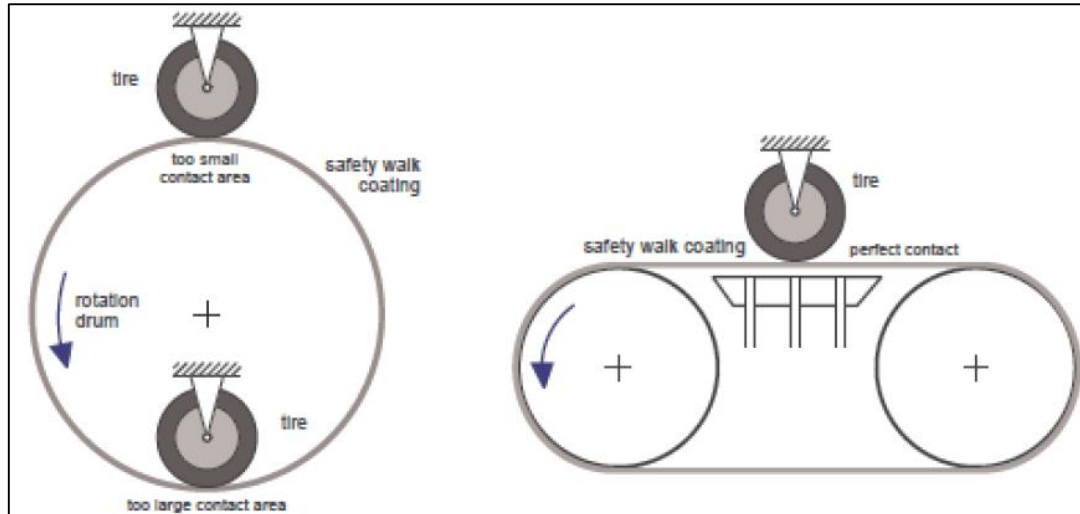


Figure 2-13: Left: Drum tyre testing equipment Right: Flat belt tyre testing equipment (Rill, 2006)

Indoor tyre testing rigs have the advantage that both static as well as dynamic tests may be conducted on the tyre being tested. Although the road surface may not be simulated as accurately as a real-life road surface, indoor tyre testing rigs boast the benefits of being weather-independent and have the ability to conduct easily repeatable tyre tests.

2.3.2 Outdoor tyre testing equipment

Outdoor tyre testing equipment usually comprises of a truck or a trailer being used to determine tyre characteristics. Unlike the indoor tyre testing equipment the outdoor tyre testing equipment is able to conduct testing procedures on actual road surfaces and under real-life conditions.

To determine tyre force and moment generation, a specialized hub is usually implemented to investigate the tractive and handling properties of the tyre being tested. The hub may be designed and implemented in such a way that the slip angle, the camber angle, the castor angle, the kingpin angle as well as a braking moment is adjustable. Load cells or strain gauges on the hub are generally used to measure forces and moments generated by the tyre during testing procedures. Figure 2-14 shows the TNO (2014) outdoor tyre testing truck which utilizes an adjustable hub to test various types of tyres.



Figure 2-14: Tyre testing rig with mounted motorcycle tower (TNO, 2014)

The outdoor tyre testing equipment used by the VDG of the University of Pretoria to conduct dynamic tyre tests for SUV tyres is shown in Figure 2-15. The outdoor tyre testing equipment consists of a main frame, a sub frame and the test tyres. The sub frame is attached to the mainframe with six load cells. These load cells are used to constrain the sub frame in all of its degrees of freedom and measure the forces and moments generated by the tyres during the testing procedure.

Adjustable hubs mounted to the outdoor tyre testing equipment allow the slip angle, the castor angle and the camber angle of the tyres to be varied to investigate handling properties of the tyre. Furthermore, a pneumatic and hydraulic braking system allows for a braking torque to be applied to the wheels to investigate tractive properties of the tyres.



Figure 2-15: Tyre testing rig during outdoor tyre testing procedure

Outdoor tyre testing equipment provides the benefit of obtaining tyre data on various road surfaces and under real-life weather conditions. The drawbacks of outdoor tyre testing equipment include tests not being easily repeatable and weather dependant.

2.4 Chapter summary

From the literature survey the following conclusions are drawn.

The handling and tractive properties of a tyre have been discussed and how these affect tyre performance.

Several existing tyre and contact models were discussed in detail. Many tyre models are available to predict tyre behaviour on smooth road surfaces. However, it was found that when encountering short length undulations and obstacles on road surfaces most of these tyre and contact models perform poorly in predicting tyre behaviour characteristics.

The physics-based FTire model was found to perform well on even and uneven road surface simulation events and manoeuvres. Therefore, the decision was made to parameterize an FTire model to predict static and dynamic tyre behaviour of an SUV all-terrain tyre on smooth and uneven road surfaces.

The FTire model is discussed in great detail. The key features, as well as the structural, tread and thermal model were discussed. It is decided that the tread and thermal model will not form part of the parameterization of the FTire model since these do not form part of this study.

Indoor and outdoor tyre testing equipment is discussed in detail and, based on available resources, it is decided upon to conduct dynamic tyre tests by utilizing outdoor tyre testing equipment.

2.5 Problem statement

The need for a tyre model that is able to accurately predict tyre behaviour of an all-terrain tyre on smooth and rough road surfaces exists, as discussed in the previous Sections. Therefore, this research project is aimed at parameterizing and validating an FTire model of an all-terrain tyre.

Based on the findings of this Chapter the research question for this paper may be defined as: Can an FTire model of an all-terrain tyre be used to predict handling and longitudinal tyre behaviour over smooth road surfaces and vertical tyre behaviour over uneven road surfaces?

2.6 Thesis outline

To answer the research question the procedure, as depicted in the following thesis outline, is followed.

Chapter 3 discusses the acquisition of parameterization and validation data. The parameterization data acquisition and testing methodology is discussed in detail. Static as well as dynamic parameterization tests are conducted to acquire parameterization data while the data acquisition of the dynamic validation tests conducted is discussed in detail.

Chapter 4 focuses on the parameterization process of the FTire model. Static and dynamic parameterization data, which was acquired in Chapter 3, is used to parameterize the FTire model. The correlation between the parameterization data and the parameterized FTire model is discussed in detail.

In Chapter 5 the FTire model validation is discussed. The MSC Adams (2013) model used to simulate the FTire model is discussed in detail. The simulation results are compared to the dynamic validation test results, obtained in Chapter 3. The dynamic response validation of the FTire model is discussed with validation metrics and procedures.

Chapter 6 summarizes the research project with a conclusion and recommendations for future research efforts.



3 Parameterization and validation data acquisition

The ability of a tyre model to predict tyre behaviour relies heavily on the underlying formulation of the model and whether this is detailed enough to predict the required behaviour. From the literature studied it was identified that FTire is the model that is most likely to be able to capture the required behaviour of the tyre due to its formulation. Sufficient experimental data is therefore required to parameterize the FTire model such that it is an accurate representation of the physical tyre.

The outcome of the validation process depends on the accuracy of the experimental data as well as on how accurately the physical system being implemented can be modelled.

3.1 Introduction

The FTire model is based on static and dynamic parameterization data and is characterized by a large number of parameters which are required to be optimized numerically in the tyre modelling process. The acquisition of parameterization data involves extensive testing and data capturing of tyre behaviour. Static parameterization data is obtained from laboratory testing while dynamic parameterization and validation test results are obtained by conducting tests with outdoor tyre testing equipment.

3.2 FTire model parameterization procedure

To construct an FTire model, Cosin's FTire/fit (2014) is implemented to process the parameterization data obtained in static and dynamic parameterization tests. FTire/fit (2014) is laid out in such a way that it guides the user through a step by step process to correctly parameterize the tyre model.

The FTire model parameterization process is initiated by extensively defining the physical tyre being modelled within FTire/fit (2014). After having defined the tyre a large amount of parameterization data is required to be imported into the model software. The required parameterization data consists of static and dynamic parameterization test results.

FTire/fit (2014) requires static vertical tyre stiffness and tyre footprint data which is implemented to establish basic tyre characteristics. Once this data have been successfully imported into FTire/fit, static cleat test parameterization data is considered. The static cleat test data gives information about the tread and sidewall stiffnesses of the tyre.

Static in-plane and out-of-plane tyre stiffness test data, which captures the lateral, longitudinal and torsional stiffnesses of the tyre, is imported into FTire/fit (2014) and serves to parameterize the handling and traction parameters of the FTire model.

Tyre modal analysis test results are required by FTire/fit (2014) to parameterize the vibrational response and damping parameters of the FTire model. Furthermore, dynamic cleat test data is imported to parameterize the damping characteristics of the FTire model.

The acquisition of parameterization test data forms a vital part in the parameterization process of the FTire model. The methods and experimental setups and procedures used to obtain the static and dynamic parameterization data for the FTire model are discussed in detail in the following sections while the parameterization process of the FTire model is discussed in more detail in Chapter 4.

3.3 Tyres

The tyre being analysed is a Michelin LTX LT235/85R16 AT² all-terrain tyre. The tyre itself, as well as its tread pattern is shown in Figure 3-1.



Figure 3-1: Michelin LTX LT235/85R16 AT² all-terrain tyre (Michelin, 2013) and tyre tread pattern

According to Michelin (2013), the tyre is a non-directional, tubeless tyre designed with a durable tread compound which increases tread life, as well as off-road performance. The tyre's construction and design allows for both on-road and off-road use. Three circumferential grooves on the tread increase water displacement and thereby minimize the risk of hydroplaning when travelling on smooth, wet road surfaces.

The tyre carcass is designed with a spiral nylon wrap which increases high-speed endurance. The weight of the tyre itself is measured to be 21kg and the weight of the tyre including the rim and wheel force transducer (WFT) (Becker et al., 2012) is found to be 55 kg.

The tyre tread stiffness is determined experimentally by means of a ShoreA hardness tester. The tread stiffness is measured on numerous tread elements across the tyre itself and is found to have an average ShoreA value of 70.

3.4 Static parameterization tests

The tyre being tested is mounted on a fixed stationary pedestal in such a way that the centreline of the tyre coincides with the centreline of a 16kN hydraulic actuator used to apply a vertical load on the tyre, as seen in Figure 3-2.

All static parameterization tests are conducted with the same tyre throughout the testing procedures to ensure consistency of experimental results. Furthermore, the static parameterization tests are conducted at inflation pressures of 1 bar and 2 bar and three different camber angles, namely 0°, 3°, and 5°.

Wheel force transducers (WFT) (Becker et al., 2012) are implemented to measure and verify the forces and moments generated by testing tyres during static and dynamic tests.

Each WFT consists of six load cells which connect two cylindrical subassemblies. The first subassembly is connected to a wheel hub while the other is connected to the wheel itself. A modified rim allows for the WFT to be implemented, as stated by Becker et al. (2012).

During tyre tests the WFT measures the forces and moments generated by the tyre in tangential and radial directions. During dynamic tests, while the wheel is rotating, it is necessary to measure the angular position of the wheel at any given point in time. Two single turn potentiometers are implemented to effectively measure the rotational displacement of the wheel. By measuring the angular position of the WFT by means of the single turn potentiometers, the measured forces and moments data is transformed into the standard global coordinate system, as defined by the SAE (2014).

The data captured by the six load cells and the two single turn potentiometers within the WFTs are transmitted wirelessly by a KMT CT8-Rotate 8 channel telemetry system.

3.4.1 Footprints and vertical tyre stiffness

FTire requires images of the size and shape of the contact patch area, also termed the footprint, of the tyre at certain vertical loads, camber angles and tyre pressures. With the aim of visually capturing the footprint, a rig is constructed which allows for a camera system to capture the contact patch through a pane of bullet proof glass.

A hydraulic actuator is used in displacement control to deflect the tyre in its vertical direction in a sinusoidal manner. A load cell is mounted in-line with the hydraulic actuator to measure the vertical load exerted on the tyre. Great care is taken to ensure that the testing rig is concentric with the hydraulic actuator and that the bullet proof glass plate is perpendicular to the tyre contact patch. The experimental setup is shown in Figure 3-2.

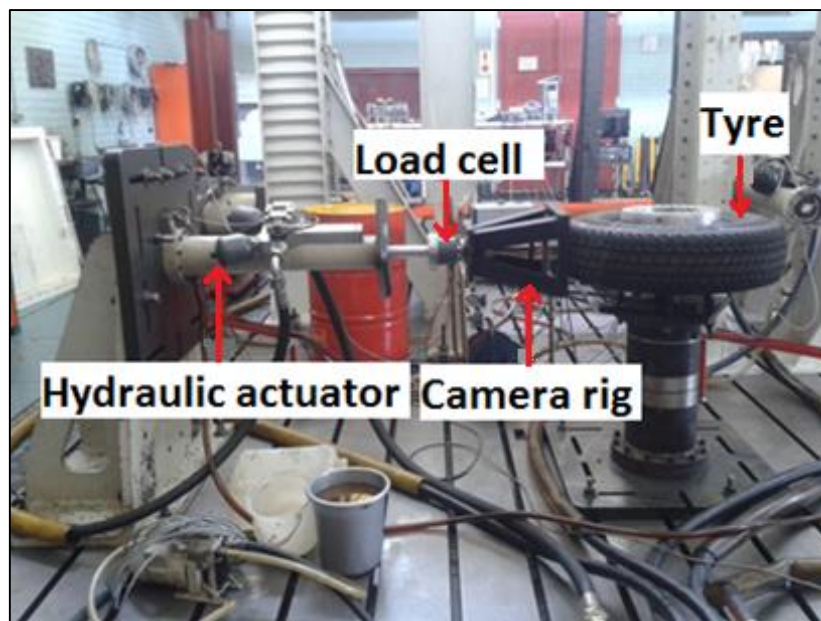


Figure 3-2: Flat plate experimental setup

The vertical displacement, exerted by the hydraulic actuator, is applied for varying amplitudes in a sinusoidal manner and at a very low speed. The hysteresis effect of the tyre, as an effect of loading and unloading the tyre, is depicted in Figure 3-3.

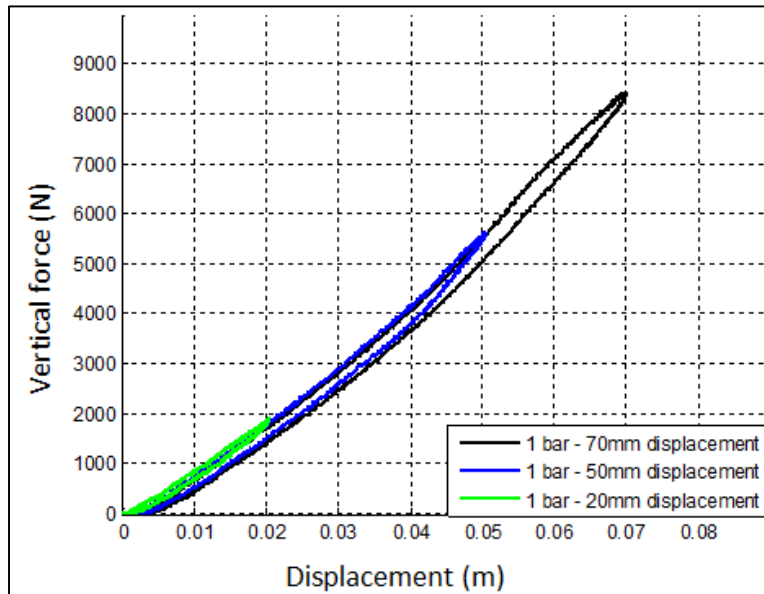


Figure 3-3: Experimental results for flat plate static test at 0 degrees camber and 1 bar inflation pressure

The displacement of the test rig during the testing procedure is measured by both the hydraulic actuator control unit as well as an Acuity (2014) AR700-8 displacement measuring laser. To verify the experimental results obtained by the load cells, a WFT (Becker et al., 2012) is implemented to validate the forces acting on the tyre. The experimental setup is depicted in Figure 3-4.

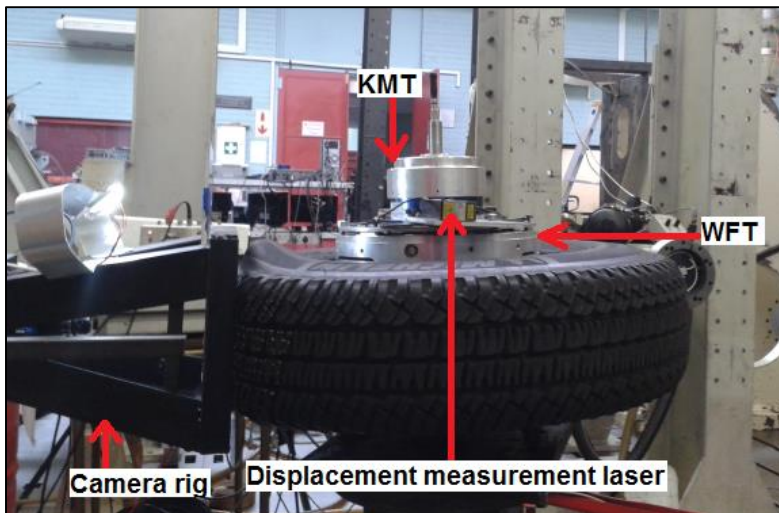


Figure 3-4: Footprint experimental setup at a camber angle of 5 degrees

Several methods to capture the tyre footprint with cameras are attempted. However, it proves to be challenging to establish the actual size and shape of the footprint. The decision is made to implement a stereovision camera system to identify the size and the shape of the tyre footprint on the glass pane accurately. Stereovision, as discussed by Guthrie (2014), is an effective manner in which a three dimensional object or profile can be captured and analysed.

The stereo vision footage is processed to generate a three dimensional image of the tyre’s footprint pressing against the bullet proof glass. By varying the vertical load experienced by the tyre in a sinusoidal manner a large number of footprint images are obtained from a single experimental test.

The cameras are controlled by means of a trigger signal generated from the hydraulic actuator displacement controller. The trigger signal is recorded to enable alignment and synchronization of measured data and captured images. It is thus possible to determine the vertical load of the tyre at a given frame of the footprint.

To make the footprint images useable for FTire, information regarding the size and shape of the footprint is required. Cosin (2014) specifies that a red line with predefined length should be added to the image to allow FTire/fit to scale the footprint image accurately. Therefore, a red line with a predefined length of 100mm relative to the tyre contact patch size is added to the footprint images.

A footprint, as depicted by the stereovision camera system, is shown in Figure 3-5. The red line allows FTire to determine the actual size and shape of the footprint. According to Cosin (2014), the red line of specified length should not coincide or interfere with the tyre footprint in the bitmap image.

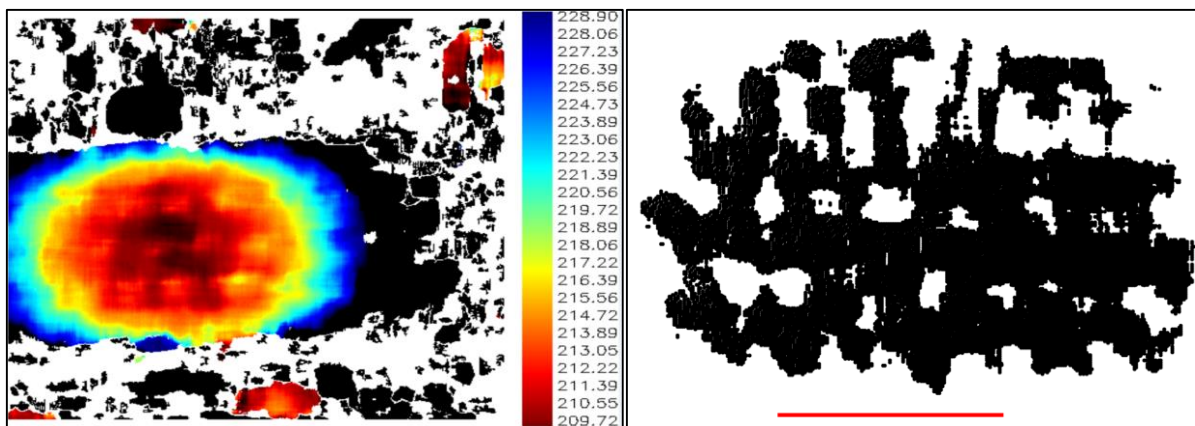


Figure 3-5: Left: Footprint captured by the stereo-vision camera system. Right: Footprint bitmap image

3.4.2 Static cleat tests

The vertical tyre stiffness on static longitudinal, transversal as well as oblique (at 45 degrees) cleats are obtained by static cleat tests. A testing rig is constructed to hold both a 25x25mm and a 32x32mm cleat on a flat steel plate. The rig holding the cleats is a flat steel plate with the cleats positioned in such a way that these are in the centre of the contact patch area of the tyre. The steel plate, to which the cleats are attached, is mounted to the hydraulic actuator and is pressed against the tyre, as depicted in Figure 3-6. The rig is designed in such a way that it can be rotated to allow the cleat to be positioned in the longitudinal, transversal, as well as in the oblique (45 degree angle) position, relative to the tyre.

The WFT (Becker et al., 2012) and the Acuity (2014) AR700-8 displacement measurement laser are used to verify the measured vertical forces and displacements relative to the tyre during the experimental procedure.

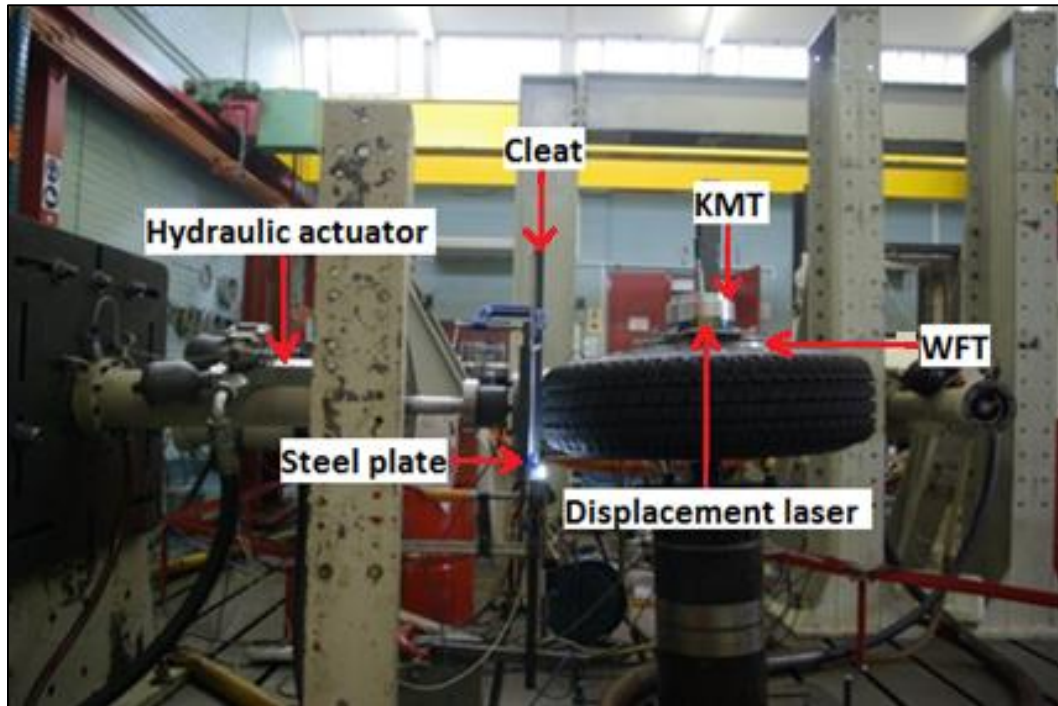


Figure 3-6: Static cleat test experimental setup for 2 bar inflation bar at 3° camber angle

It is vital that the rig is displaced far enough so that the tyre's tread envelopes the cleat to measure the change in the tyre's vertical stiffness as the tread deforms. Figure 3-7 shows how the tyre tread envelopes the static transversal cleat.

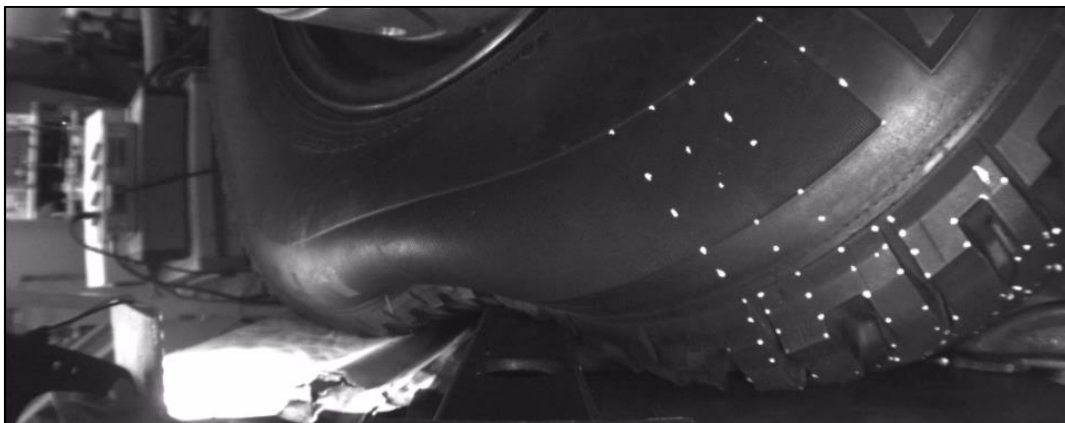


Figure 3-7: Static 25x25mm oblique cleat test at 1 bar inflation pressure

Figure 3-8 shows the static parameterization test results for a 25x25mm cleat. A distinct increase in vertical tyre stiffness is observed as the tyre tread envelopes the cleat. The effect of the transversal and oblique cleats on the vertical stiffness of the tyre is much larger than that of the longitudinal cleat. The longitudinal cleat does not cause a significant change in vertical tyre stiffness as the tread envelopes the cleat. However, the effect of hysteresis is much more prominent in the longitudinal static cleat test than the oblique and transversal static cleat tests. This may be attributed to the fact that the construction of the tyre limits the tread to envelope an obstacle (such as a cleat) in the longitudinal direction due to the construction of the radial tyre.

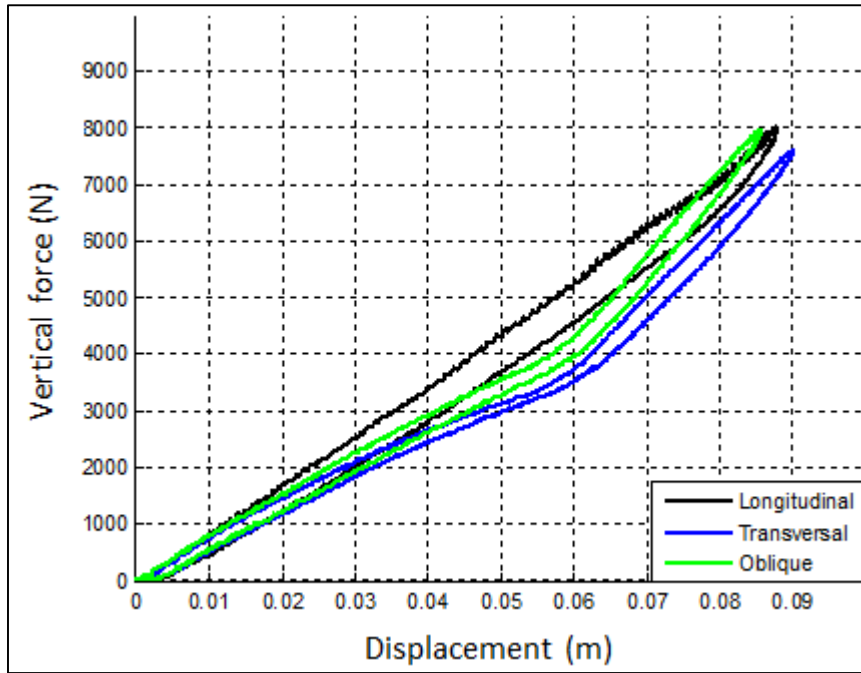


Figure 3-8: 25x25mm static cleat test experimental results at 0 degrees camber and 1 bar inflation pressure

3.4.3 Static in-plane and out-of-plane tyre stiffness tests

The lateral, longitudinal and torsional stiffnesses of the tyre are determined experimentally by inducing the tyre to slip in the lateral, longitudinal and torsional directions, respectively. The longitudinal tyre slip forms the in-plane measurements while the lateral and torsional slip are considered as out-of-plane measurements. Tyre slip is induced by applying a constant vertical load of 8000N to the static tyre with a steel plate mounted to a hydraulic actuator and then translating the plate in the respective planar direction by means of a linear rail/guide system.

The displacement of the steel plate is measured in the vertical direction as well as in the longitudinal and lateral directions, relative to the tyre, by making use of two Acuity (2014) AR700-8 displacement measurement lasers. A load cell is placed in-line with the hydraulic actuator to measure the vertical load on the tyre. A second load cell is mounted in between the steel plate and a block and tackle system to the longitudinal or lateral forces being exerted on the tyre as the steel plate is being translated along the linear guides in the longitudinal or lateral directions relative to the tyre, respectively.

The WFT (Becker et al., 2012) is implemented to verify the forces measured by the two load cells. The experimental setup is shown in Figure 3-9. It should be noted that the tests were conducted with the tyre placed directly against the steel plate with no abrasive surface coating on the steel plate itself.

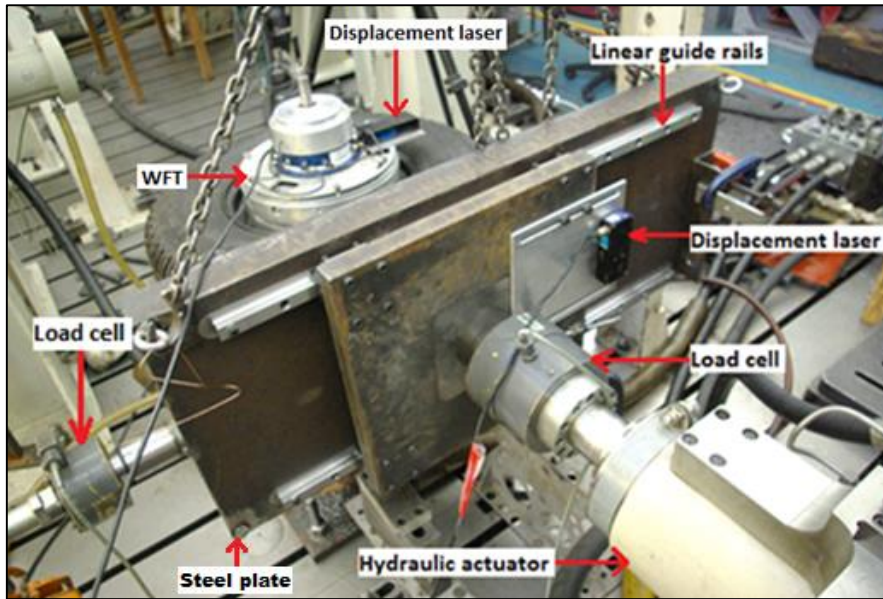


Figure 3-9: In-plane experimental setup in the longitudinal direction

The steel plate is translated horizontally or longitudinally, relative to the tyre, by means of a three ton block and tackle system. The block and tackle system is operated manually and it is imperative that the hauling chain is pulled at a constant speed such that the tyre deflects and, ultimately, slips at a constant rate. Therefore, great effort is undertaken to ensure that the steel plate is translated at a constant rate.

It should be noted that Figure 3-9 depicts the experimental setup for the in-plane longitudinal tyre stiffness tests. To execute the out-of-plane lateral tyre stiffness tests the steel plate mounted to the hydraulic actuator should be rotated by 90 degrees such that the linear guide/rail system is able to translate the steel plate in the lateral direction, relative to the tyre.

Longitudinal and lateral tyre stiffness data results, which are shown in Figures 3-10 and 3-11, respectively, show that the tyre has a constant in-plane stiffness as the tyre deflects. The longitudinal and lateral stiffnesses saturate at the point where the tyre starts slipping.

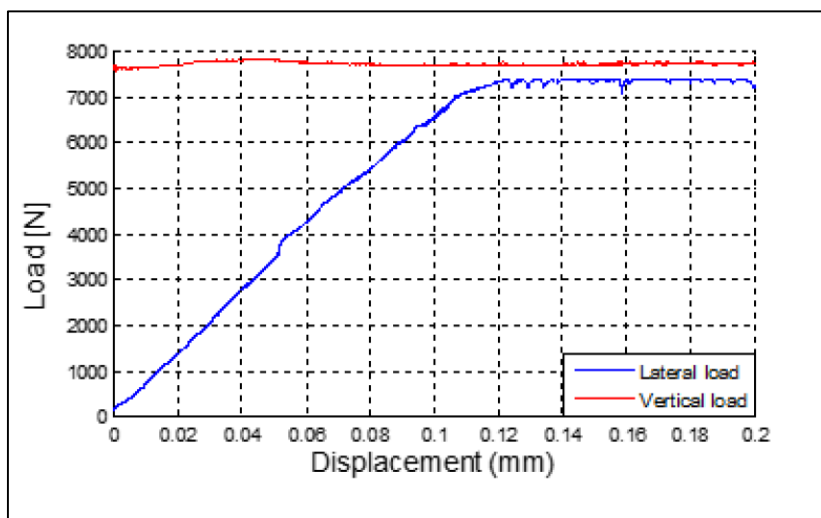


Figure 3-10: In-plane lateral force experimental results at 7000N vertical load and 2 bar inflation pressure

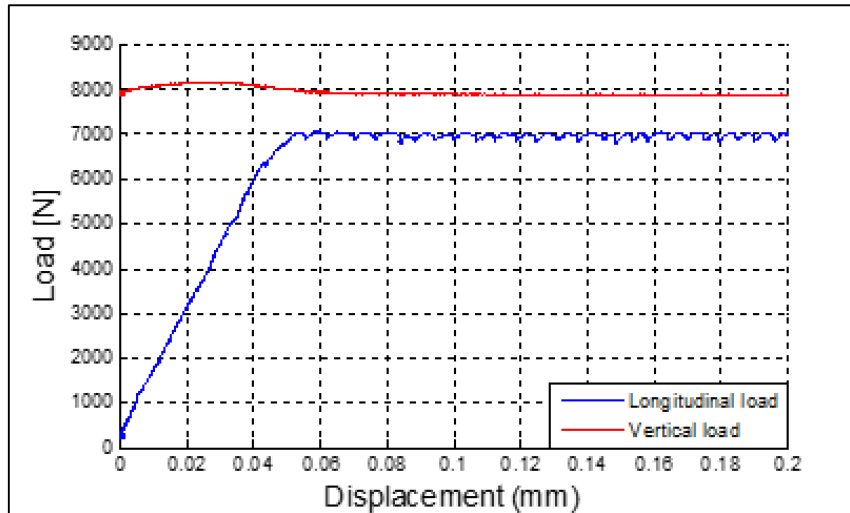


Figure 3-11: In-plane longitudinal force experimental results at 8000N vertical load and 2 bar inflation pressure

When considering the torsional stiffness of the tyre pure rotation of the steel plate is vital. Therefore, to prevent translation of the steel plate along its linear guides, its translational degree of freedom is restrained by fixing the steel plate to the hydraulic actuator. This provides a purely rotational degree of freedom of the steel plate around the hydraulic actuator’s centreline.

The two Acuity (2014) AR700-8 displacement lasers are mounted on the top and bottom of the steel plate from which each laser measures the distance to an adjacent vertical post which is fixed to the ground. This configuration allows the angle of the steel plate to be determined at any given point of the rotation of the steel plate by means of a trigonometric analysis, as shown schematically in Figure 3-12.

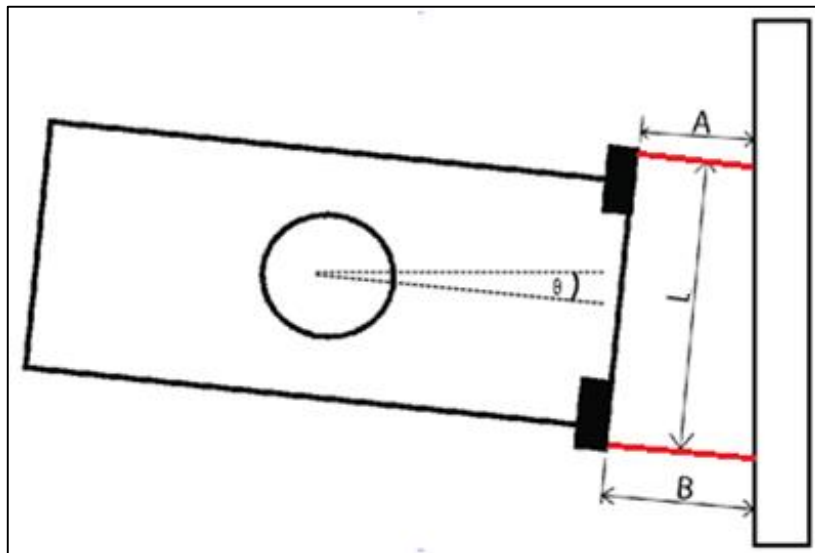


Figure 3-12: Schematic representation of determining the angular position of the steel plate

A trapezium method approach is used to determine the angular position of the steel plate as shown below.

$$\theta = \sin \frac{B-A}{l} \tag{1}$$

The rotation of the steel plate is induced by suspending the block and tackle from an overhead crane hook and attaching the other end to the top right-hand corner of the steel plate. The steel plate is then rotated about the centreline of the hydraulic actuator by operating the hauling chain of the block and tackle system.

Figure 3-13 shows the results of the in-plane torsional stiffness experimental investigation. Similar to the lateral and longitudinal tyre stiffness analysis, the torsional tyre stiffness is seen to gradually increase as the angular displacement increases. The torsional tyre stiffness saturates after which it starts to decrease as the tyre begins to slip.

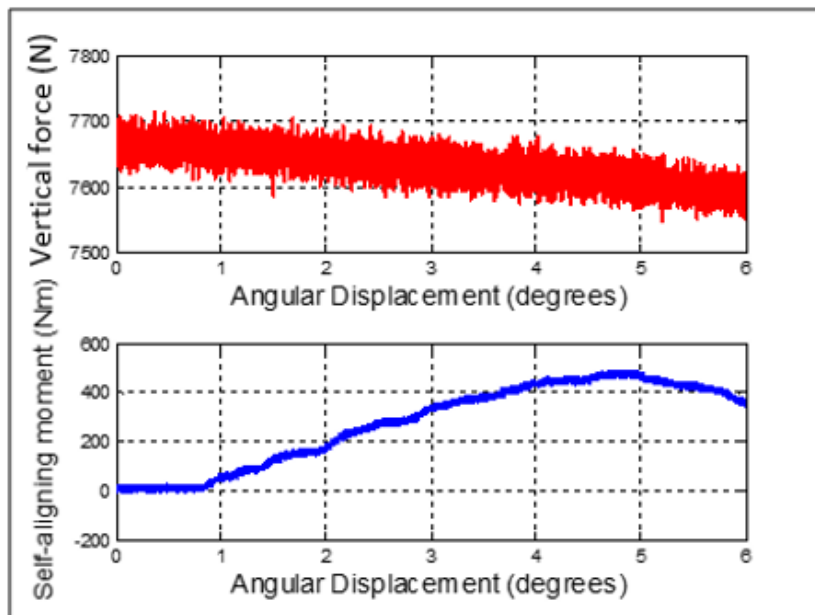


Figure 3-13: In-plane torsional moment experimental results at 7680N vertical load

3.4.4 Modal analysis

The first six vibrational tyre modes are determined by means of a modal analysis. The first six modal shapes of an unloaded tyre are shown in Figure 3-14.

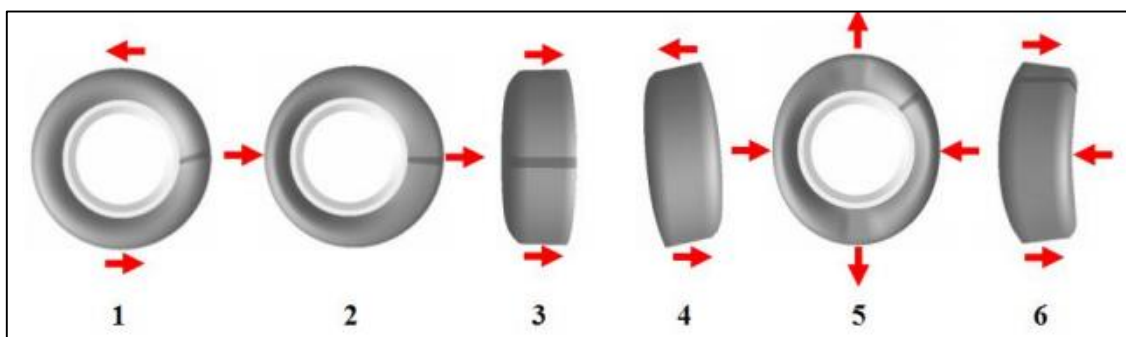


Figure 3-14: First six vibrational modes of an unloaded tyre with a fixed rim (Gipser, 2013)

The tyre being tested is mounted horizontally on the pedestal used in previous static parameterization tests. The tyre is then excited by an impulse from a hydraulic actuator. The impulse excites a large range of frequencies and the corresponding mode shapes of the tyre.

A load cell is mounted in-line with the hydraulic actuator to measure the magnitude of the impulse. A Polytec PSV – 400 (Polytec, 2014) scanning laser vibrometer is utilised to capture the vibrational response of the tyre. Reflective tape was placed onto the tread and sidewall of the tyre as reference points which the Polytec PSV – 400 (Polytec, 2014) follows consecutively during the modal analysis testing procedure.

The Polytec PSV – 400 (Polytec, 2014) scanning laser vibrometer is placed directly above the tyre to measure the vibrational response of each piece of reflective tape on the sidewall of the tyre (see Figure 3-15). This allows the Polytec PSV – 400 (Polytec, 2014) scanning laser vibrometer to capture vibrational modes 3, 4 and 6 as depicted in Figure 3-14.



Figure 3-15: Left: Experimental setup of the modal analysis from the top. **Right:** Tyre, as captured by the Polytec PSV – 400 (Polytec, 2014) scanning laser vibrometer from the top

To capture vibrational modes 2 and 5 the Polytec PSV – 400 (Polytec, 2014) scanning laser vibrometer is placed in front of the tyre to capture the vibrational response of each piece of reflective tape on the tread of the tyre, as depicted in Figure 3-16.

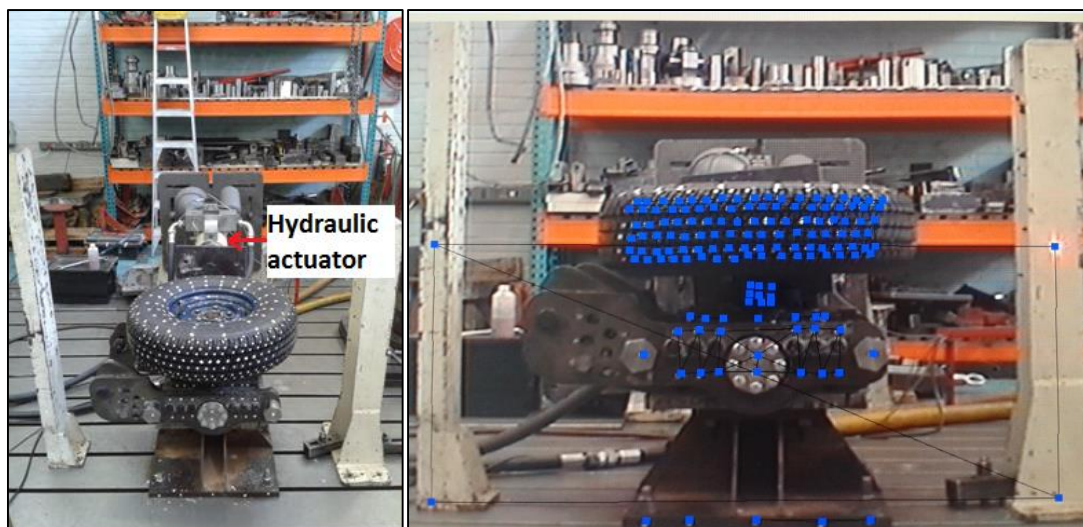


Figure 3-16: Left: Experimental setup of the modal analysis from the front. **Right:** Tyre, as captured by the Polytec PSV – 400 (Polytec, 2014) scanning laser vibrometer from the front

By making use of a PSV Software package, which generates an FRF of the measured vibrational response of the tyre, the frequencies at which the respective vibrational mode shapes occur are identified. The FRF displays an operational deflection shape of all measured points (reflective tape strips) which were analysed during the testing procedure from which the respective frequencies and corresponding mode shapes are identified.

The first mode shape, as shown in Figure 3-14, represents the in-plane rigid-body rotation natural frequency response. To determine at which frequency this mode shape occurs the tyre is excited torsionally by means of a moment-arm connected to the WFT (Becker et al., 2012). The wheel hub is allowed to rotate freely while the moment arm is excited with an increasing sinusoidal displacement sweep (0 – 40Hz) facilitated by a 16kN hydraulic actuator. The experimental setup is shown in Figure 3-17.

The torsional natural frequency is determined from the moment about the wheel's spin axis. The angular tyre displacement is measured by the WFT (Becker et al., 2012) single turn potentiometers, which are able to accurately measure 0.5 degrees of rotational displacement.

A frequency response function (FRF) is constructed based on the angular displacement measurements captured by the WFT (Becker et al., 2012) single turn potentiometers and the frequency at which the in-plane rigid-body rotation mode occurs is estimated based on the resulting FRF. The modal analysis results are depicted in Table 3-1.

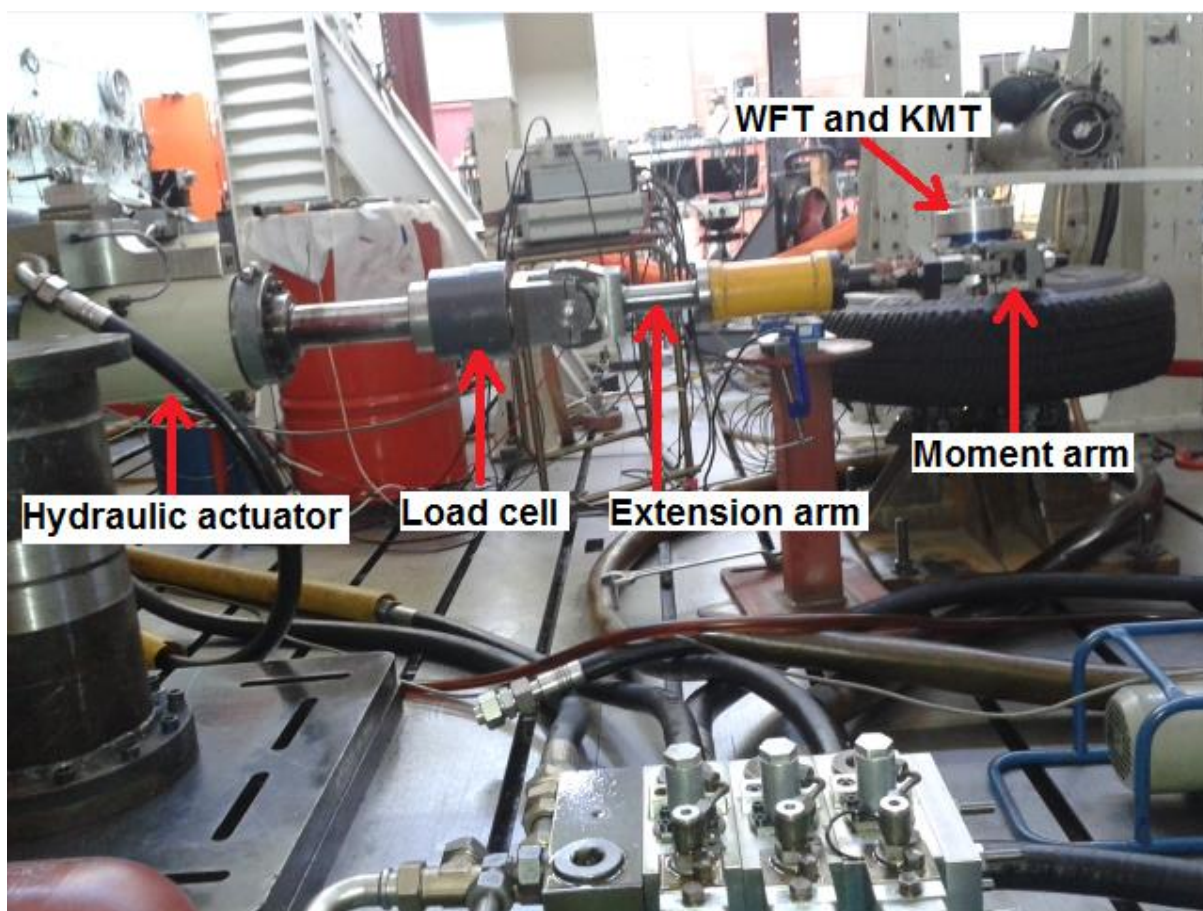


Figure 3-17: Torsional modal analysis experimental setup

Table 3-1: Modal analysis results

Mode shape	1 bar inflation pressure		2 bar inflation pressure	
	Frequency (Hz)	Damping (%)	Frequency (Hz)	Damping (%)
1	26.1	-	28.4	-
2	24.2	4.21	26.1	3.87
3	32.5	3.17	37.9	3.53
4	46.9	2.48	49.9	2.10
5	52.6	0.92	55.9	0.04
6	64.4	0.43	68.2	0.12

3.5 Dynamic parameterization and validation tests

An outdoor tyre testing rig is used to conduct dynamic parameterization and validation tests and is shown in Figure 3-18. The outdoor tyre testing comprises of a main frame and a sub frame connected by six load cells. The six load cells measure the forces and moments acting on the tyres in the lateral, longitudinal and vertical direction during testing procedures. The outdoor tyre testing equipment is depicted schematically in Figure 3-18 where the load cells, as well as their corresponding measurement directions are indicated.

Due to the fact that the outdoor tyre testing equipment does not make use of a suspension system all forces and moments measured by the load cells are attributed to the forces generated by the tyres. The WFT (Becker et al., 2012) and KMT system is implemented to verify the forces and moments measured by the load cells. The forces and moments measured by the WFT (Becker et al., 2012) prove to give smoother and more reliable results over the dynamic testing procedures and the decision is made to use the WFT (Becker et al., 2012) force and moment measurement results for the dynamic testing validation.

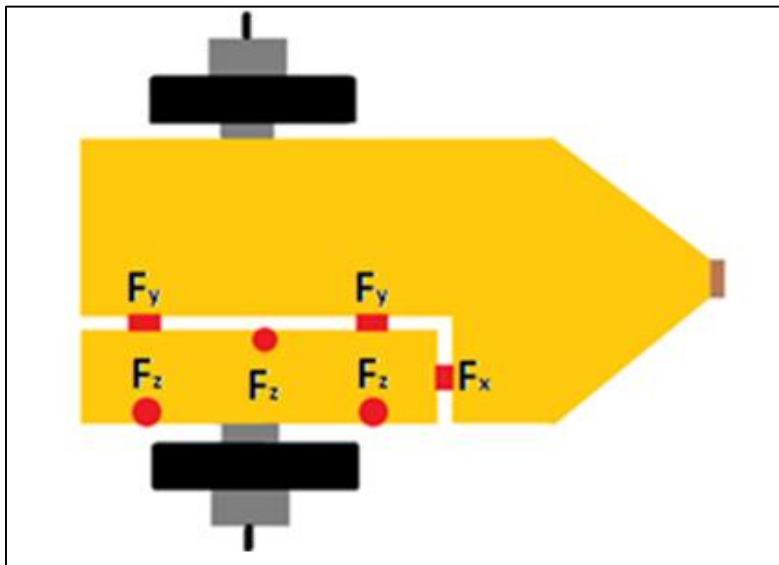


Figure 3-18: Outdoor tyre testing equipment load cell orientation

Previous dynamic tests revealed that the outdoor tyre testing equipment has a tendency to pull skew and bounce while being translated along a test track under testing conditions. Therefore, a damping system is employed which consists of two dampers and two cables, one on each side, which are located between the tyre testing rig and the towing vehicle. The stabilization system, as implemented in the dynamic tests, is shown in Figure 3-19.



Figure 3-19: Outdoor tyre testing equipment stabilisation system

It is found that the stabilisation system reduced the effect of the outdoor tyre testing equipment from pulling skew but bouncing was observed to persist during testing procedures. The bouncing or hopping motion of the tyre testing equipment is observed during all dynamic tests but is most noticeable during handling validation tests.

During the dynamic testing procedure a towing vehicle is used to translate the outdoor tyre testing equipment longitudinally over a testing track. The velocity at which the tyre testing equipment is being translated is measured by making use of a Racelogic (2014) VBOX, which is a GPS data logging device.

The outdoor tyre testing equipment is equipped with adjustable hubs which are designed to vary the slip angle, camber angle as well as the castor angle of the tyre. The camber angle adjustment ranges from -5 to +5 degrees, in 1 degree increments, while the castor angle adjustment ranges from 0 to 10 degrees, in 1 degree increments. Both the camber and castor angles are varied manually while the slip angle can be swept from -2 to 15 degrees during a testing procedure by means of linear actuators. Linear variable displacement transducers (LVDT) are implemented to measure the angle between the tyre and the tyre testing equipment during testing procedures.

During the handling validation tests the slip angle is measured by means of a Correvit (2014) which is a non-contact optical slip sensor. It is found that the Correvit (2014) has difficulties to accurately measure the absolute slip angle of the testing tyre at low speeds when implemented on the tyre testing rig. This may be due to the fact that the tyre testing rig has no suspension and is, therefore, exposed to the bouncing which the outdoor tyre testing equipment experienced during testing procedures.



A Land Rover Defender 110 rear differential has been fitted to the tyre testing rig. A braking torque is applied to each of the wheels by applying a brake pressure on the input shaft of the differential by means of brake callipers. Two brake disks are mounted to the differential input shaft and, correspondingly, two brake callipers apply a brake pressure on the shaft.

Due to the dynamics of the open differential both wheels are able to turn individually at different speeds and directions for manoeuvrability of the testing rig. The brake callipers are actuated by a single hydraulic master cylinder which supplies an equal brake pressure to each of the two brake callipers.

A Festo DNC-50-25-PPV-A linear pneumatic actuator is implemented to actuate the hydraulic brake system master cylinder. The pneumatic linear actuator is controlled by means of an electronic pressure regulator valve. A hydraulic pressure transducer is utilized to measure the hydraulic pressure in the brake line.

Point Grey Flea 3 stereo vision cameras are implemented to measure wheel slip. The cameras are mounted to the outdoor tyre testing equipment and face the inside of the tyre. The cameras are positioned in such a way that they are able to observe the road surface as well as the sidewall of the tyre. Therefore, the stereo vision system is able to determine the longitudinal slip based on the wheel speed as well as the longitudinal velocity of the tyre testing equipment relative to the ground speed.

The outdoor tyre testing equipment is designed to test commercial vehicle tyres with a vertical load of up to 2 metric tons per wheel. The vertical load exerted on the tyres can be varied by adding or removing steel plates on top of the tyre testing rig or removing these in order to increase or decrease the vertical load on each tyre, respectively.

For the dynamic parameterization tests and the vertical validation tests only one load case is considered. The load case being considered (LC0) consists of the weight of the outdoor tyre testing rig only, as indicated in Table 3-2. During the dynamic parameterization tests and the vertical validation tests the detachable braking system is removed. Furthermore, the tests were conducted at a tyre inflation pressure of 2 bar.

For the dynamic validation tests three vertical load cases are considered. For the first vertical load case (LC0) no additional load is added to the tyre testing rig. Thus, only the outdoor tyre testing equipment's own weight accounts for the vertical load. For the second load case (LC1) a steel plate with a mass of approximately 200kg is placed on the tyre testing rig. The third load case (LC3) consists of three 200kg steel plates placed on the tyre testing rig. The three vertical load cases are summarized in Table 3-2 and are chosen in a way to obtain a sufficient vertical load data spectrum while not exceeding the maximum static load of 8000N of the tyre.

The handling validation tests are conducted with load cases LC1 and LC3 while the traction validation tests are conducted with load cases LC0, LC1 and LC3. Both the dynamic handling and dynamic traction validation tests are conducted with the braking system attached to the tyre testing rig and at an inflation pressure of 2 bar.

Table 3-2: Three load cases considered during validation field tests (As measured by the WFT)

Load case	Vertical load (N) per tyre (with pneumatic braking system)	Vertical load (N) per tyre (without pneumatic braking system)
LC0	4387	3582
LC1	5143	N/A
LC3	6954	N/A

3.5.1 Vertical field tests

Dynamic parameterization and validation tests are conducted to acquire experimental data by towing the outdoor tyre testing equipment over obstacles using a Land Rover Defender 110 Tdi. It is vital that the towing vehicle does not negotiate any of the obstacles utilized in the testing procedures. Therefore, the tyre testing rig is hitched to the Land Rover in an offset position as shown in Figure 3-20.



Figure 3-20: Tyre testing rig offset position

Dynamic vertical field tests are conducted on the suspension track of the Gerotek Test Facilities (2013). The tracks on which tests are conducted include the Belgian paving and the Fatigue track. Dynamic cleat tests are performed on a smooth road surface and form part of dynamic parameterization and validation tests.

The outdoor tyre testing equipment is translated over each of the tracks at a constant longitudinal velocity. The dynamic parameterization and validation tests are conducted at two different speeds. The driver of the Land Rover Defender selects the first gear for the lower speed (3.5 m/s) and the second gear for the higher speed (6 m/s) while the vehicle is let to drive on idling speed.

3.5.1.1 Dynamic parameterization tests

Dynamic cleat tests over 25x25mm, 32x32mm and 50x50mm cleats are conducted. Figure 3-21 shows the outdoor tyre testing equipment negotiating a 50x50mm cleat during a dynamic parameterization test run.



Figure 3-21: Dynamic cleat test (LC0)

Figure 3-22 shows two 50x50mm dynamic cleat tests that are conducted. Other vertical parameterization tests show similar results. It is, therefore, concluded that the dynamic parameterization testing results are consistent and are repeatable.

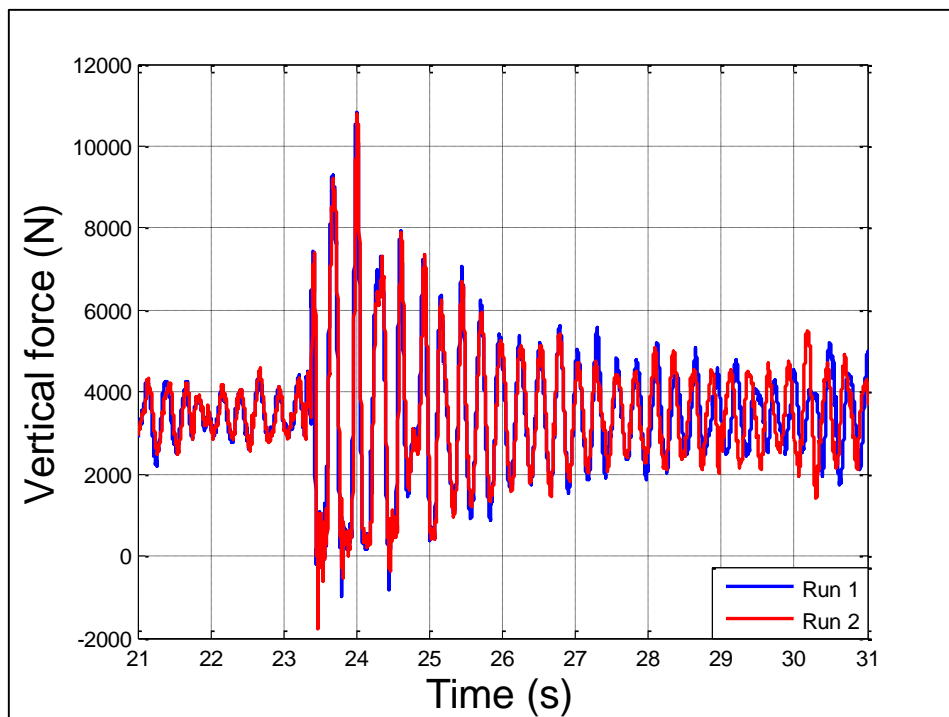


Figure 3-22: 50x50mm dynamic cleat test result

3.5.1.2 Validation tests

The outdoor tyre testing equipment is towed by the Land Rover in the offset position over the Belgian paving and the Fatigue track. The right-hand side tyre, which is attached to the sub frame, negotiates the test track while the left-hand side tyre and the towing vehicle's tyres do not negotiate the test track at all and roll on the smooth concrete road surface, as shown in Figure 3-23. The dynamic cleat tests discussed in Section 3.5.1.1 also form part of the dynamic vertical validation tests.



Figure 3-23: Dynamic validation test conducted on the Belgian paving

3.5.2 Handling validation tests

Dynamic handling validation tests are conducted on the oval (high speed) track at the Gerotek Test Facilities (2013). A SAMIL military truck is used to tow the tyre testing rig at a constant longitudinal velocity while the tests are conducted. It is observed that the outdoor tyre testing equipment has a considerable bouncing motion while conducting the handling validation tests which influences the resulting data acquired during the tests.

During the handling validation testing procedure the effect of varying the slip angle as well as the camber angle of the tyres is investigated. As the tyre testing rig is translated longitudinally, the slip angle is varied between -1 and 9 degrees in 1 degree increments. The camber angle is changed manually in between individual tests and thus stays constant during each of the dynamic handling validation tests. Camber angles vary from -2 to 2 degrees in 2 degree increments for the handling validation tests. Figure 3-24 shows a handling validation test being conducted at a large slip angle and at 2 degrees camber angle.



Figure 3-24: Handling validation test (LC3) at 2 bar inflation pressure



Figure 3-25 shows testing results obtained from dynamic handling validation tests which are conducted as described above. Other dynamic handling validation tests show similar results and it is thus concluded that the testing results are consistent and repeatable.

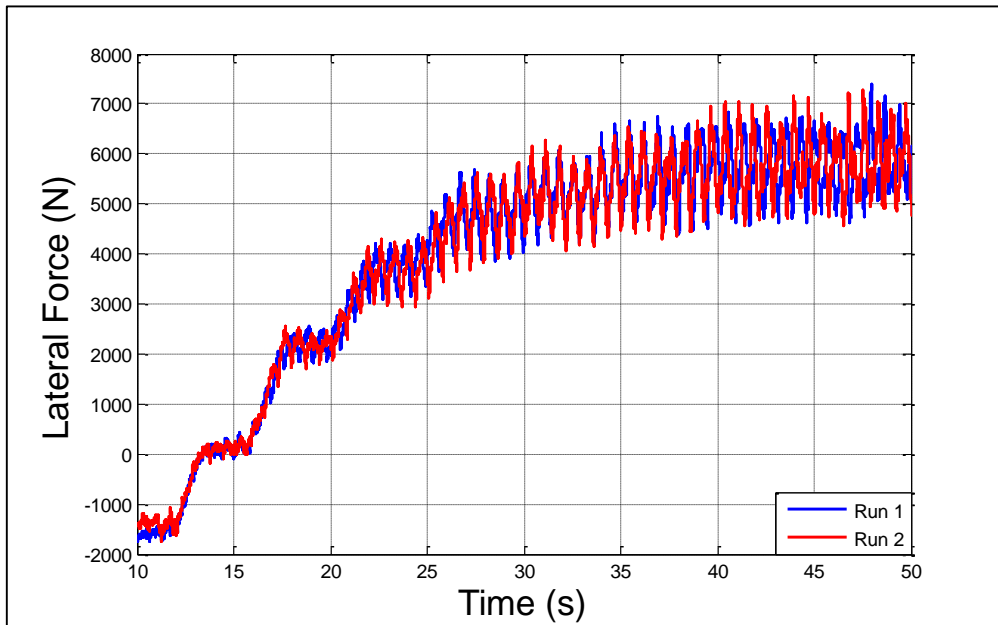


Figure 3-25: Handling validation test results (LC3) at 0° camber angle

Figure 3-26 shows the slip angle, as measured by the LVDT, during a handling validation test while Figure 3-27 gives the corresponding lateral force generated by the tyres as a result of the varying slip angle and Figure 3-28 gives the resulting lateral force vs. slip angle relationship.

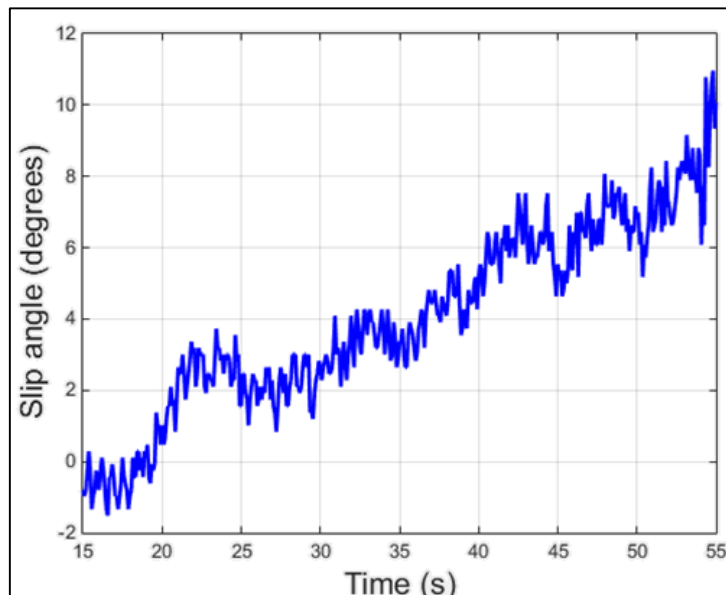


Figure 3-26: Varying slip angle during a handling validation test (LC1) at 0° camber

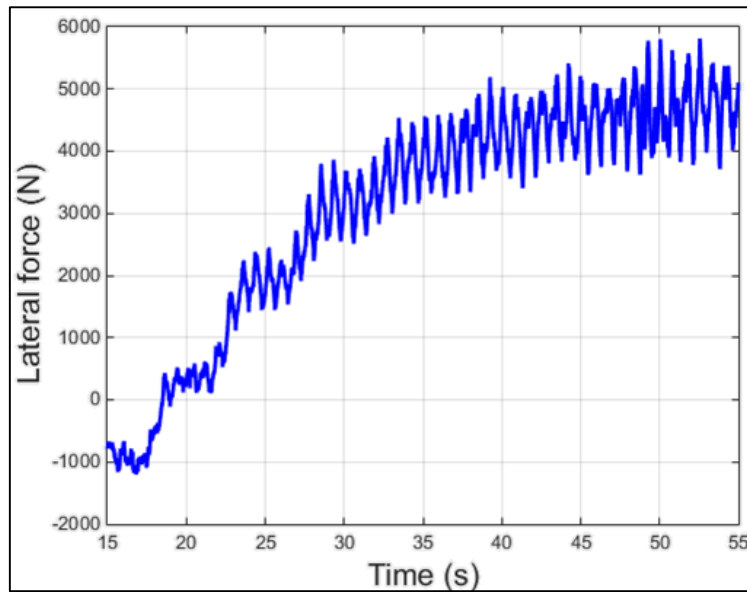


Figure 3-27: Varying lateral force during a handling validation test (LC1) at 0° camber

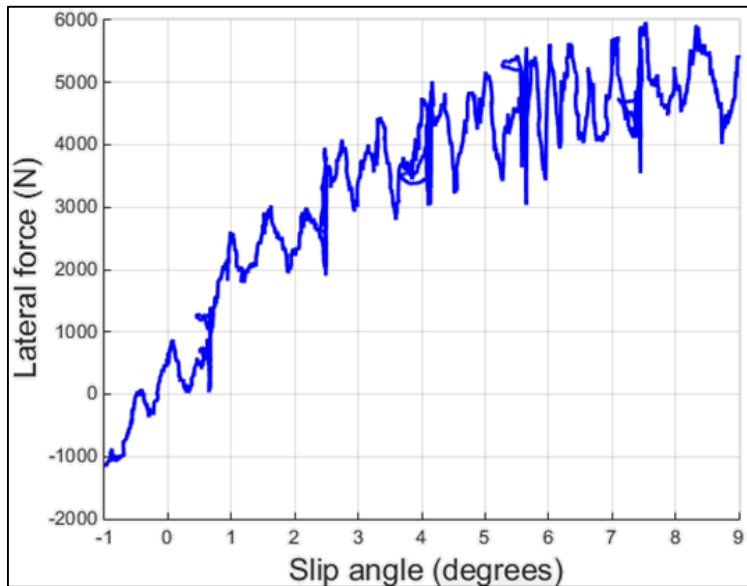


Figure 3-28: Lateral force vs. slip angle relationship during handling validation test (LC1) at 0° camber

3.5.3 Traction validation tests

Dynamic traction validation tests are conducted on the oval (high speed) track at the Gerotek Test Facilities (2013). The outdoor tyre testing equipment is hitched to the tow bar of the SAMIL military truck which translates the tyre testing rig at a constant velocity.

The braking system is controlled by a linear pneumatic actuator. By measuring the brake pressure in the brake line with a hydraulic pressure transducer, the brakes are actuated in such a way that the brake pressure is increased constantly from zero until the wheels of the tyre testing rig are locked, thus inducing longitudinal slip between 0% and 100%.

Figure 3-29 shows a traction validation test being conducted at the instant where 100% slip is attained as seen by the skid marks behind the tyre.



Figure 3-29: Traction validation test (LC1) at 2 bar inflation pressure

Figure 3-30 shows testing results obtained from dynamic traction validation test which are conducted as described above. Other dynamic traction validation tests show similar results and it is thus concluded that the testing results are consistent and repeatable.

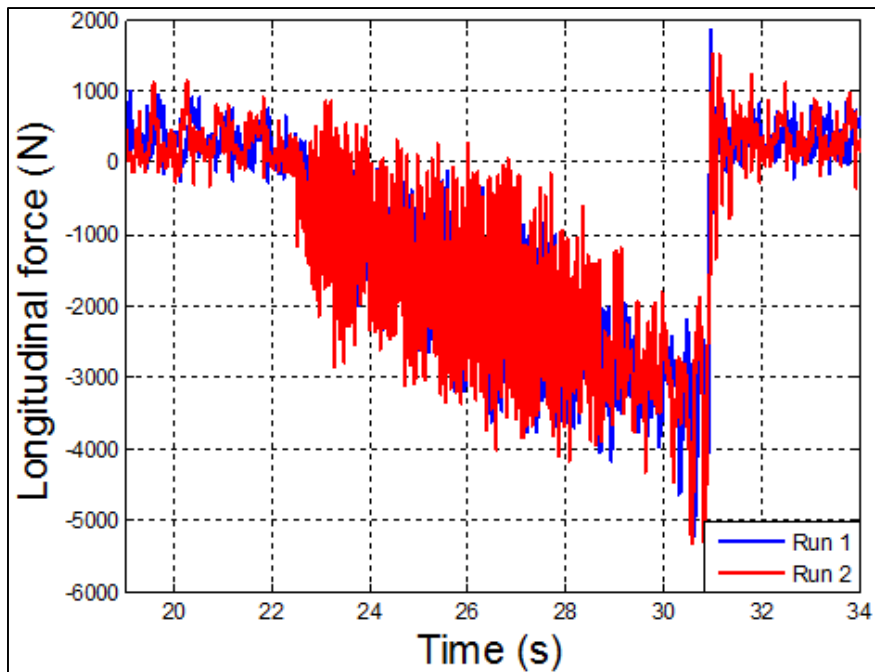


Figure 3-30: Traction validation test results (LC1)

Figure 3-31 shows the longitudinal velocity of the outdoor tyre testing equipment during a dynamic traction validation test. The angular velocity of the wheel is shown in Figure 3-32 as determined from the angular position measurements from the WFT (Becker et al., 2012). The longitudinal slip, as measured by the stereo-vision camera system is shown in Figure 3-33 while Figure 3-34 shows the longitudinal force generated by the tyre as a result of the applied brake pressure. Finally, Figure 3-35 depicts the resulting longitudinal force vs. longitudinal slip relationship for a dynamic traction validation test.

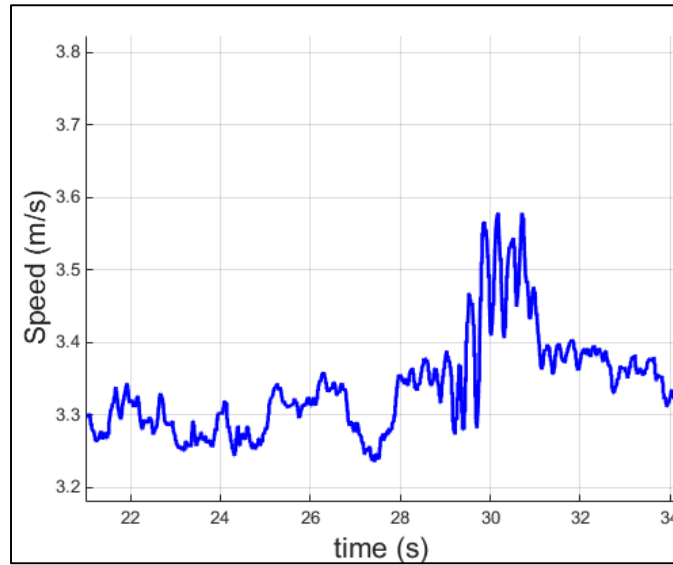


Figure 3-31: Velocity during a dynamic traction validation test (LC1)

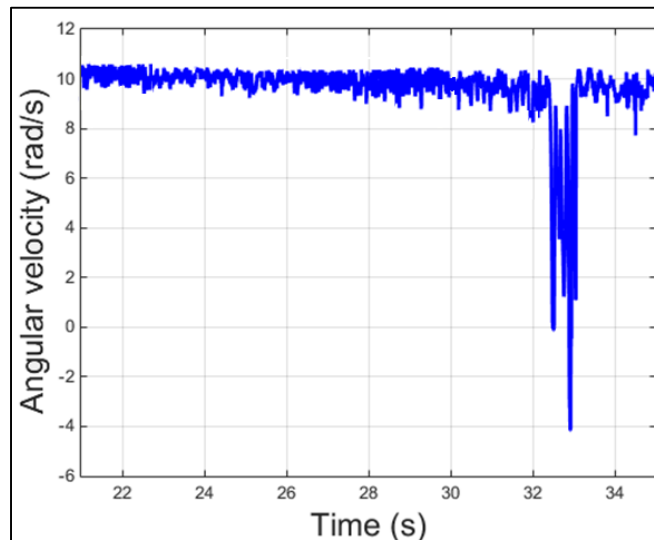


Figure 3-32: Angular velocity of the wheel during a dynamic traction validation test (LC1)

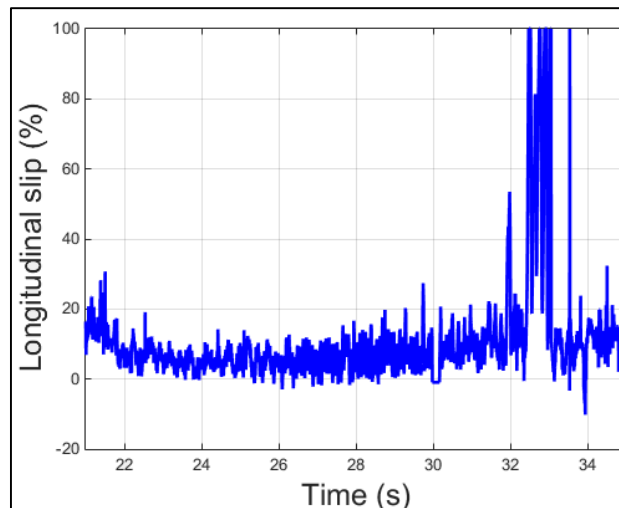


Figure 3-33: Longitudinal slip of the wheel during a dynamic traction validation test (LC1)

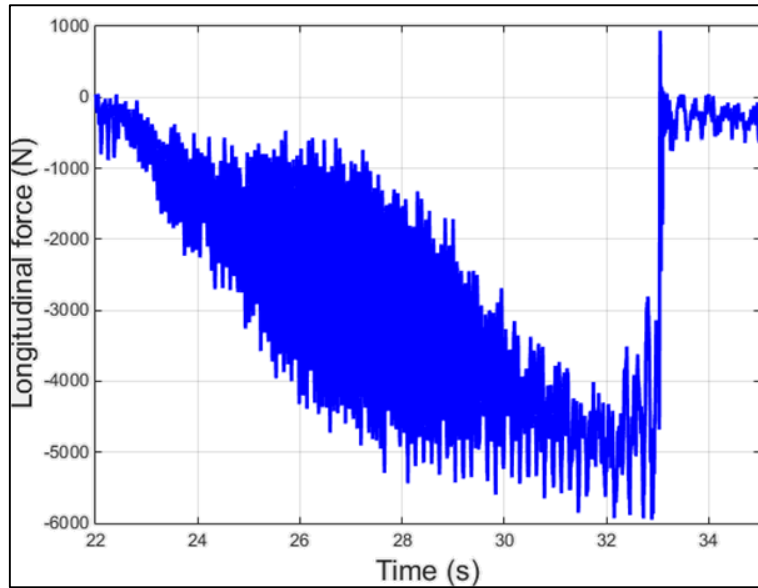


Figure 3-34: Longitudinal force during a dynamic traction validation test (LC1)

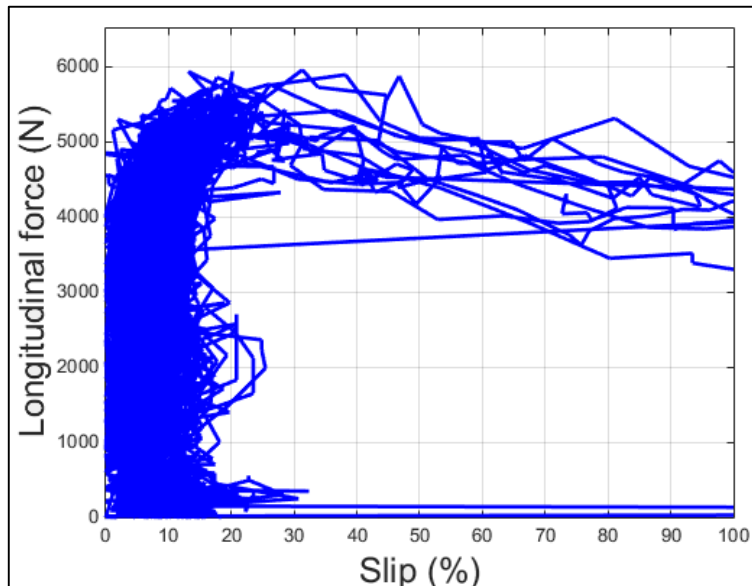


Figure 3-35: Longitudinal force vs. slip relationship for a dynamic traction validation test (LC1)

The longitudinal force vs. longitudinal slip characteristics acquired from the dynamic traction validation tests, shown in Figure 3-35, are not as expected. Further investigation reveals that the right-hand side tyre is rotating in reverse, as seen in Figure 3-32, while the left-hand side tyre experiences 100% slip. This is discovered by considering the KMT potentiometer data results. The reason for this occurrence is due to the nature of the open differential which is implemented in the braking system of the outdoor tyre testing equipment.

Other dynamic traction tests show similar results and it is found that the longitudinal force vs. longitudinal slip testing results are inconclusive due to the dynamics of the open differential utilized in the outdoor tyre testing equipment and are, therefore, omitted for the rest of this study. It is, therefore, decided to consider only the longitudinal force characteristics while neglecting the longitudinal slip data results for the rest of the study.



Based on these findings the recommendation is made to that a locked or lockable differential should be implemented in future dynamic traction tests to prevent the wheels to turn independently during the testing procedure.

3.6 Chapter summary

The FTire parameterization process as well as the required parameterization data is briefly discussed. The testing equipment used and procedures implemented to acquire static and dynamic tyre parameterization data were discussed in detail. Laboratory tests were conducted to capture static tyre parameterization data while field tests were conducted to capture dynamic parameterization and validation data.

Static parameterization tests consisted of capturing the size and shape of the tyre footprint, determining vertical and in-plane tyre stiffnesses as well as conducting static cleat tests. Static parameterization tests yielded consistent and repeatable results for multiple inflation pressures, camber angles and vertical loads.

A modal analysis was performed on the tyre to determine at which frequencies the first 6 vibrational modes occur on an unloaded and loaded tyre. Furthermore, the damping factors at the first 6 mode shapes were determined experimentally.

Dynamic parameterization and validation tests were conducted to capture the tyre behaviour in the lateral, longitudinal and vertical direction at different vertical loads. The tracks and road surfaces on which the dynamic validation tests were conducted were discussed in detail.

A sufficient amount of static and dynamic parameterization test data is captured during the testing procedures to implement within FTire/fit (2014) to be able to parameterize the FTire model.

The handling and traction validation tests were conducted on a smooth concrete road surface while the vertical parameterization and validation tests were conducted on the Belgian paving, the Fatigue track as well as a number of cleats placed on a smooth concrete road surface. All dynamic tests were conducted at the Gerotek Test Facilities (2013). From the experimentally obtained data it was found that the longitudinal force vs. slip relationship data was meaningless due to the dynamics of the Land Rover differential incorporated in the outdoor tyre testing equipment. Based on these findings the decision is made to only consider the longitudinal force characteristics while disregarding the slip characteristics. The dynamic handling and vertical tests showed good experimental results.

4 Parameterization of the FTire model

The construction and parameterization of an FTire model is governed by the procedure laid out by FTire/fit (2014) and relies on parameterization data obtained in static and dynamic parameterization tests. The ability of the FTire model to predict tyre behaviour relies on the accuracy of the parameterization data as well as the optimization of the parameters within the FTire model itself.

4.1 Introduction

The FTire parameterization process consists of three main phases, namely the preparation, the identification/validation and the finishing phases which are used to define the tyre model based on parameterization data, as shown in Figure 4-1. It is of utmost importance that the user is familiar with the tyre model software structure in order to understand the tyre model dynamics. The user should thus familiarise him or herself with the tyre model structure before attempting to parameterize and create a tyre model.

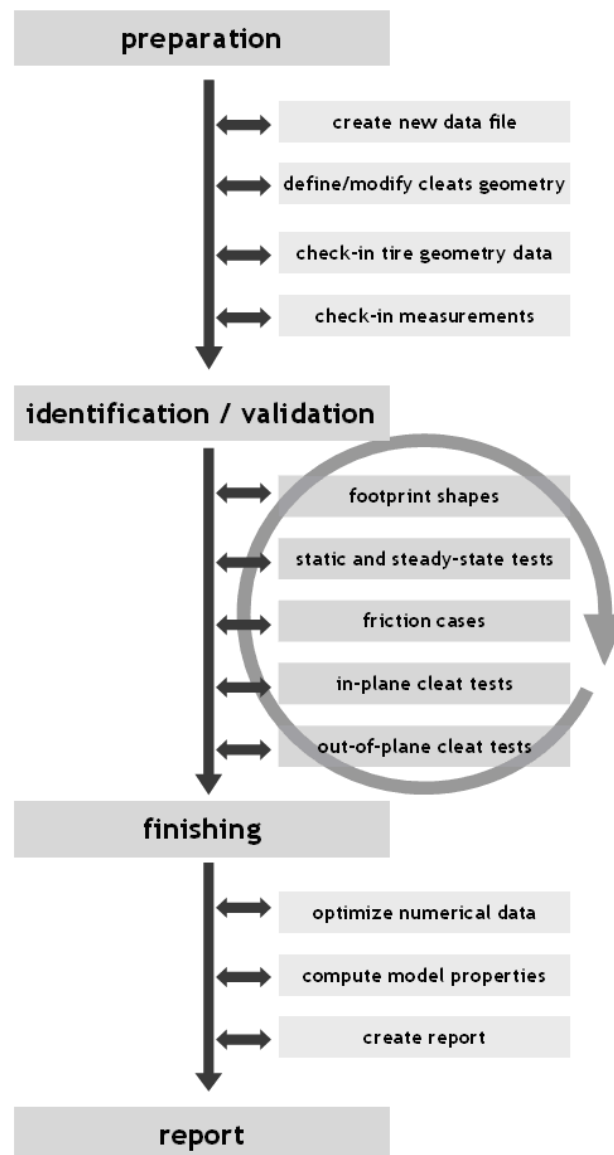


Figure 4-1: FTire parameterization procedure (Gipser, 2002)

4.2 Preparation phase

The tyre model parameterization process begins by creating a tyre property file which is based on an existing tyre property (.tir) file with similar tyre characteristics as the tyre being parameterized. It is of great importance that the existing tyre model file, used to initialize the tyre model, has similar characteristics to that of the tyre being modelled. It is found that no existing tyre model files have similar characteristics of the Michelin LTX tyre. Therefore, a tyre property file with similar tyre characteristics is generated incrementally. This proves to be a very long and arduous process since the FTire/fit solver implemented is rudimentary and requires an adequately good initial guess for its optimization process to converge to a stable tyre model.

Once the tyre property file has been created, an obstacle definition file is generated and imported into FTire. This obstacle definition file defines the types of obstacles which have been implemented in the static parameterization tests, discussed in Section 3.4. The obstacle definition file allows FTire/fit to relate a specific obstacle used in the static parameterization tests. A section of the cleat definition file created and implemented for the parameterization of the FTire model is shown in Figure 4-2.

```

* A 25x25 mm      0 deg (transversal)
* B 25x25 mm      45 deg (oblique)
* C 25x25 mm      90 deg (longitudinal on flat surface)
* D 32x32 mm      0 deg (transversal)
* E 32x32 mm      45 deg (oblique)
* F 32x32 mm      90 deg (longitudinal on flat surface)

$obstacle_A !* 25x25 0 deg *****
type drum; v vdrum/3.6; number_cleats 1; mu_factor 1.0; mu_factor_cleat 0.5
diameter          9999 ! [m] negative if outer drum
cleat_height       25   ! [mm]
cleat_length       25.3 ! [mm]
cleat_bevel_edge_length 1.8 ! [mm]

$obstacle_B !* 25x25 45deg *****
type drum; v vdrum/3.6; number_cleats 1; mu_factor 1.0; mu_factor_cleat 0.5
diameter          9999 ! [m] negative if outer drum
cleat_direction    -45  ! [deg]
cleat_height       25   ! [mm]
cleat_length       25.3 ! [mm]
cleat_bevel_edge_length 1.8 ! [mm]

$obstacle_C !* 25x25 90deg *****
type drum; v vdrum/3.6; number_cleats 1; mu_factor 1.0; mu_factor_cleat 0.5
diameter          9999 ! [m] negative if outer drum
cleat_direction    90   ! [deg]
cleat_height       25   ! [mm]
cleat_length       25.3 ! [mm]
cleat_bevel_edge_length 1.8 ! [mm]
  
```

Figure 4-2: Section of the cleat definition file

The physical tyre dimensions and geometry, as well as the speed and load ratings, as stated by the tyre manufacturer, are defined in an FTire generation data file. Two tyre inflation pressures at which parameterization tests were conducted are also defined in this window. Figure 4-3 shows the FTire generation file window in which tyre properties are specified.

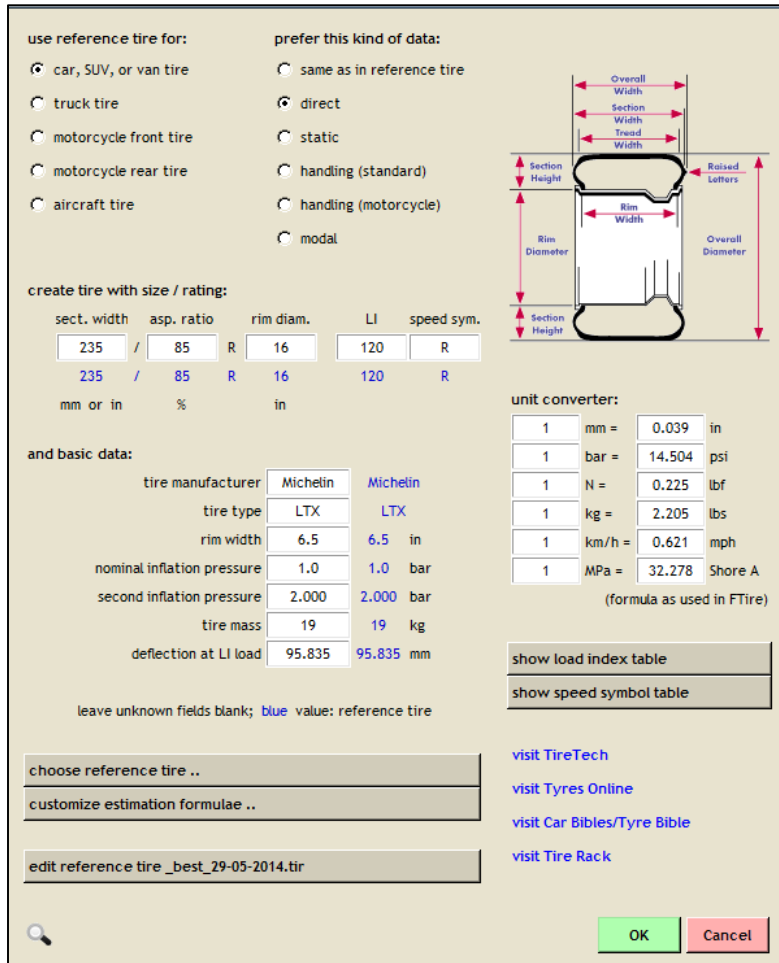


Figure 4-3: FTire generation file window

It is vital to conduct parameterization tests at two different inflation pressures that the effect of inflation pressure is identified by FTire/fit. Not only does this give information about the effect of inflation pressure on the tyre but also tyre characteristics such as the carcass stiffness are captured more accurately.

If the tyre were only parameterized based on a single inflation pressure it would be impossible to distinguish between the effects of the inflation pressure and carcass stiffness during the FTire/fit parameterization of the FTire model. Similarly, static parameterization tests are conducted at different camber angles for FTire/fit to be able to investigate the effect of the lateral sidewall stiffness on the overall characteristics of the tyre.

Finally, relevant parameterization test data from each parameterization test is imported and checked into FTire/fit. The footprint images are imported in a bitmap image format while other static and dynamic parameterization test data is imported in the form of TYDEX (Unrau et al., 1997) files. FTire/fit attempts to recognize the type of parameterization test that was conducted based on the information provided in the TYDEX (Unrau et al., 1997) file of each parameterization test conducted.

Information including obstacle definition and several measured channels are considered to identify the parameterization test that was conducted. After having identified each of the imported TYDEX (Unrau et al., 1997) and bitmap files FTire/fit sorts these based on the type of test that was conducted.

It is found that a large number of measured channels from the parameterization test data are required for FTire/fit to recognize a parameterization test that was conducted. Furthermore, the acquired test data should be as smooth as possible with no large differences between measured data points within the test data.

Numerous attempts are made to import handling and traction validation test data, discussed in Section 3.5. However, it is found that the validation test data is very noisy even after filtering the data. The FTire/fit solver shows great difficulty in identifying tests if the data is noisy and fails to import the data. Therefore, it is not possible to include the dynamic handling and traction validation test data in the parameterization process of the FTire model and the decision is made to omit these data sets in the parameterization process.

4.3 Identification/validation phase

Once the preparation phase has been completed the identification/validation phase is initiated. In this phase FTire/fit identifies and validates the parameters which define and predict certain tyre characteristics. The correct parameter identification order should be followed, as stated by Cosin (2014). Based on this information the tyre footprint bitmap images are considered first.

The footprint bitmap images which are obtained from static parameterization tests, discussed in Section 3.4.1, give information about the in-plane, lateral, longitudinal and twist bending stiffness parameters of the tyre belt. It is found that a combination of parameter values are required to be parameterized manually in parallel for the parameterization test results and the FTire/fit prediction data sets to correlate.

The FTire/fit footprint size and shape parameterization turns out to be the most complex parameterization process due to the number of parameters that have to be adjusted simultaneously. It is paramount that FTire/fit is able to accurately approximate the tyre footprint for a number of load cases and camber angles since a good approximation of the contact patch size and shape is vital to predicting tyre behaviour.

Figures 4-4 and 4-5 show the correlation between the actual footprint and the footprint predicted by FTire/fit. It is concluded that the correlation is good between the measured and estimated footprints.

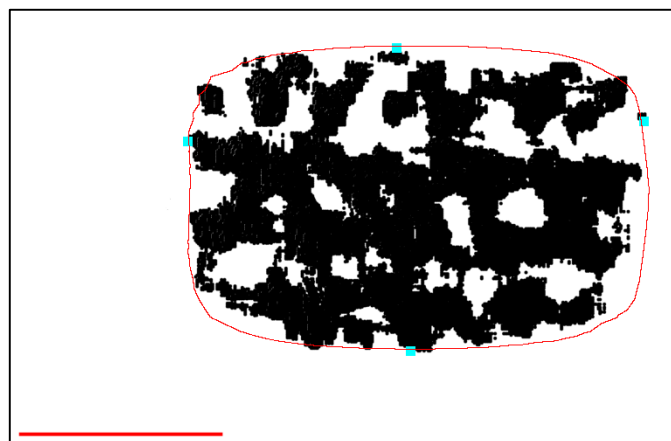


Figure 4-4: Footprint at 1 bar inflation pressure, 0 degrees camber and 3496N vertical load

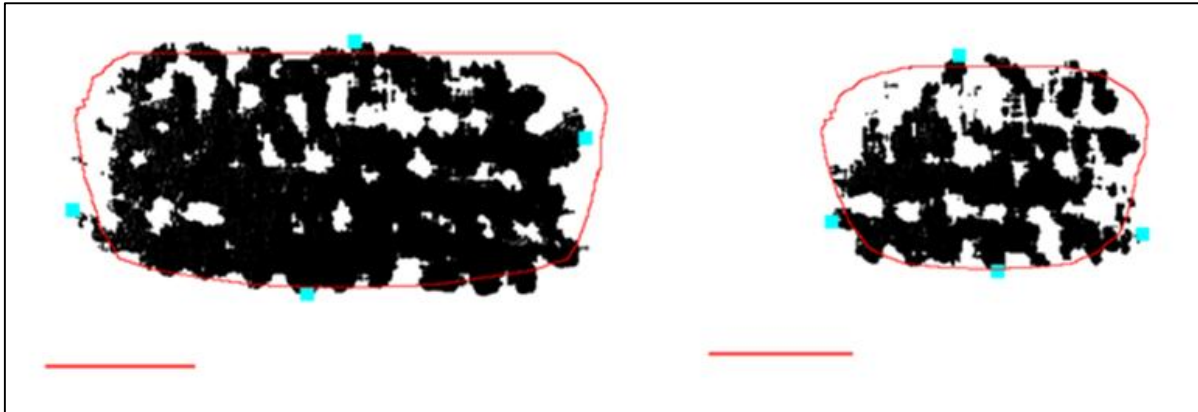


Figure 4-5: Footprint images at 2 bar inflation pressure. Left: 8123N vertical load (3° camber). Right: 1845N vertical load (5° camber angle)

The static and steady state tests are the next step in the identification process. It is found that the static vertical stiffness test data, discussed in Section 3.4.1, is used to parameterize the radial stiffness parameters. The parameters for both inflation pressures are altered simultaneously. Figures 4-6 and 4-7 show the measured data and the FTire/fit data at 1 bar and 2 bar inflation pressure, respectively. From these figures it is concluded that the parameter has been approximated well by FTire/fit. Further static and steady-state tests, which were conducted on a flat steel plate at camber angles of 0°, 3°, and 5° are approximated well by FTire/fit.

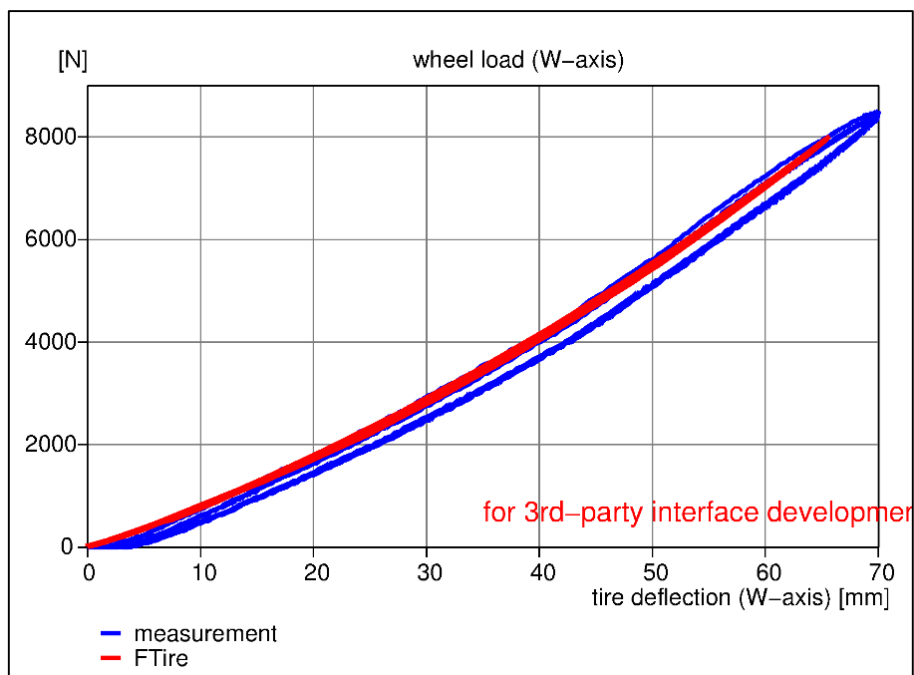


Figure 4-6: Vertical stiffness on a flat plate at 1 bar inflation pressure and 0 degrees camber

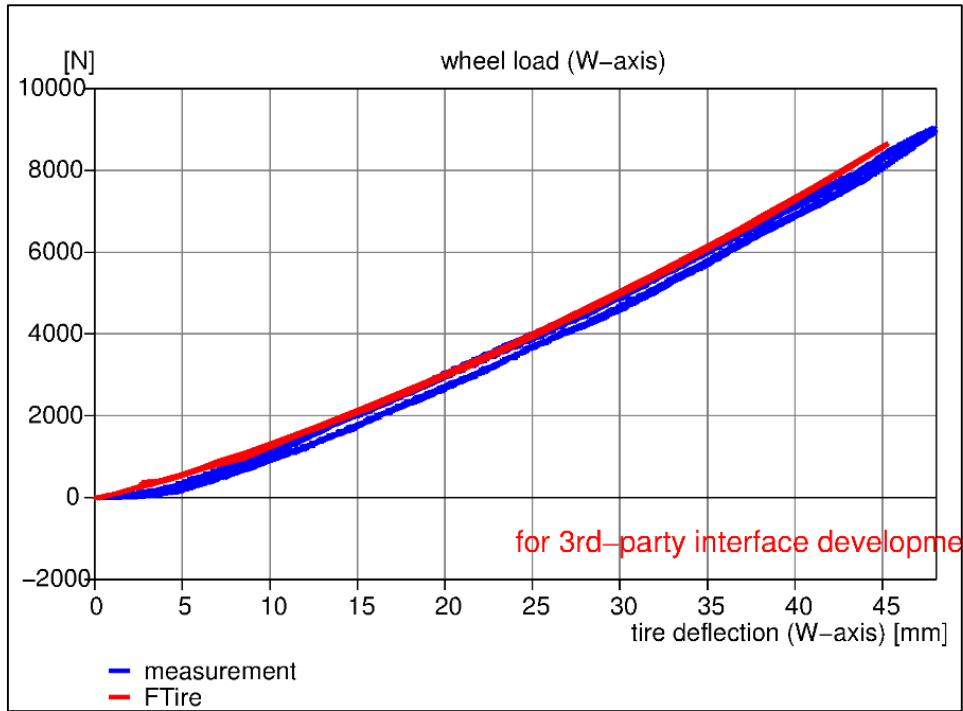


Figure 4-7: Vertical stiffness on a flat plate at 2 bar inflation pressure and 6 degrees camber

The static cleat parameterization test data obtained from static cleat tests, discussed in Section 3.4.2, influence the lateral, longitudinal, torsional twist as well as the in-plane bending tyre stiffnesses. Figures 4-8 and 4-9 show that the parameterization data and the FTire/fit model prediction data correlate well for the in-plane cleat tests.

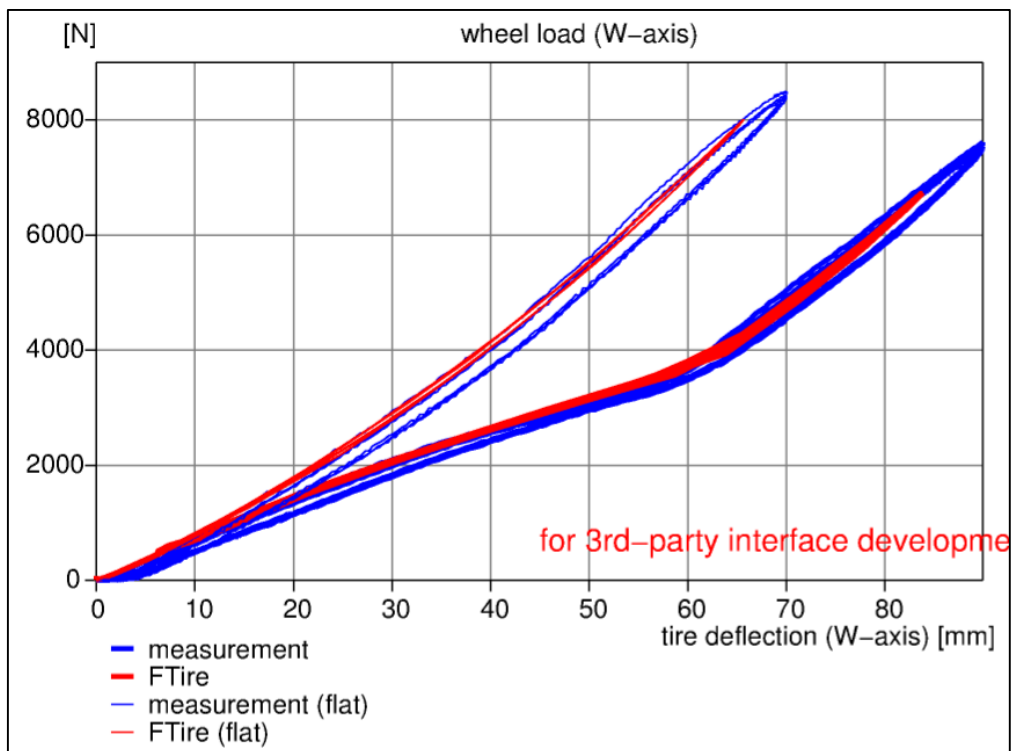


Figure 4-8: Vertical tyre stiffness on a 25x25mm transversal cleat at 0 degrees camber and 1 bar inflation pressure



Figure 4-9: Vertical tyre stiffness on a 32x32mm transversal cleat at 0 degrees camber and 2 bar inflation pressure

In-plane and out-of-plane parameterization test data, discussed in Section 3.4.3, is used to parameterize the in-plane and out-of-plane parameters which prove to be very difficult to adjust. The solver does not converge when adjusting these parameters even after numerous attempts are made to redefine the TYDEX (Unrau et al., 1997) files which define the static parameterization tests conducted. Therefore, it is decided to leave the parameters as they were initially estimated.

Figures 4-10 and 4-11 show the correlation of the longitudinal, lateral and torsional tyre stiffnesses, respectively. It is clearly seen that the initial in-plane and out-of-plane stiffnesses estimated by FTire are higher than those of the experimental results in the longitudinal and lateral directions, respectively. Furthermore, the friction coefficient in the longitudinal direction is estimated to be lower by FTire/fit than the experimental results while the lateral friction coefficient is estimated well by FTire/fit. These differences in coefficients of friction are likely to be attributed to the fact that tests were conducted on a steel plate rather than an abrasive surface such as concrete.

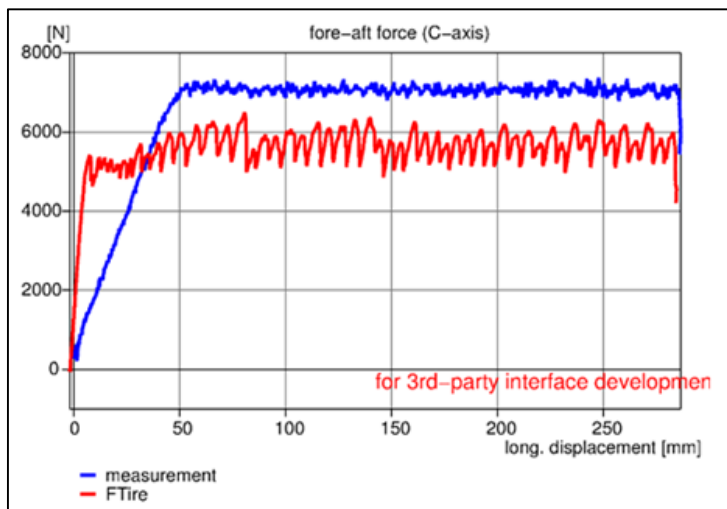


Figure 4-10: Longitudinal tyre stiffness at 1 bar inflation pressure, 0 degrees camber and 8.61 kN vertical load

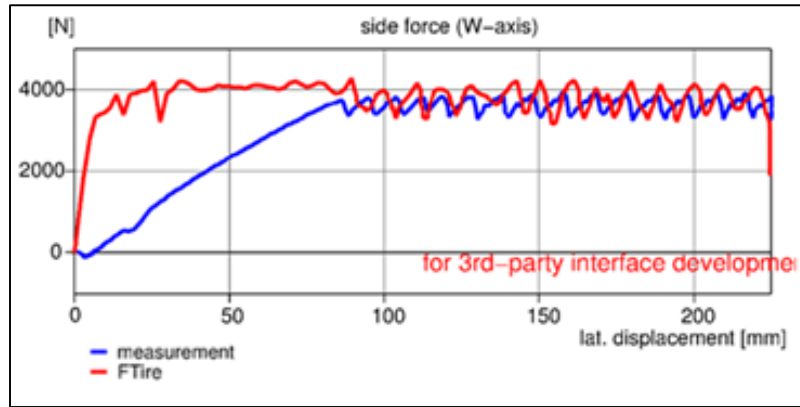


Figure 4-11: Lateral tyre stiffness at 1 bar inflation pressure, 0 degrees camber and 3.61 kN vertical load

Figure 4-12 shows that the initial torsional stiffness, estimated by FTire/fit, is higher than that of the experimental test results. On the other hand, the estimated friction coefficient is seen to be lower than the experimental results.

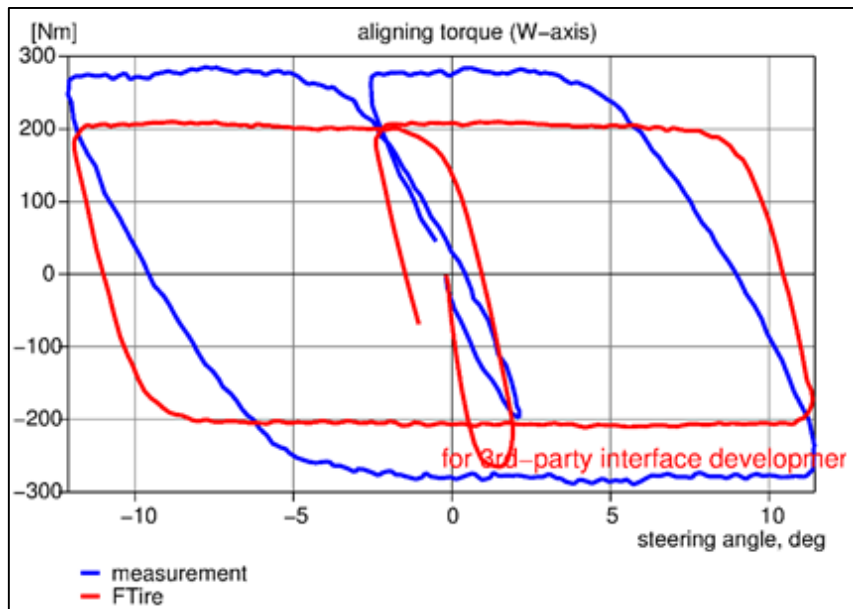


Figure 4-12: Torsional tyre stiffness at 1 bar inflation pressure, 0 degrees camber and 5 kN vertical load

According to Cosin (2014), damping parameterization tests should be performed dynamically on a drum tyre testing rig with a cleat mounted onto the running surface of the drum. Due to the fact that no drum tyre testing rig is available to conduct these parameterization tests, these cannot be performed, as required by FTire/fit. It is attempted to import the dynamic cleat test data from the field tests conducted at the Gerotek Test Facilities (2014), as discussed in Section 3.5.1.1. However, the dynamic cleat test data proves to be too noisy to be recognized by FTire/fit and, therefore, these tests cannot be used to parameterize the necessary parameters in FTire/fit.

Stallmann (2014) suggests that the tyre damping parameters can be parameterized manually by making use of the dynamic cleat test data which is obtained from the dynamic validation and parameterization tests, as discussed in Section 3.5.1.1. An initial estimate of the damping behaviour is made by considering the damping factors obtained from modal analysis tests, discussed in Section 3.4.4.

An FTire model is created with the initial tyre damping estimation and implemented in a dynamic cleat test simulation, as discussed in Section 5.2.5. It is found that the damping factors obtained from the modal analysis results are too low and these are adjusted incrementally until the measured dynamic cleat test data results correlate with the FTire model prediction behaviour, as shown in Figure 4-13. This method of adjusting the tyre damping parameters proves to be a cumbersome but effective process.

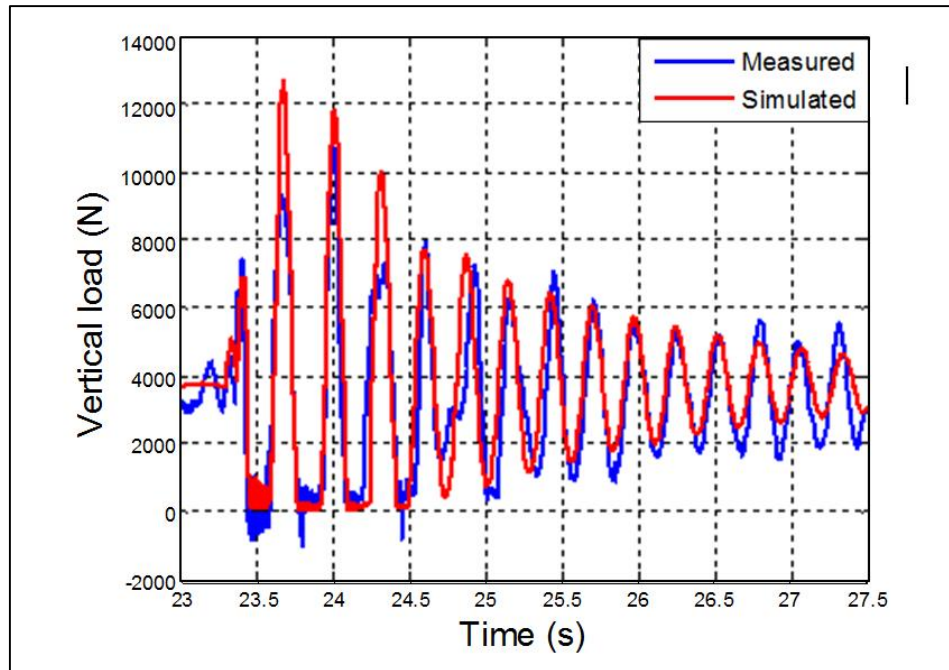


Figure 4-13: 50x50mm cleat test damping correlation at 3.5 m/s

There is a distinct visual difference in amplitude between the measured and simulated results when considering the first and third peaks of the tyre response after having negotiated the cleat. This difference in amplitude can be attributed to measurement noise and disturbances caused by external factors such as road undulations or slightly misaligned cleat plates. While the simulated tyre response oscillations regress constantly, the measured tyre response is seen to have a more irregular characteristic.

It is found that certain parameterization test types require the same parameters to be parameterized (e.g. the footprint and static cleat tests). However, the tuning of the parameters can only be done for one type of test at a time. This means that tuning the parameter for one type of parameterization test might improve the FTire/fit estimation results of that type of test but this may lead to the FTire/fit estimation of another test to deteriorate. Therefore, a compromise is made for each of such cases. It is found that the FTire/fit estimation results correlate well with the overall measured parameterized test data after the validation/identification process is performed repeatedly.

4.4 Finishing phase

After having completed the identification/validation phase the finishing phase is initiated. In this phase a report is created by FTire/fit which depicts all parameterization results in form of images for each of the parameterization tests and FTire/fit estimations considered during the identification/validation phase. From this report the user can visually inspect the correlation between the parameterization data and the FTire/fit estimation results for each type of test considered.

Based on the results presented in the report the identification/validation phase is reinitiated to refine the necessary FTire/fit parameter estimation for certain parameterization tests. Finally, after having completed the parameterization process of the FTire model a tyre (.tir) file is created to be used for tyre behaviour prediction during simulations.

4.5 Chapter summary

In this chapter, the parameterization of the FTire model, which is based on parameterization data obtained from static and dynamic experimental testing, has been discussed.

The parameterization process conducted to develop an FTire model of the all-terrain tyre was discussed in detail and was heavily based on static parameterization data acquired in static laboratory tests. The relevant parameters to parameterize the tyre model were adjusted manually to obtain a correlation between the parameterization data and the tyre model data since the FTire/fit solver was found to be rudimentary.

The FTire/fit estimation was found to give a good correlation with the static parameterization test data on flat surfaces and over cleats for different camber angles.

The static in-plane and out-of-plane tyre behaviour was not estimated as well as it was for the vertical behaviour of the tyre. Possible reasons for this include a difference in friction coefficient estimation and a difference in stiffness estimations between the FTire model and the actual tyre. However, due to the FTire/fit solver instability the FTire model could not be modified to an extent for the results to correlate.

The tyre damping and dynamic response parameterization was initially based on modal analysis results and fine-tuned by considering dynamic cleat parameterization test results. A tyre model was created and implemented in a dynamic vertical parameterization test simulation to fine-tune the damping behaviour of the FTire model.

5 Validation

For simulation models that are constructed to represent real-life physical systems, validation forms an integral part of the modelling process. The validation process is aimed at comparing simulation results to experimental results. The comparison of these data sets may readily show correlations or discrepancies between the two data sets. Furthermore, the validation may reveal anomalies, aberrations and irregularities in either of the data sets.

Generally the measurement data set abnormalities occur due to inconsistently varying factors while executing tests or due to measurement imprecisions. Model data set abnormalities generally occur due to mathematical errors, incorrect model approximations, model inputs or a faulty model.

5.1 Introduction

A tyre model such as the FTire is expected to give meaningful results when considering the tyre forces and moments generated by the tyres during dynamic tests conducted. These tests may include tests over smooth road surfaces, rough road surfaces as well as over rough terrain. To determine whether the FTire model gives acceptable results, the forces and moments predicted by the tyre model during simulations are validated against the forces and moments generated by the actual tyre during validation tests.

When validating data sets against one another, an objective method or metric must be incorporated which is able to relate one data set to another and vice versa. According to Kat et al. (2012) several methods have been developed and, in general, these methods may be classified in two categories.

The first type is a method that looks at the difference between each of the data points in the given data sets rather than the data sets as a whole. This means that the error between the data sets may be represented by a vector which has the same size as the data sets being considered. This vector gives information about the relative error between the data sets and thus an error may be located easily in the data set. An example of this method is the relative error percentage (%RE) method.

The second type is a method that looks at the difference between given data sets as a whole. Therefore, the data sets are compared to one another in the form of a single numerical value. This means that if an error between data sets exists it will not be easily found since the method cannot identify the error patterns between the data sets. Nonetheless these methods are preferred when comparing data set results against one another due to the fact that the comparison is much simpler than that of an error vector. An example of this method is the root mean square (RMS) error method.

For this investigation it is decided to use both the RMS and %RE methods to compare the measured and simulated data sets to one another. The RMS method, which is a measure of the magnitude of a varying quantity, gives a good cumulative error prediction between two or more data sets and may be defined mathematically as follows.

$$RMS = \sqrt{\frac{1}{n} \sum_{i=1}^n (s_i - p_i)^2} \quad (2)$$

The relative error method, which is the absolute error divided by the magnitude of the exact value, defines the percentage of the error between each data point so as to simplify the comparison and validation of the measured and simulated data sets being analysed. One of the data sets has to be identified as being the correct or exact result. Thus, for the sake of the validation process, it is assumed that the measured data set yields the exact results. Therefore, the relative error percentage (%RE) is defined as follows.

$$\%RE = \frac{p-s}{p} \times 100 \quad (3)$$

A validation metric developed by Kat et al. (2012), which is based on relative error is able to quantify the correlation between measured and simulated responses by evaluating the resulting relative error percentage. In order to extract a single value from the %RE method for validation purposes the mean of the relative error percentage (m%RE^m) as well as the mean of the relative error percentage below a specified relative error percentage (m%RE^s) of 15% is calculated, as depicted by Kat et al. (2012). The mean of the relative error percentage results are interpreted as depicted by the following example.

m%RE^m = 5.6% P(76.120%) 76.120% of the %RE vector entries lie at or below a mean %RE of 5.6%.

m%RE^s = 15% P(92.490%) 92.490% of the %RE vector entries lie at or below the specified %RE of 15%.

5.2 Adams modelling

A high fidelity MSC Adams (2013) model of the outdoor tyre testing rig, which was created by the Vehicle Dynamics Group (VDG) of the University of Pretoria, is implemented to validate the FTire tyre model, as seen in Figure 5-1.

The FTire model is implemented in the simulations by importing the tyre (.tir) file, discussed in Section 4.4. The FTire model is attached to the hubs of the outdoor tyre testing equipment model in MSC Adams (2013). The forces and moments generated by the outdoor tyre testing equipment, as predicted by the FTire model, are compared to measured forces and moments generated by the tyres during dynamic validation tests, as discussed in Sections 3.5.1 to 3.5.3.

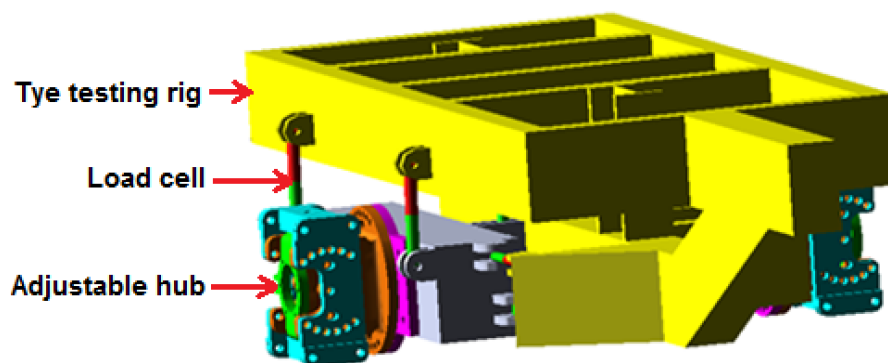


Figure 5-1: MSC Adams (2013) model of the outdoor tyre testing equipment

5.2.1 Experimental determination of moments of inertia of the tyre testing rig

The mass and moment of inertia properties of the outdoor tyre testing equipment have previously been determined experimentally. However, amongst other components, a Land Rover Defender rear differential coupled to a Land Rover Defender brake assembly, as well as a pneumatic detachable brake system and adjustable hubs have been added to the outdoor tyre testing equipment to conduct dynamic lateral and longitudinal tyre characteristics tests. Therefore, the decision is made to re-establish the position of the C. O. G. as well as the pitch and roll moments of inertia of the outdoor tyre testing equipment experimentally.

5.2.1.1 Determination of the position of the centre of gravity of the tyre testing rig

In order to determine the position of the C. O. G. in all three Cartesian directions two sets of experimental tests are conducted. The first set of tests is implemented to determine the in-plane position of the C. O. G. while the second set determines the vertical position of the C. O. G. of the outdoor tyre testing equipment.

5.2.1.1.1 In-plane position of the centre of gravity of the tyre testing rig

The outdoor tyre testing equipment is supported at three points while the vertical load on these points is measured using wheel scales. From these three vertical load measurements it is then possible to determine the position of the in-plane C. O. G. as follows.

As stated by Meriam et al. (2009), the position of the in-plane C. O. G. is determined by making use of the following equations.

$$CG_x = \frac{\sum m_i \bar{r}_{x,i}}{\sum m_i} \quad (4)$$

$$CG_y = \frac{\sum m_i \bar{r}_{y,i}}{\sum m_i} \quad (5)$$

for $i = 1, 2, 3$

Where $\bar{r}_{x,i}$ and $\bar{r}_{y,i}$ depict the distance between each of the measuring points to a predetermined reference point on the outdoor tyre testing equipment in the Cartesian x- and y- direction, respectively.

5.2.1.1.2 Vertical position of the centre of gravity

The second set of experimental tests are conducted to determine the vertical position of the C. O. G. by supporting the front of the outdoor tyre testing equipment on a wheel scale while lifting the rear up using an overhead crane, as seen in Figure 5-2.



Figure 5-2: Experimental setup to determine the vertical position of the C. O. G. with pneumatic brake system

While the front load, R , is measured by a wheel scale, the rear lifting force, F , is measured by a five ton load cell. As the crane is hoisted up, the tyre testing rig is positioned at an increasing angle relative to the ground. The vertical position of the C. O. G. is determined by taking the moments about R , as shown in Figure 5-3. The following equation, as developed by Uys et al. (2006) is used to determine the vertical position of the C. O. G.

$$LF \cos \theta - HF \sin \theta - mgb \cos \theta - mgh \sin \theta = 0 \quad (6)$$

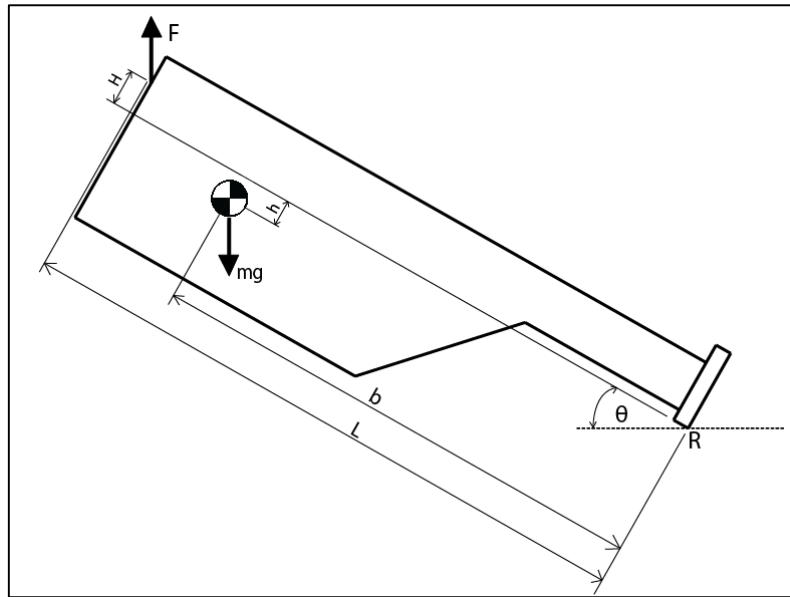


Figure 5-3: Locating the vertical position of C. O. G. without pneumatic brake system

5.2.1.2 Determination of the moments of inertia of the tyre testing rig

A pendulum method, as discussed by Uys et al. (2006) is used to determine the pitch and roll moments of inertia of the outdoor tyre testing equipment. The method is based on a rigid body oscillation about a pivoting point where a restoring force is given by a spring, as seen schematically in Figure 5-4.

The pitch and roll moments of inertia around the pivoting point are determined by considering the period of oscillation of the outdoor tyre testing equipment, as stated by Uys et al. (2006). The pitch and roll moments of inertia of the outdoor tyre testing equipment are then determined by applying the parallel axis theorem.

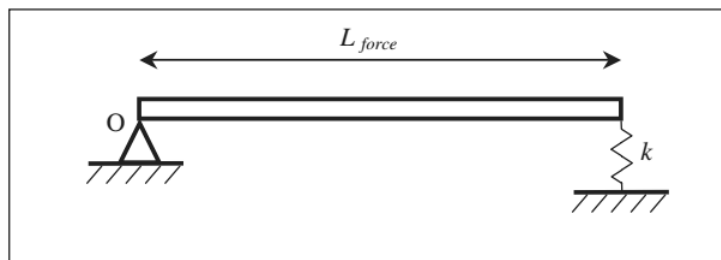


Figure 5-4: Schematic representation of the rotation of a rigid body (Uys et al., 2006)

5.2.1.2.1 Pitch moment of inertia of the tyre testing rig

To determine the pitch moment of inertia the outdoor tyre testing equipment is pivoted about its wheel hubs. This setup allows the tyre testing rig to rotate freely about its drive shafts but restricts any other movement.

A spring is mounted between the nose of the outdoor tyre testing equipment and a load cell, which is connected to the ground at the front of the tyre testing rig, as shown in Figure 5-5. An Acuity (2014) AR700-8 displacement measurement laser is used to measure the vertical displacement of the spring which is excited vertically to induce an oscillation of the tyre testing rig about its hubs.

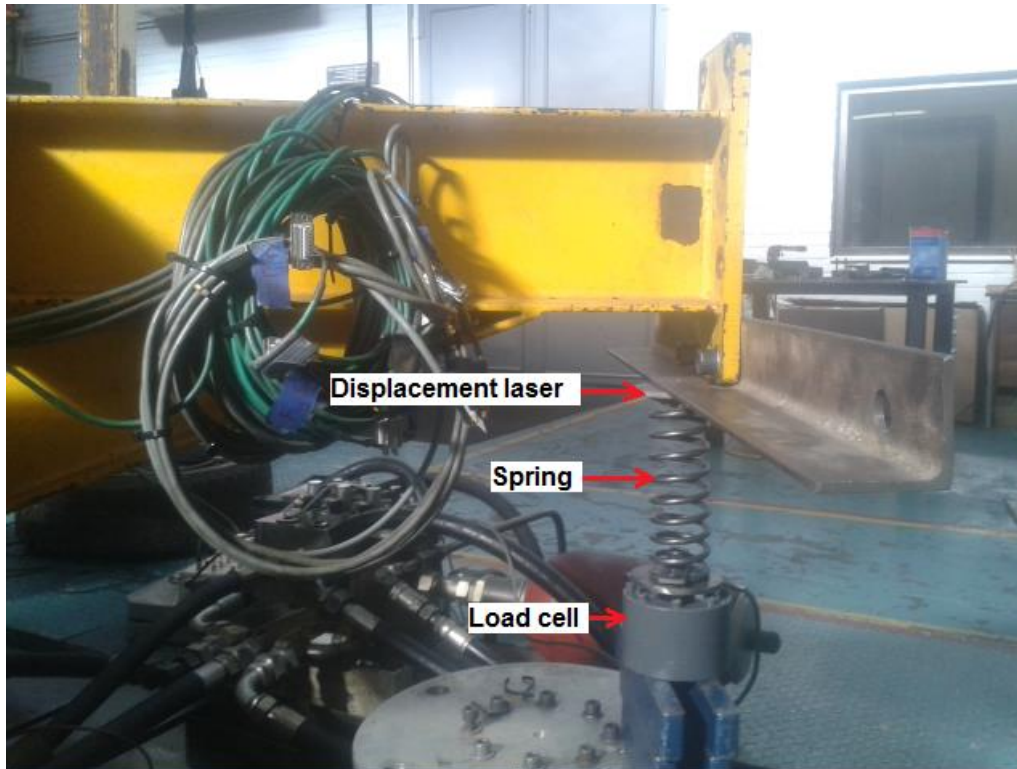


Figure 5-5: Measurement equipment setup to determine the pitch moment of inertia

According to Uys et al. (2006) the pitch moment of inertia of the tyre testing rig about its drive shafts is defined as follows.

$$I_o = \frac{\tau^2 k L^2 force}{2\pi} \quad (7)$$

The spring stiffness is determined by loading a set of known weights above the spring and measuring the resulting deflection of the spring.

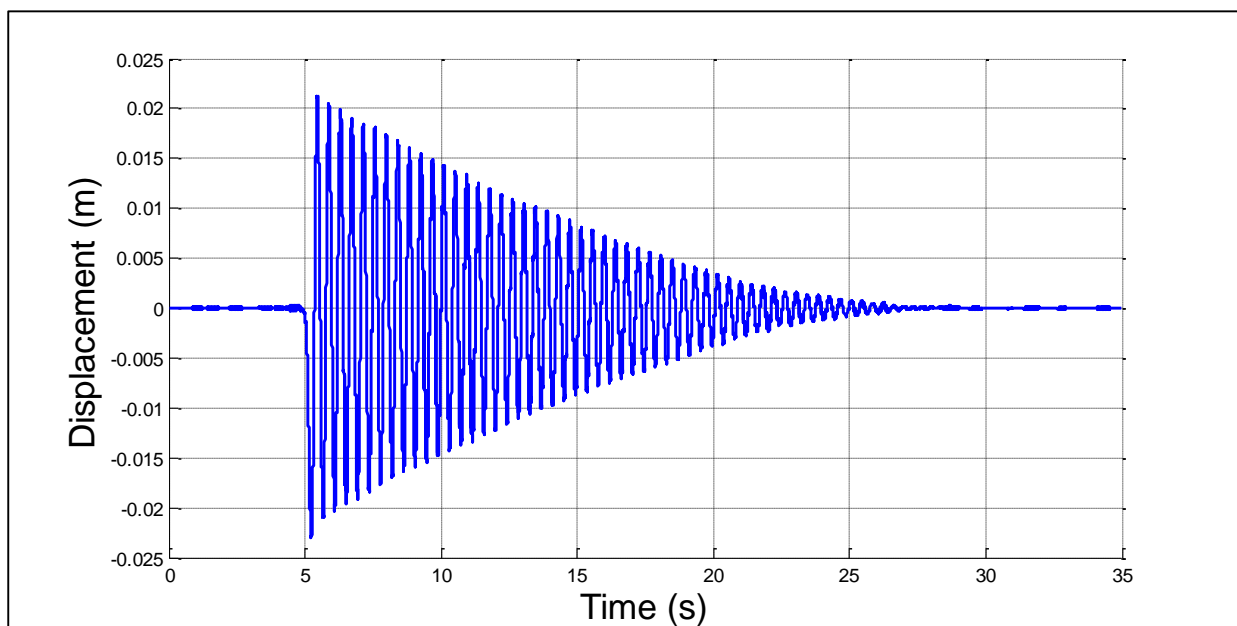


Figure 5-6: Pitch moment of inertia experimental results

The laser displacement measurement, seen in Figure 5-6, gives information about the damped period of the outdoor tyre testing equipment. Therefore, the natural frequency is determined to calculate the undamped natural period. From the displacement curve the logarithmic decrement, δ , is determined as follows.

$$\delta = \ln \frac{x_1}{x_2} \quad (8)$$

Thus the damping ratio, ζ , is calculated as follows.

$$\zeta = \frac{\delta^2}{\sqrt{\delta^2 + (2\pi)^2}} \quad (9)$$

The undamped natural period is determined by the following relation.

$$\tau = \sqrt{1 - \zeta^2} \tau_d \quad (10)$$

From these results the pitch moment of inertia of the tyre testing rig is calculated around the point of rotation by making use of Equation 7.

The parallel axis theorem is used to determine the pitch moment of inertia of the outdoor tyre testing equipment about its C. O. G. as follows.

$$I_{pitch,CG} = I_o - m(L_x^2 + L_z^2) \quad (11)$$

Where L_x and L_z depict the distances from the drive shaft centre line to the position of C. O. G. in the Cartesian x - and z -directions (determined in Sections 4.2.1.1.1 and 4.2.1.1.2), respectively. Based on the distance between the reference point and the position of the C. O. G. as well as the mass of the tyre testing rig, the pitch moment of inertia about the C. O. G. of the tyre testing rig are determined. Table 5-1 shows the results which are obtained for the pitch moments of inertia of the outdoor tyre testing equipment.

Table 5-1: Results of pitch moment of inertia

	Pitch moment of inertia
Without pneumatic braking system	171 kgm ²
With pneumatic braking system	185 kgm ²

5.2.1.2.2 Roll moment of inertia of the tyre testing rig

The roll moment of inertia of the tyre testing rig is determined using the same method as the pitch moment of inertia. However, the outdoor tyre testing equipment is pivoted about its longitudinal centreline axis on knife edges.

The spring, which supplies the restoring force, is mounted to the left-hand side wheel hub and is connected to a load cell which is mounted to the ground, as seen in Figure 5-7. The displacement of the spring is measured by the Acuity (2014) AR700-8 displacement measurement laser.

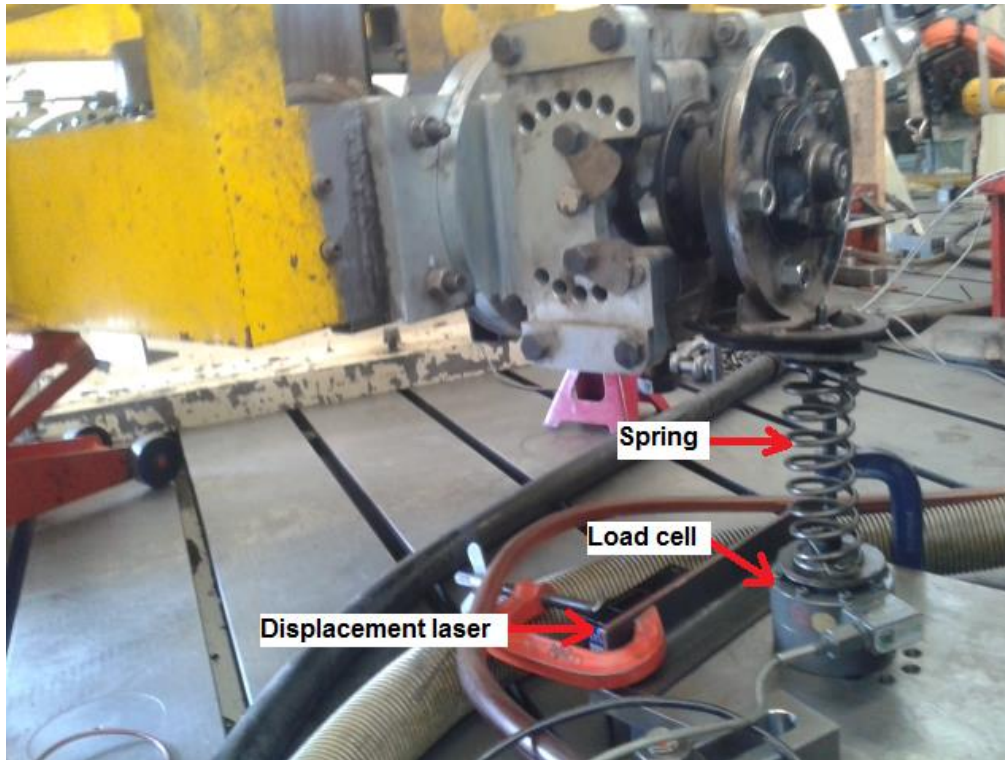


Figure 5-7: Measurement equipment setup to determine the roll moment of inertia

A small vertical excitation input is given to the system by hand above the spring to induce an oscillation of the outdoor tyre testing equipment about its pivoting axis.

To determine the roll moment of inertia about the C. O. G. of the outdoor tyre testing equipment the following equation is implemented:

$$I_{roll,CG} = I_o - m(L_y^2 + L_z^2) \quad (12)$$

where L_y and L_z depict the distances from the pivoting centre line to the position of C. O. G. in the Cartesian y - and z -directions (as determined in Sections 5.2.1.1.1 and 5.2.1.1.2), respectively. Table 5-2 shows the results which were obtained for the roll moments of inertias.

Table 5-2: Results of roll moment of inertia

	Roll moment of inertia
Without braking system	86 kgm ²
With braking system	90 kgm ²

The pendulum method is very sensitive to distance measurements and accurate determination of the C. O. G.. An existing CAD model of the tyre testing rig is used to validate all measured distances during the testing procedures.

5.2.2 Simulation velocity input

A longitudinal driving force is applied to the tow hitch of the MSC Adams (2013) outdoor tyre testing equipment model. The longitudinal driving force simulates a towing vehicle translating the outdoor tyre testing equipment on a road surface. A PID controller is implemented to control the driving force longitudinally at the same velocity at which dynamic validation tests were conducted.

The tow hitch of the outdoor tyre testing equipment model is simulated as a spherical joint which is free to rotate in all three Cartesian axes directions while translation in the vertical and lateral directions are prevented in the towing system model. During dynamic tests the towing vehicle is likely to have given vertical and lateral translation inputs to the outdoor tyre testing equipment through the tow hitch due to the effects of the towing vehicle's suspension, steering and speed fluctuations.

5.2.3 Handling simulation inputs

The inputs to the handling test simulations include the longitudinal velocity as well as slip and camber angles of the left-hand side and right-hand side wheels. The slip angles of the left-hand side and right-hand side tyre are given as variable inputs to the adjustable hub models in MSC Adams (2013), as shown in Figure 5-1. The slip angle simulation inputs are the same inputs as given to the linear actuators utilized to vary the slip angles of the tyres during dynamic validation tests, as discussed in Section 3.5.2. The variable velocity and slip angle inputs to the handling simulations are shown in Figure 5-8.

Similarly, the camber angles for the left-hand side and right-hand side wheels are given as inputs to the model. However, it should be noted that due to the construction of the adjustable hubs, these stayed constant during each test run and are therefore defined as constant variables in the simulation model.

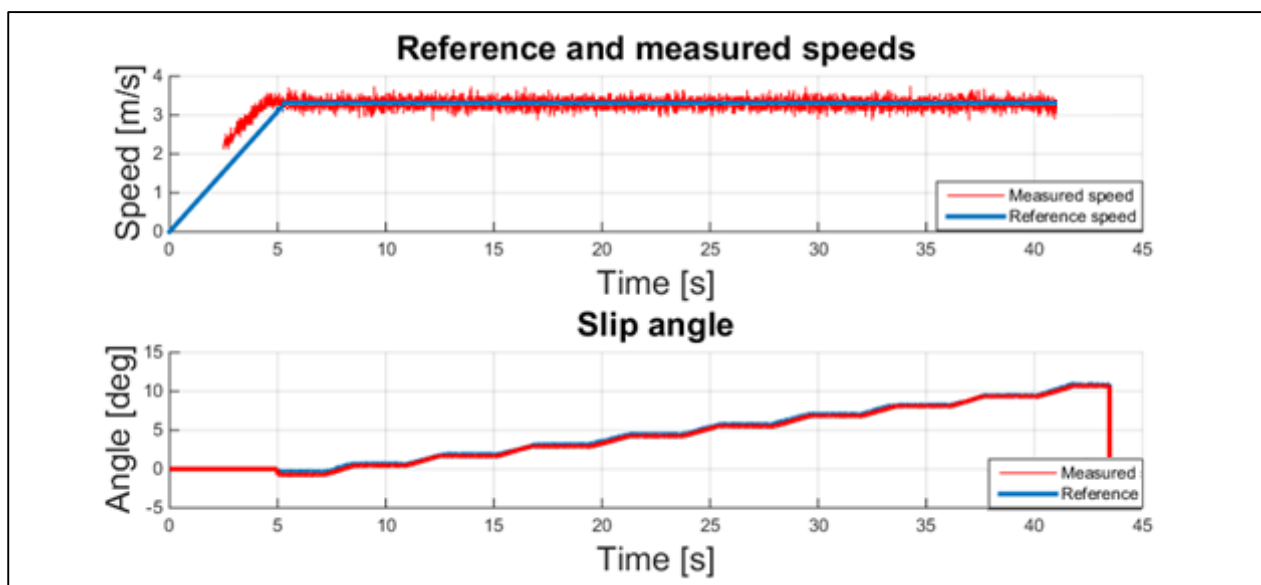


Figure 5-8: Handling test simulation inputs

The camber and castor angles are defined by constant values which are implemented to revolute joints within the outdoor tyre testing equipment model. The varying slip angles of the left-hand side and right-hand side tyres are implemented by means of variable inputs to revolute joints within the outdoor tyre testing equipment model.

This method of implementation ensures that the handling simulations approximate the handling validation tests as closely as possible. The handling MSC Adams (2013) simulations are run in co-simulation with Matlab (2013) by means of a Matlab (2013) Simulink model.

5.2.4 Traction simulation inputs

The longitudinal velocity as well as the left-hand side and right-hand side brake torques are variable inputs for the modelling of the dynamic traction validation tests. The velocity and brake torque variable inputs are depicted in Figure 5-9. The brake torques act on revolute joints between the hub and the wheel and are modelled as variable inputs. The brake torques, which are not physically measured during the dynamic traction validation tests (discussed in Section 3.5.3), are derived from the brake pressure applied to the brake callipers as follows.

According to Budynas et al. (2010), the brake torque for brake callipers, based on a uniform wear model, is expressed as

$$T_{brake} = \frac{1}{2}(\theta_2 - \theta_1)\mu_f p_a r_i (r_o^2 - r_i^2) GR \quad (13)$$

where

$\theta_2 - \theta_1 = 64^\circ$, as defined by Hamersma (2013)

μ_f = a value of 0.4 is estimated, based on the findings of Budynas (2010)

GR = 3.58, as defined by Land Rover (2006)

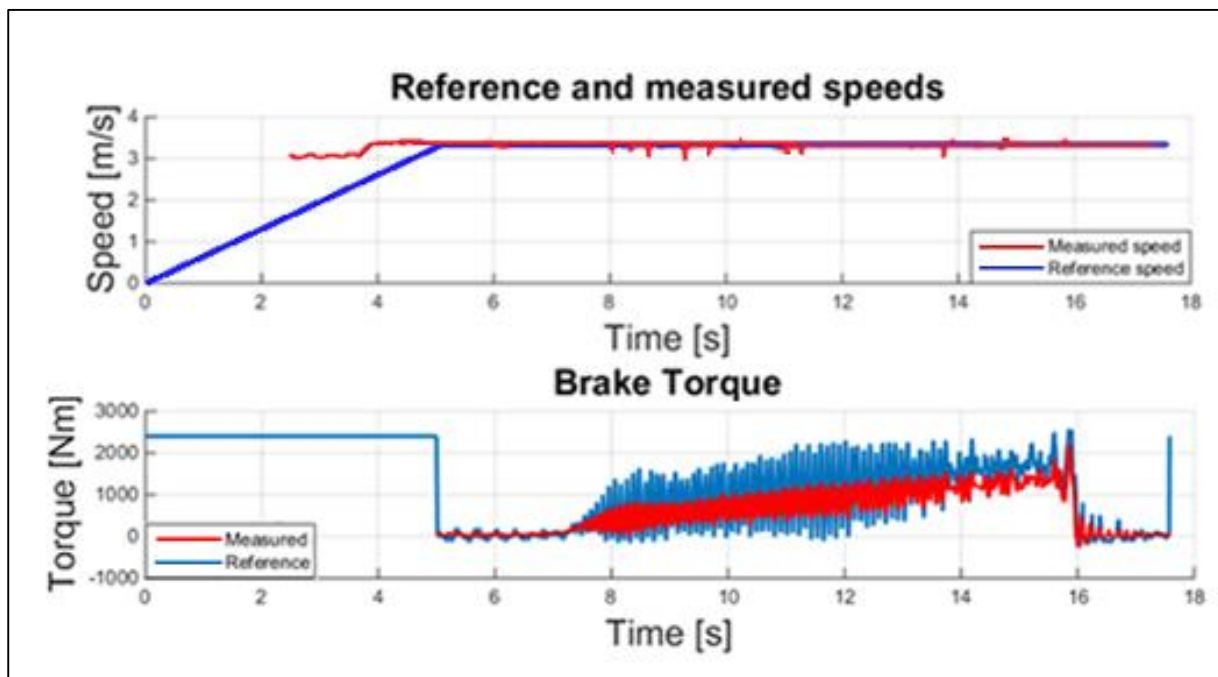


Figure 5-9: Longitudinal test simulation inputs

The brake torque applied to the left-hand side and right-hand side wheels is defined as a variable torque which is applied to the left-hand side and right-hand side wheel joints of the MSC Adams (2013) outdoor tyre testing equipment model, respectively. The variable brake torque inputs ensure that the dynamic traction test simulations approximate the dynamic traction validation tests as closely as possible. The traction MSC Adams (2013) simulations are run in co-simulation with Matlab (2013) by means of a Matlab (2013) Simulink model.

5.2.5 Vertical simulation inputs

The vertical simulations require very specific road surface inputs to conduct the simulations as the dynamic vertical validation tests (discussed in Section 3.5.1) were conducted. The Belgian paving and Fatigue track profiles have been measured previously by Becker et al. (2014) with the Can-Can profilometer. Based on the findings of Becker et al. (2014) CRG road definition files (seen in Figure 5-10) are created to be used in the simulation environment, as stated by Stallmann (2014).

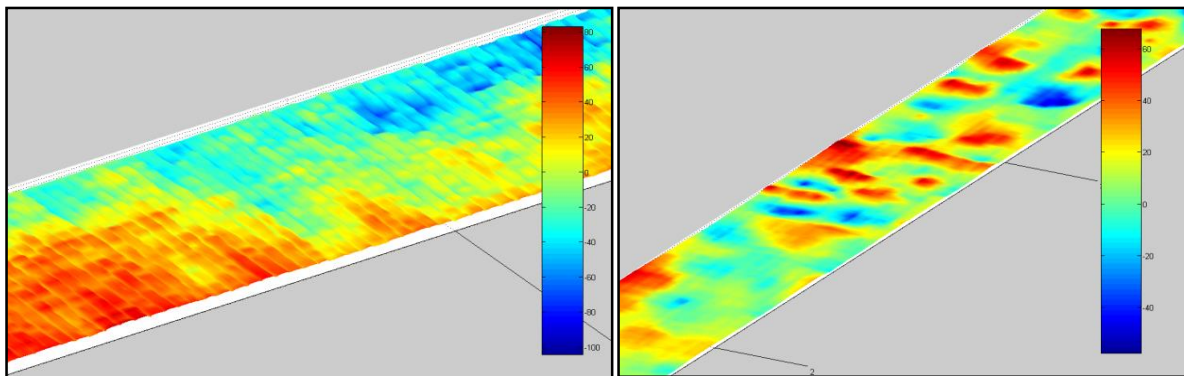


Figure 5-10: Left: Profiled Belgian paving, Right: Profiled Fatigue track (right) (Becker, 2008)

Three different types of cleat roads are used during simulations, namely roads with 25x25mm, 32x32mm and 50x50mm cleats. These roads are created by defining specified cleat sizes on a flat road surface. These road files are based on findings by Stallmann (2014).

The velocity input to the vertical simulations is the same as for the handling and traction simulations. Based on these inputs the vertical simulations are conducted under the same conditions as the dynamic validation tests were conducted, as discussed in Section 3.5.1. The simulation velocity inputs are depicted in Figures 5-11 and 5-12. The vertical MSC Adams (2013) simulations are run in co-simulation with Matlab (2013) by means of a Matlab (2013) Simulink model.

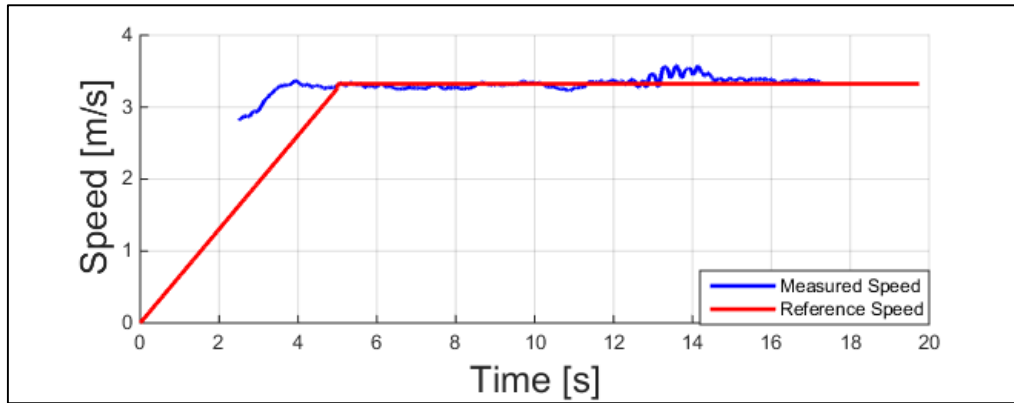


Figure 5-11: First gear simulation speed input for vertical test simulations

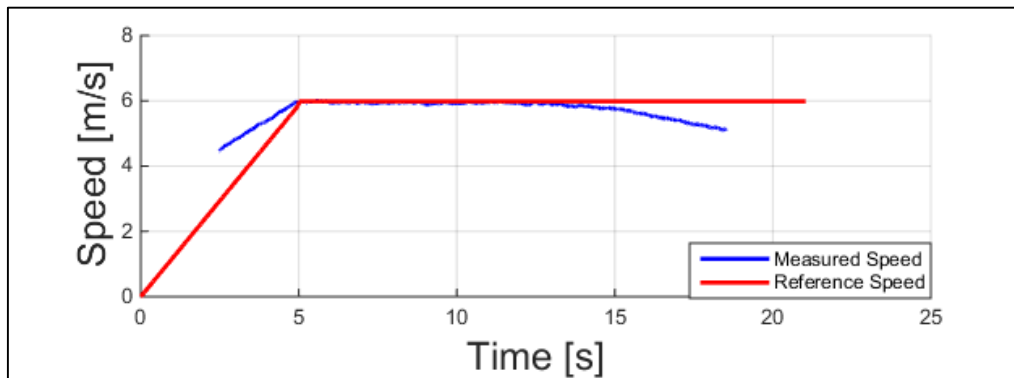


Figure 5-12: Second gear simulation speed input for vertical test simulations

5.3 Lateral tyre properties validation

The validation of the tyre model in the lateral direction is divided into two separate parts, namely the lateral force vs. slip angle and the self-aligning moment vs. slip angle validation. In both these validation parts the camber angle is taken into account. For the lateral tyre properties validation two load cases (LC1 and LC3) and three different camber angles are considered for the validation process while the inflation pressure remains constant at 2 bar.

5.3.1 Lateral force vs. slip angle validation

The lateral force, generated by the tyre due to a change in slip angle as well as camber angle, is being considered. The lateral forces generated by the tyre during validation field tests are simulated by varying the slip and camber angles of the wheels in the simulation environment, as discussed in Section 5.2.3.

The lateral forces, generated by the tyres during dynamic field tests, are validated against those generated by the FTire model in the simulation environment. Two load cases are considered, namely LC1 and LC3.

Figure 5-13 shows the measured and the simulated data for lateral forces generated by the tyres at 2 bar inflation pressure (LC1) at 0° camber angle.

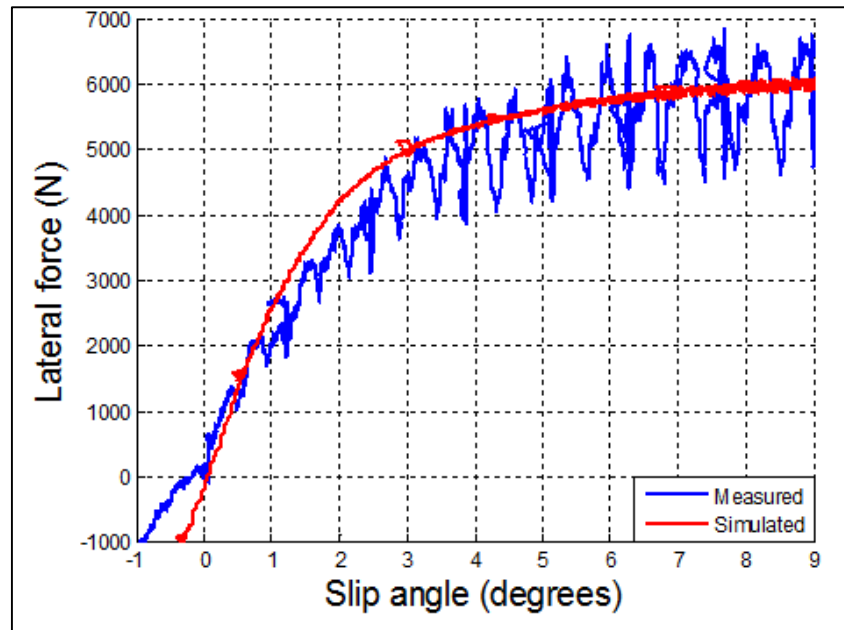


Figure 5-13: Lateral force vs. slip angle (LC1) at 0 degrees camber angle

From Figure 5-13 it is seen that the lateral forces generated by the tyre and those generated by the FTire model follow a similar trend at slip angles greater than 0 degrees. However, the measured data appears to have some form of an oscillatory disturbance within the signal.

This oscillatory disturbance is likely to have originated from a combination of the nature of longitudinal translation and road undulations. It was observed during the testing procedure that the left-hand side wheel wobbled during the testing procedure and which may likely have contributed to the oscillatory disturbance in the measured signal. Furthermore, a distinct bouncing motion of the outdoor tyre testing equipment was observed during the dynamic validation tests, as discussed in Section 3.5.

When considering the simulation signal, the same phenomenon may be seen. High frequency low amplitude oscillatory noise is observed in the signal, increasing as the slip angle is increased. However, it should be noted that the road defined in the simulation environment is a perfectly flat road which has no imperfections or undulations in the road surface.

The RMS error and the %RE are calculated for all lateral force vs. slip angle tests and corresponding simulations. The conclusion is drawn is that the tyre model tyre behaviour prediction gives results which do not correlate due to the noisy experimental data results. Due to the difference in nature between the measured and simulated data signals a direct validation is not possible. Therefore, the following attempt is made to validate the measured and simulated data signals against one another.

Due to the nature of the sweeping of the slip angle in one degree increments during the handling validation field test runs, as described in Section 3.5.2 and shown in Figure 5-8, a cluster of data is available for certain slip angles.

Therefore, the mean of each of these data clusters for each one degree slip angle increments is determined. The mean of each of these clusters, as well as the slip angle at which these occur are superimposed over the measured and simulated data results, as shown in Figure 5-14. And are seen to correlate better to the simulated data results. Therefore, the validation process is repeated for all handling tests and simulations conducted, based on the validation test cluster data sets and the simulated data sets at the corresponding slip angles.

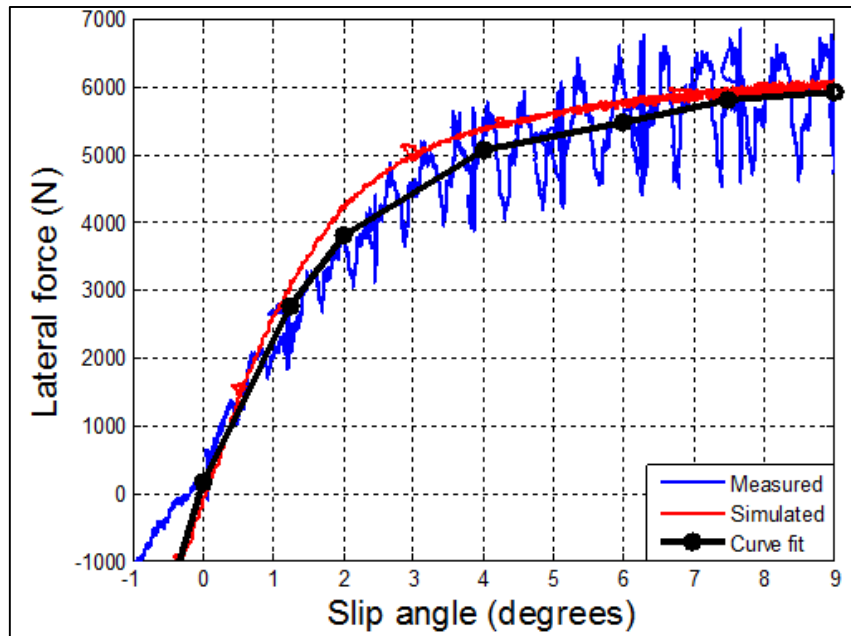


Figure 5-14: Validation method in the lateral direction

Table 5-3 depicts the validation results between measured and simulated signals for the lateral force vs. slip angle for three load cases and camber angles. All lateral force vs. slip angle validation test results are shown graphically in Appendix A.

Table 5-3: Validation results for lateral force vs. slip angle for three load cases and camber angles

Load case	Camber angle (degrees)	RMS (N)	m%RE ^m	m%RE ^s
LC1	-2	263.834	13.765% P(71.020%)	15% P(74.850%)
	0	240.745	9.876% P(69.320%)	15% P(83.620%)
	2	201.653	10.035% P(75.810%)	15% P(84.320%)
LC3	-2	432.514	12.729% P(69.820%)	15% P(76.760%)
	0	387.995	10.604% P(76.460%)	15% P(87.510%)
	2	319.642	9.743% P(70.760%)	15% P(82.190%)

From the results listed in Table 5-3 it becomes clear that the results for the lateral force vs. slip angle validation between the curve fit data points of the measured results and simulated data signals correlate well. The relative error percentage does not exceed 14% in any of the test validations. The RMS values depicted in Table 5-3 depict the difference between the curve fit measurement results and simulated data results.

5.3.2 Self-aligning moment

The self-aligning moment generated by the tyres due to the effect of varying slip and camber angles is validated against the self-aligning moment predicted by the FTire model in the simulation environment. The variation of the slip and camber angles is simulated and the resulting moment predicted by the FTire model is obtained.

Three vertical load cases are considered and Figure 5-15 shows the measured and simulated data results of a dynamic handling validation test run at 2 bar inflation pressure, LC1 and at 0° camber angle.

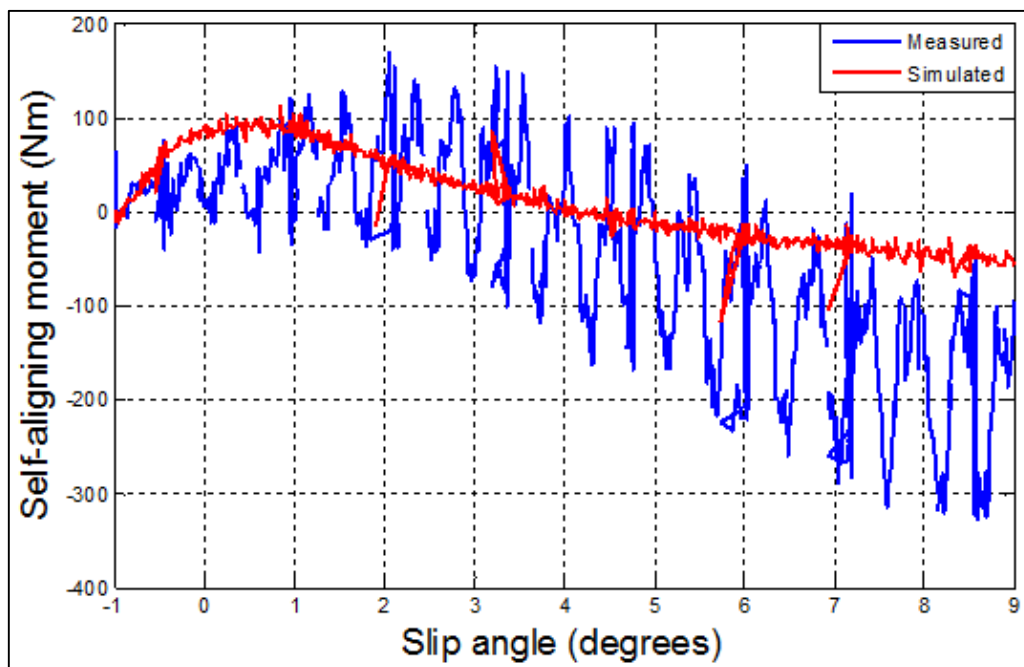


Figure 5-15: Self-aligning moment vs. slip angle (LC1) at 0 degrees camber angle

From Figure 5-15 it is seen that the self-aligning moment generated by the tyre and that predicted by the FTire follow a similar trend. The same methodology as implemented in Section 5.3.1 is implemented to validate the measured and simulated signals against one another. The results of the validation are given in Table 5-4. All self-aligning moment vs. slip angle validation test results are shown graphically in Appendix A.

Table 5-4: Validation results for self-aligning moment vs. slip angle for three load cases and camber angles

Load case	Camber angle (degrees)	RMS (Nm)	m%RE ^m	m%RE ^s
LC1	-2	73.987	43.078% P(67.060%)	15% P(20.050%)
	0	68.768	69.067% P(74.920%)	15% P(9.490%)
	2	71.479	39.021% P(68.030%)	15% P(22.640%)
LC3	-2	156.786	49.978% P(77.940%)	15% P(14.070%)
	0	145.752	52.037% P(81.940%)	15% P(8.280%)
	2	132.970	32.981% P(68.400%)	15% P(18.930%)

From Table 5-4 it is found that the self-aligning moment vs. slip angle validation results do not correlate as well as the lateral force vs. slip angle validation results. The mean of the %RE for all cases does not fall below a threshold of 32%. This means that the validation of the measured and simulated results of the self-aligning moment yield a correlation that is not favourable. The RMS values depicted in Table 5-4 depict the difference between the curve fit measurement results and simulated data results.

5.4 Longitudinal tyre properties validation

The validation of the tyre model in the longitudinal direction is divided into two separate parts, namely the longitudinal force and the braking moment validation. Due to the dynamics of the outdoor tyre testing equipment's braking system the braking force vs. longitudinal slip and braking moment vs. longitudinal slip characteristics cannot be validated. Therefore, the longitudinal force vs. time and braking moment vs. time measurements and simulations are validated against one another. Three load cases (LC0, LC1 and LC3) are considered in the longitudinal tyre properties validation while the tyre inflation pressure is kept at a constant 2 bar.

5.4.1 Longitudinal force

The longitudinal force generated by the tyre due to a braking torque applied is being considered. The longitudinal forces generated by the tyre during the dynamic validation field tests, as discussed in Section 3.5.3, are simulated by applying a brake torque on the wheels in the simulation. Figure 5-16 shows the measured and simulated result data set for LC0.

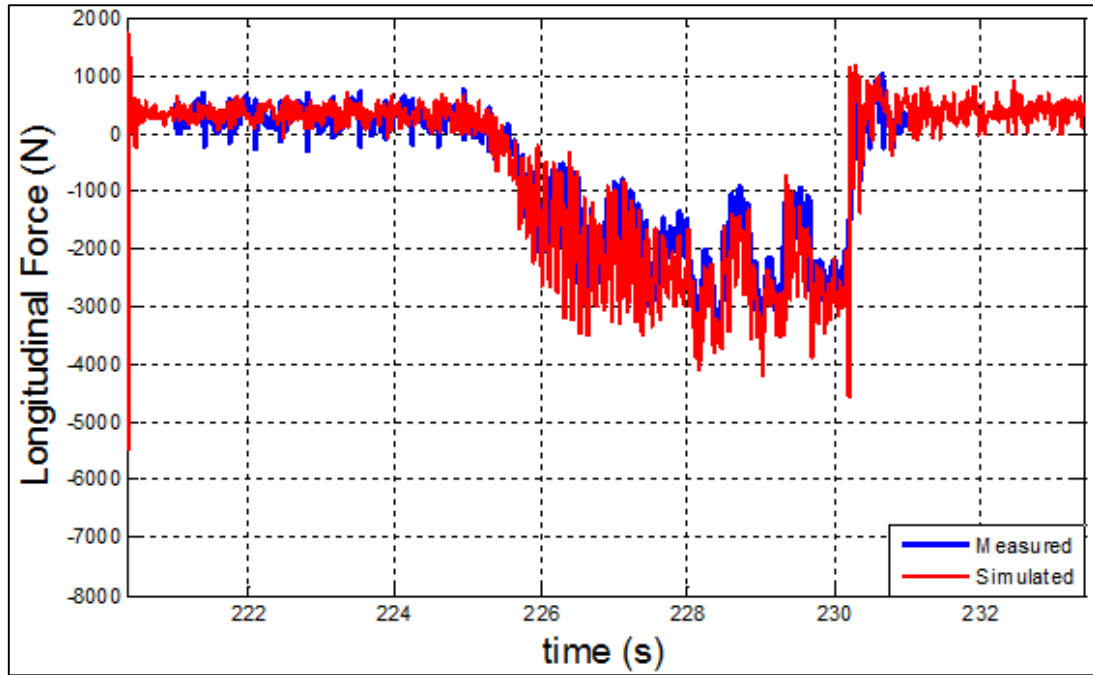


Figure 5-16: Longitudinal force (LC0) at 2 bar inflation pressure

At first glance the correlation of the measured and simulated data sets is good. The metrics utilized to validate the measured and simulated data sets are shown in Table 5-5 below where it is seen that the RMS error clearly increases as the vertical load increases while the %RE remains relatively constant. All longitudinal force validation test results are shown graphically in Appendix A.

Table 5-5: Validation results of longitudinal force for three load cases

Load case	RMS (N)	m%RE ^m	m%RE ^s
LC0	601.9	7.2% P(86.380%)	15% P(95.150%)
LC1	780.8	6.4% P(82.500%)	15% P(94.380%)
LC3	1264.3	8.8% P(83.970%)	15% P(91.530%)

From the results listed in Table 5-5 it becomes clear that the results for the longitudinal force validation between the measured and simulated signals correlate well. The relative error percentage does not exceed 8.8% in any of the validation cases. In all cases the number of points of the relative error percentage for a mean relative percentage of 15% does not fall underneath a 91% threshold. Therefore, the longitudinal force validation yields a good correlation between the measured and simulated result signals. The RMS values depicted in Table 5-5 depict the difference between the measured and simulated data results.

5.4.2 Braking moment

The braking moment, generated by the tyres during braking, is validated against the moment generated by the tyre model in the simulation environment. The brake torque applied to the wheels during the dynamic validation tests, as discussed in Section 3.5.3, is simulated and the resulting moment generated by the FTire model is obtained. Figure 5-17 shows the measured and simulated data set results for the braking moment at LC0.

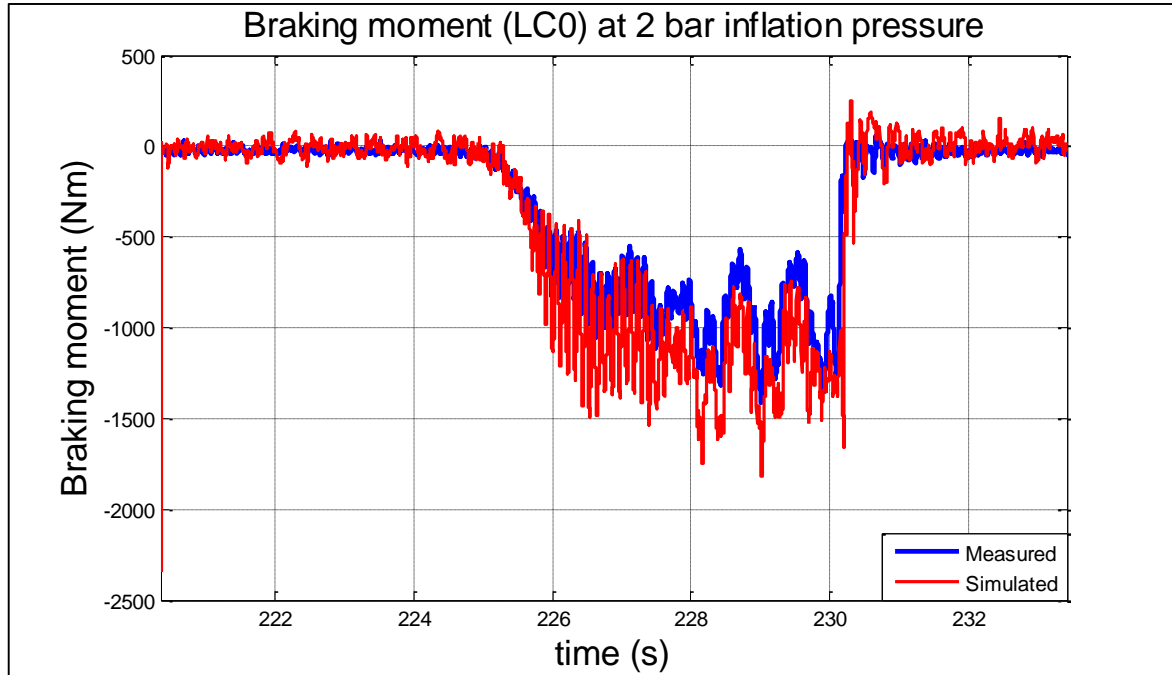


Figure 5-17: Braking moment (LC0) at 2 bar inflation pressure

To validate the correlation between the two data results the RMS error as well as the %RE metrics are calculated. The validation results may be seen in Table 5-6. All braking moment validation test results are shown graphically in Appendix A.

Table 5-6: Validation results of the braking moment for three load cases

Load case	RMS (Nm)	m%RE ^m	m%RE ^s
LC0	208.2	7.8% P(81.080%)	15% P(95.970%)
LC1	365	6.7% P(86.710%)	15% P(98.580%)
LC3	431.8	10.0% P(77.140%)	15% P(93.080%)

From the results listed in Table 5-6 it becomes clear that the results for the braking moment validation between the measured and simulated signals correlate well. The relative error percentage does not exceed 10% in any of the validation cases. In all cases the number of points of the relative error percentage for a mean relative percentage of 15% does not fall underneath the 93% threshold.

Therefore, the braking moment validation yields a good correlation between the measured and simulated results. The RMS values depicted in Table 5-6 depict the difference between the measured and simulated data results.

5.5 Vertical tyre properties validation

The validation of the FTire tyre model in the vertical direction consists of two sections. The first section deals with the validation of the FTire model over discrete obstacles and the second section deals with the validation of the tyre model over rough terrain. One vertical load (LC0) is considered at two different speeds (3.5m/s and 6 m/s) while the tyre inflation pressure is kept at a constant 2 bar.

5.5.1 Discrete obstacles

The discrete dynamic obstacle tests, as discussed in Section 3.5.1.1, include dynamic cleat tests which were performed. The dynamic cleat tests consist of three distinct phases which are classified as before impact, during impact and after impact phases.

The before impact phase holds no significant information other than the equilibrium forces and moments of the tyre. The impact phase is the most important phase as it is used in validating the extent to which the FTire model is able to capture and predict the tyre's behaviour while negotiating a discrete obstacle. The after impact phase consists of the tyre's behaviour after negotiating the obstacle and holds information of the dynamic damping of the tyre.

It is decided to make use of the second and third phases of the cleat tests to validate the FTire model for discrete obstacles. Figure 5-18 depicts an example of the dynamic cleat tests and the two parts of the validation are depicted graphically as the impact phase (green) and the after-impact phase (red).

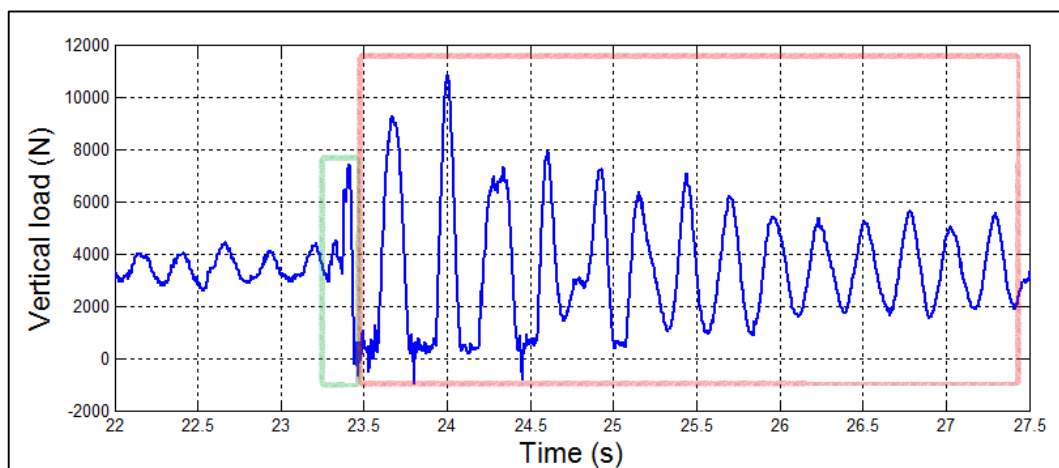


**Figure 5-18: Vertical validation phases for a 50x50mm cleat test (LC0) at 6m/s Green: Impact phase.
Red: After impact phase**

Figure 5-19 shows the measured and simulation results of a 50x50mm cleat test (LC0) at 6 m/s. It can be seen that the cleat impact phase is approximated well by the simulation model. The after-impact phase is seen to deviate slightly between the measured and simulated signals. This is largely attributed to measurement noise and externally introduced disturbance factors as discussed in Section 3.5.1.1.

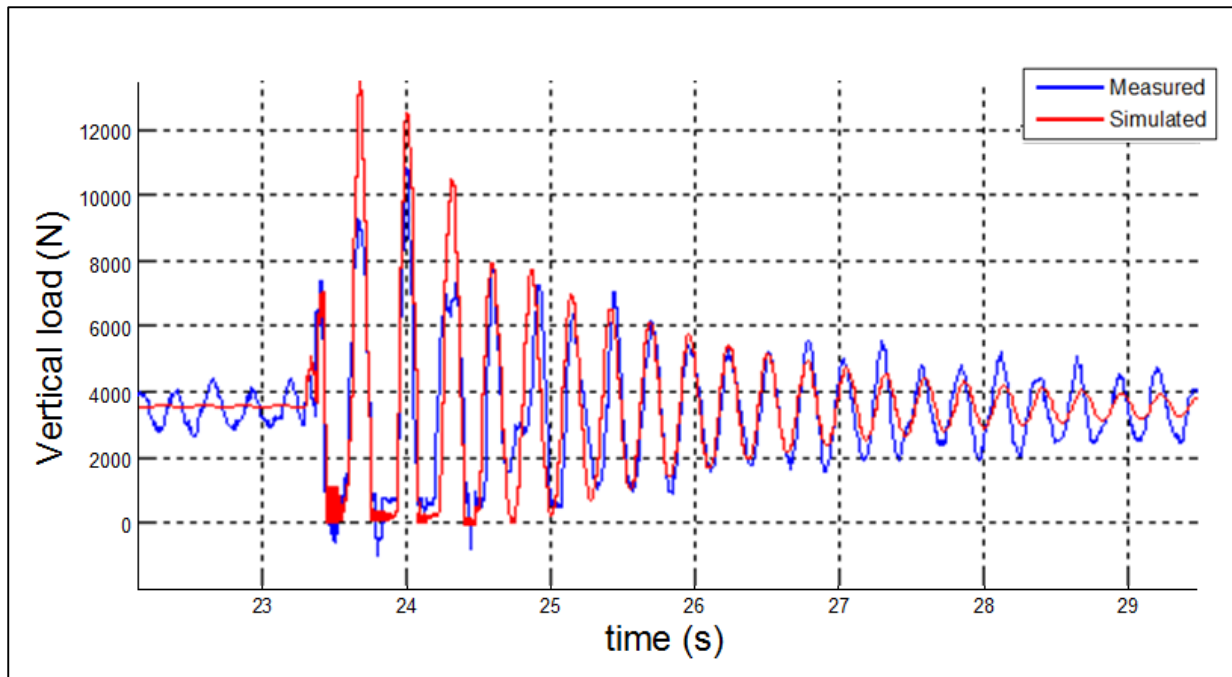


Figure 5-19: Measured and simulated 50x50mm cleat test (LC0) at 6m/s

The two phases of the cleat tests are validated by implementing the RMS error and %RE metrics. However, from Figure 5-19 it is seen that the second phase of the simulated and measured data sets vary in oscillatory period. Therefore, a direct validation of the signals would hold no valuable information.

It is, therefore, decided that only the oscillatory peaks of the measured and simulated signals are considered in the after impact phase for the validation since these hold valuable information about the tyre's response behaviour after having encountered the obstacle. The results of the validation for the measured and simulated data sets are shown in Tables 5-7 and 5-8. All dynamic cleat test validation results are shown graphically in Appendix A.

Table 5-7: Cleat test validation results for 3.5 m/s test for LC0 at 2 bar inflation pressure

Cleat size	Impact phase			After impact phase		
	RMS (N)	m%RE ^m	m%RE ^s	RMS (N)	m%RE ^m	m%RE ^s
25x25mm	288.443	7.207% P(68.330%)	15% P(88.890%)	231.027	4.529% P(70.050%)	15% P(92.700%)
32x32mm	210.634	12.833% P(81.730%)	15% P(90.845%)	1555.721	13.933% P(72.160%)	15% P(82.153%)
50x50mm	316.894	5.451% P(64.600%)	15% P(92.105%)	1317.917	15.248% P(68.290%)	15% P(64.450%)

The results for the 3.5 m/s cleat test validation between the measured and simulated signals correlate well. The relative error percentage does not exceed 12% in any of the obstacle encounter and 15.2% for the after obstacle validation cases. In all cases the number of points of the relative error percentage for a mean relative percentage of 15% does not fall underneath a 82% threshold.

Therefore, the 3.5 m/s cleat test validation yields a good correlation between the measured and simulated result signals. The RMS values depicted in Table 5-7 depict the difference between the measured and simulated data results.

Table 5-8: Cleat test validation results for 6 m/s test for LC0 at 2 bar inflation pressure

Cleat size	Impact phase			After impact phase		
	RMS (N)	m%RE ^m	m%RE ^s	RMS (N)	m%RE ^m	m%RE ^s
25x25mm	371.496	9.988% P(67.210%)	15% P(81.970%)	862.424	13.338% P(85.980%)	15% P(90.000%)
32x32mm	522.919	11.353% P(71.570%)	15% P(82.280%)	806.289	11.590% P(76.540%)	15% P(85.000%)
50x50mm	590.6467	8.438% P(66.010%)	15% P(87.952%)	1538.012	14.376% P(76.450%)	15% P(74.950%)

The results for the 6 m/s cleat test validation between the measured and simulated signals correlate well, as shown in Table 6-6. The relative error percentage does not exceed 11.4% in any of the obstacle encounter and 14.4% for the after obstacle validation cases. In all cases the number of points of the relative error percentage for a mean relative percentage of 15% does not fall underneath a 74.9% threshold. Therefore, the 6 m/s cleat test validation yields a good correlation between the measured and simulated result signals. The RMS values depicted in Table 5-8 depict the difference between the measured and simulated data results.

5.5.2 Rough terrain

The tracks on which the dynamic rough terrain tests are conducted, as discussed in Section 3.5.1.2, are located at the Gerotek Test Facilities (2013) and include the Belgian paving and the Fatigue track.

Figure 5-20 shows the measured and simulated data sets obtained over the Belgian paving track at 3.5 m/s while Figure 5-21 shows the measured and simulated data sets obtained over the Fatigue track at 3.5 m/s. Both data sets do not correlate well in the time domain due to the fact that, even a slight path deviation over the test track, may result in a significant difference in vertical force response.

In Figure 5-21 large negative peaks are seen in the measured results. During the dynamic validation tests on the Fatigue track, discussed in Section 3.5.1.2, the tyre was observed to hop considerably with the tyres losing contact with the ground occasionally which the negative peaks in the measured response are attributed to.

From Figures 5-20 and 5-21 it is seen that the simulation results do not give a negative vertical load prediction of the tyre. This is due to the fact that the simulation model measures the forces exerted by the FTire model on the tyre itself and neglects the weight of the tyre model. Therefore, if during a simulation the tyre testing rig model experiences a loss of contact between the FTire model and the simulated road surface it predicts that the vertical load of the tyre is zero since it does not experience any load other than its own weight.

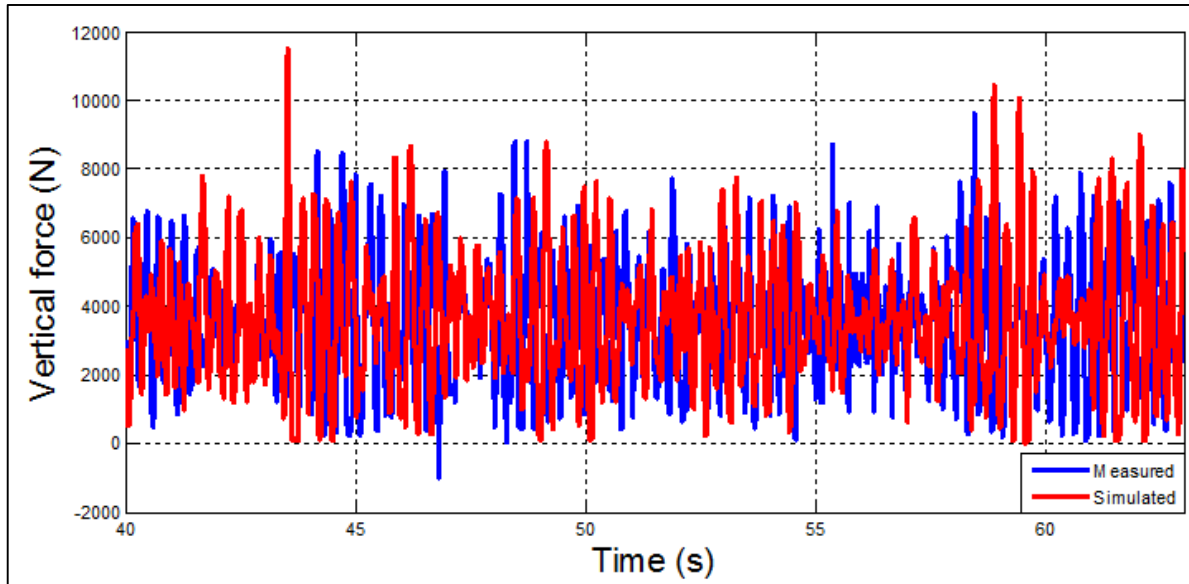


Figure 5-20: Measured and simulated results of the Belgian paving (LC0) at 3.5 m/s

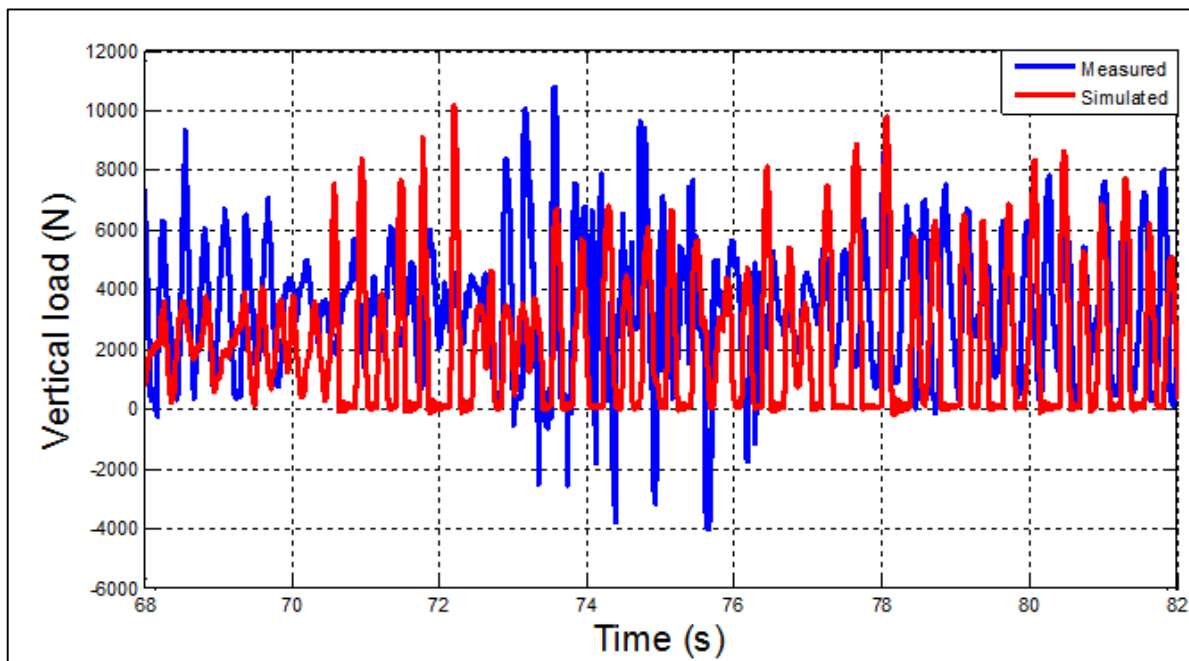


Figure 5-21: Measured and simulated results of the Fatigue track (LC0) at 3.5 m/s

The RMS and %RE errors determined in the time domain confirm that the measured and simulated signals do not correlate in the time domain. Therefore, this validation technique gives inconclusive results.

A second validation technique, namely the probability theorem is considered which involves the analysis of random phenomena. Therefore, this validation technique comprises of determining the probability that a certain vertical load is measured during a dynamic validation test as well as the corresponding simulation.

The mathematical probability theorem is applied as a validation method by considering the normal or Gaussian distribution of each of the validation test and simulation time signals. The Gaussian distribution is able to accurately predict the probability that any observation or signal will fall between any two real limits.

The Gaussian or normal distribution may be defined as follows:

$$f(x, \mu, \sigma) = \frac{1}{\sigma\sqrt{2\pi}} e^{-\frac{(x-\mu)^2}{2\sigma^2}} \quad (14)$$

The mean and the standard deviation are the parameters utilized to validate the measured and simulated data sets against one another. Figure 5-22 shows an example of a Gaussian distribution.

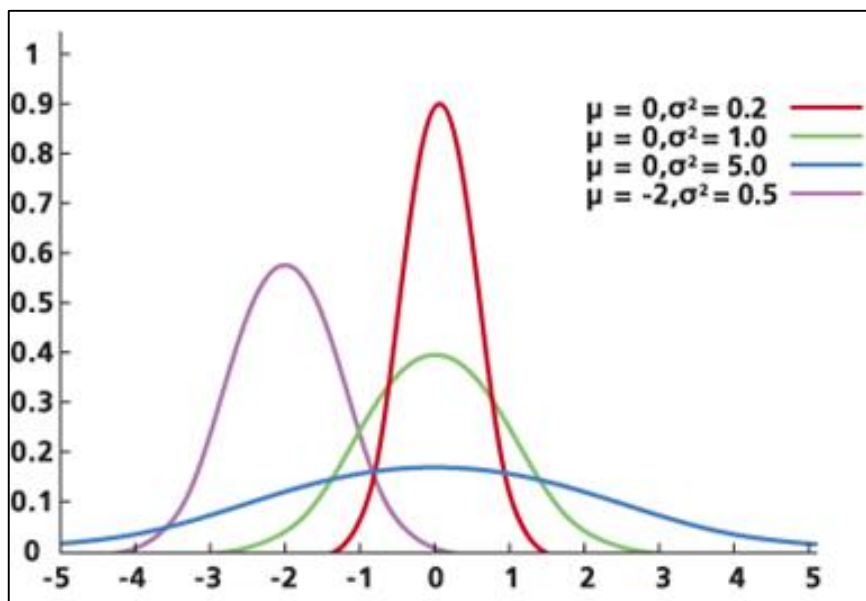


Figure 5-22: Gaussian (normal) distribution example (Distributions, 2014)

The standard deviation indicates the behaviour of the vertical load characteristics of the tyre. It is seen that the standard deviation holds more information about the accuracy of the FTire model's ability to predict tyre behaviour since it is more dominantly defined by the vertical load distribution. Furthermore, the standard deviation of the data sets may indicate a difference of the tyre damping behaviour between the tyre and the tyre model.

The mean holds information about the vertical static load. A difference in the mean between the measured and simulated signals is expected if there is a difference between the static vertical load experienced by the tyre and the tyre model or if either has significantly more ground contact loss than the other.

Based on the normal distribution of the measured and simulated signals the data sets are validated against one another by fitting a normal distribution curve to each data set. Figure 5-23 shows how the normal distribution curve is fitted over a dynamic vertical validation test data set.

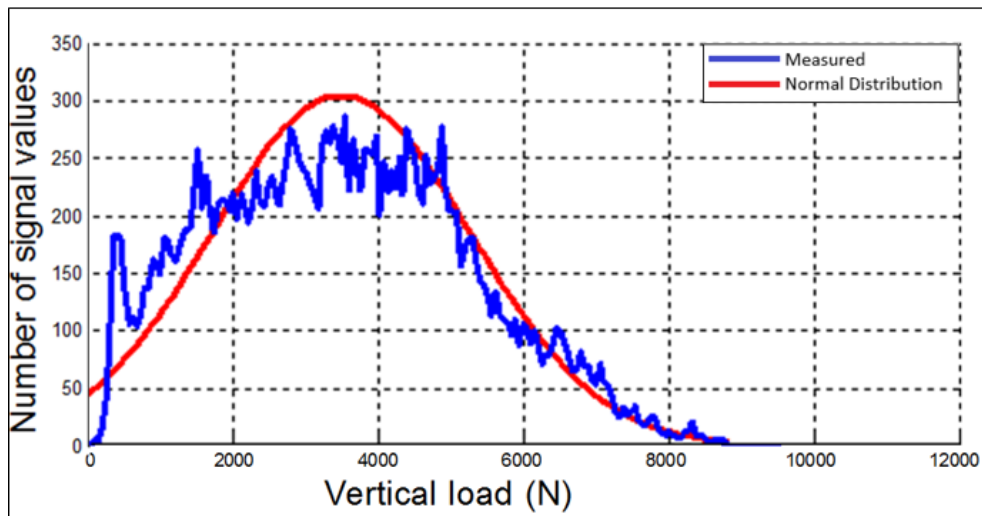


Figure 5-23: Normal distribution curve fit to vertical validation test data on the Belgian paving at 3.5 m/s

5.5.2.1 Belgian paving

The vertical load probability density behaviour over the Belgian paving is analysed by considering the normal distribution of the vertical load behaviour of the measured and simulated results, as shown in Figure 5-24. The validation results for the Belgian paving are shown in Table 5-9. All Belgian paving validation test results are shown graphically in Appendix A.

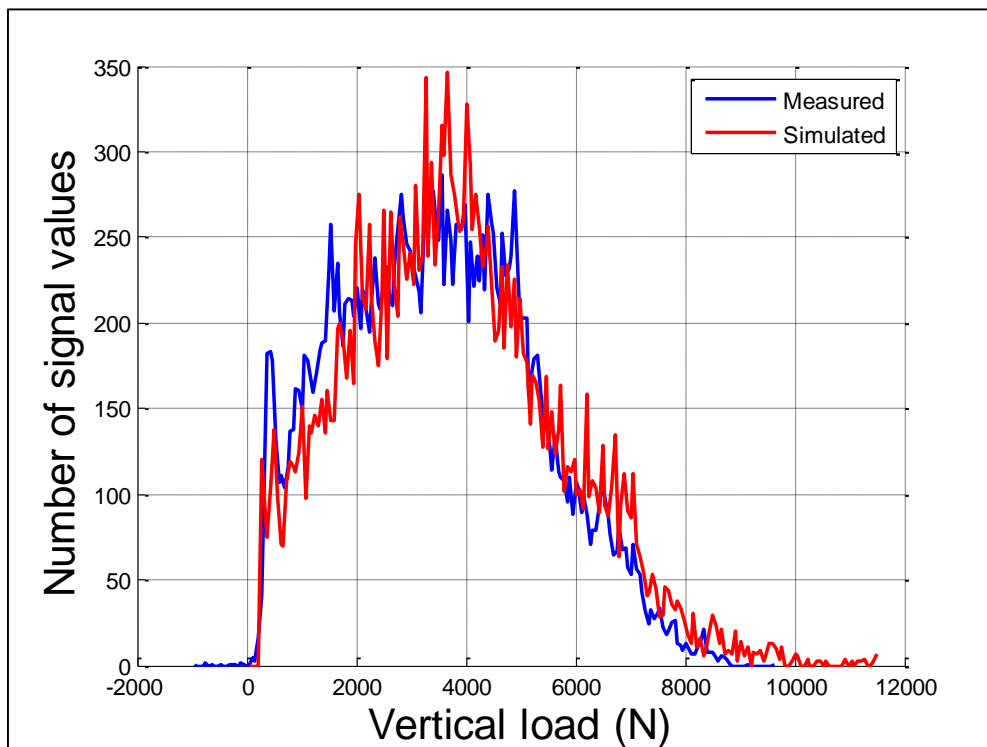


Figure 5-24: Normal distribution of the vertical load (LC0) over the Belgian paving at 3.5 m/s

Table 5-9: Validation results for the Belgian paving

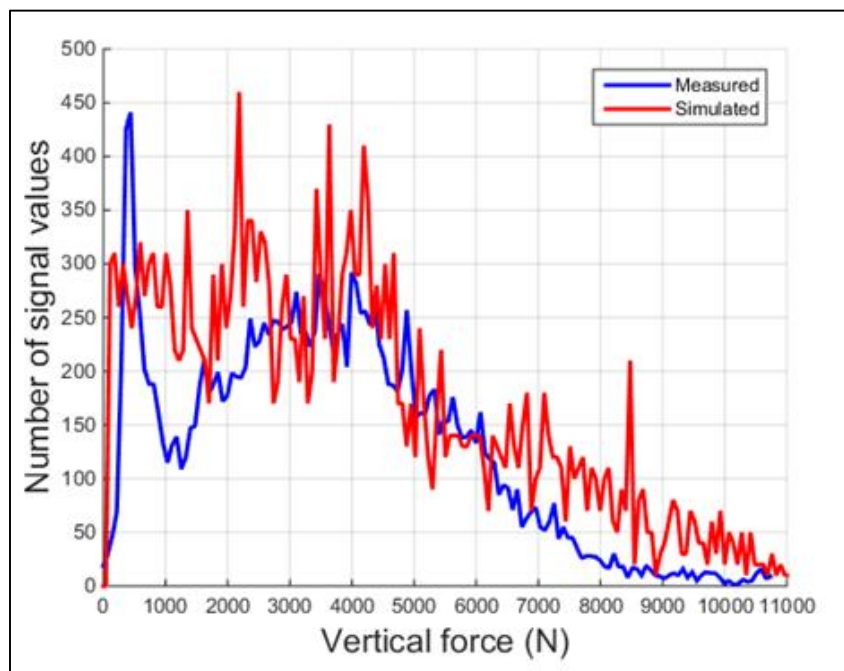
Velocity (m/s)		Measured	Simulated	%RE
3.5	Mean (μ)	3502.602	3659.440	4.483%
6		3483.942	3318.347	4.753%
3.5	Standard deviation (σ)	1781.641	1988.983	11.638%
6		2634.368	2090.179	20.657%

From the results in Table 5-9 above it is seen that the mean of the simulated and the measured data sets for both speeds do not deviate by more than 5% relative error indicating a good correlation between the data sets.

The standard deviation of the data sets is seen to deviate significantly more for the 6m/s test. The standard deviation is seen to not deviate by more than 21% relative error indicating a correlation that is not favourable between the measured and simulated data sets.

5.5.2.2 Fatigue track

The vertical load probability density behaviour over the Fatigue track is analysed by considering the normal distribution of the vertical load behaviour, as seen in Figure 5-25. The validation results for the Fatigue track are shown in Table 5-10. All fatigue track validation test results are shown graphically in Appendix A.

**Figure 5-25: Normal distribution of the vertical load (LC0) over the Fatigue track at 3.5 m/s**

From the results in Table 5-10 it is seen that the mean of the simulated and the measured data sets for both speeds do not deviate by more than 17% relative error indicating a correlation that is not favourable between the data sets.

Table 5-10: Validation results for the Fatigue track

Velocity (m/s)		Measured	Simulated	%RE
3.5	Mean (μ)	3423.028	2886.509	15.674%
6		3426.653	2899.555	16.382%
3.5	Standard deviation (σ)	2185.468	2931.099	34.118%
6		2098.520	2712.295	29.248%

The standard deviation of the data sets is seen to not deviate by more than 35% relative error indicating a bad correlation between the measured and simulated data sets. The results in Tables 5-9 and 5-10 show that the correlation between the mean and the standard deviation for both speeds over the Belgian Paving is superior to that over the Fatigue track.

5.6 Chapter summary

In this chapter the FTire model was validated against measured test data. Numerous validation metrics were discussed and it was found which metrics were applicable to which validation data sets.

The Adams model, which was used to validate the FTire model, and the simulation procedure implemented to simulate the validation tests conducted was discussed in detail. The position of the centre of gravity as well as the roll and pitch moments of inertia of the outdoor tyre testing rig, which was used to acquire dynamic parameterization and validation data, were determined experimentally. These results were applied to the outdoor tyre testing equipment model in MSC Adams (2014).

The validation of the lateral tyre behaviour yielded that the FTire model was not able to predict the tyre behaviour accurately. However, by utilizing the curve fit data in the handling validation process, as discussed in Section 5.3.1, it is found that the validation process yielded acceptable results. Based on the %RE results it was found that the correlation was not as good as the longitudinal tyre behaviour. However, it was concluded that the amount of measurement noise in the dynamic handling tests far exceeded that of the dynamic traction tests.

From the validation results it was found that the FTire model was able to accurately predict the longitudinal tyre behaviour. The %RE results between the measured and simulated data results yielded a good correlation between the signals.

The vertical tyre behaviour validation between the measured and simulated data sets was divided into two sections, namely the discrete and rough terrain obstacles. The discrete obstacle validation yielded a good tyre behaviour prediction by the FTire model.

The vertical tyre behaviour validation over rough terrain was not conducted in the time domain. A Gaussian distribution of the data sets was considered. The FTire model tyre prediction was seen to give good correlations with the measured results. It was found that the FTire model was able to predict the vertical tyre behaviour over the Belgian paving more accurately than over the Fatigue track.

The conclusion drawn from the validation process was that the FTire model was able to predict the tyre behaviour in the lateral, longitudinal and vertical direction.

6 Conclusion and recommendations

6.1 Conclusion

A literature survey was conducted from which information about pneumatic tyre construction and tyre characteristics in the lateral, longitudinal and vertical direction were considered. Factors affecting tyre handling and traction performance were discussed.

Several tyre and road contact models, ranging from the point contact model to the flexible ring model, and their application in MSC Adams (2013) were discussed in detail. It was found that the FTire model, developed by Cosin, is most suitable for handling simulations on smooth road surfaces and ride comfort simulations over rough terrain in MSC Adams (2013). Therefore, the FTire model was investigated and described in great detail.

It was argued that the FTire parameterization process relied heavily on parameterization data. The static and dynamic parameterization tests, conducted to parameterize the FTire model, were discussed in detail and it was found that the static and dynamic parameterization tests gave reliable and useful results.

The acquisition of handling, traction and ride comfort validation test data using the outdoor tyre testing equipment was discussed in detail. The traction validation test data revealed that the longitudinal force vs. slip characteristics could not be used for validation purposes since the tyre being tested was found to rotate backwards during traction validation tests.

In the detailed discussion of the FTire parameterization process, which was based heavily on static parameterization data, it was found that it was necessary to perform a large amount of parameterization iterations to obtain an FTire model with sufficient accuracy to predict tyre behaviour. The parameterization of the damping behaviour of the FTire model was based on dynamic cleat test results.

A high fidelity multi-body dynamics MSC Adams (2013) model was used to simulate the FTire model. The simulation inputs, which were based on dynamic validation test results, were discussed in detail. To ensure the validity of the simulations the position of the centre of gravity, as well as the pitch and roll moments of inertia, of the outdoor tyre testing equipment were determined experimentally. These results proved to be vital in the validation process since the simulation model was heavily based on the outdoor tyre testing equipment.

Validation metrics, which were used to validate the FTire model simulations with dynamic validation test results, were introduced. Based on the validation results it was found that the FTire model was able to predict the tyre behaviour with sufficient accuracy. Simulations of the FTire model on smooth road surfaces gave acceptable results for the handling simulations and good results for tractive simulations. The ride comfort simulations revealed that the FTire model was able to predict tyre behaviour over discrete obstacles accurately and well over rough terrain.

The conclusion was drawn that the parameterized FTire model, based primarily on static parameterization data, was able to predict the Michelin LTX all-terrain tyre behaviour over smooth road surfaces and rough terrain. This has made a unique contribution since no previous FTire model of an all-terrain tyre is available for vehicle simulations. Vehicle simulations may readily incorporate the FTire model for tyre behaviour prediction over smooth and rough terrain.

6.2 Recommendations

It is recommended that the outdoor tyre testing equipment be developed further to accommodate some form of suspension that may assist in minimizing the hopping motion of the tyre testing rig during the testing procedures. By eliminating externally induced disturbances to the dynamic tests, the acquired data may likely be used for the parameterization of the FTire model. The WFT (Becker et al., 2012) has proven to give accurate results for static and dynamic tyre tests. Therefore, the WFT (Becker et al., 2012) may be implemented with an updated outdoor tyre testing rig.

The procedure of the laboratory tests which were conducted to obtain parameterization data for the FTire model could possibly be improved. It is recommended that, when investigating the longitudinal, lateral and torsional tyre stiffnesses the tests should be conducted on various concrete surfaces, rather than on a steel plate. This could possibly improve the in-plane parameterization process and aid in parameterizing an improved FTire model.

A laboratory testing rig, implemented to conduct low speed dynamic tyre tests, should be constructed. This testing rig, which should preferably also be lined with concrete, could be used to obtain lateral and longitudinal force data by varying the slip angle and longitudinal slip, respectively, while the tyre is translated over the testing rig at a low speed giving potentially valuable parameterization data.

Lastly, it is recommended to further develop the FTire/fit solver. It was found that the FTire/fit solver was rudimentary and improving the ability of the solver to optimize the FTire/fit parameters could greatly assist in parameterizing an improved FTire model.



7 References

1. Acuity, Laser Displacement Sensor., Laser Measuring Device., Laser Sensors., 2014. *Laser Displacement Sensor, Laser Measuring Device, Laser Sensors*. [ONLINE] Available at:<http://www.acuitylaser.com/products/item/ar700-laser-displacement-sensor>. [Accessed 1 April 2014].
2. Barbosa, L. A. P., Magalhaes, P. P. G., 2015. Tire tread pattern design trigger on the stress distribution over rigid surfaces and soil compaction. *Journal of Terramechanics*, 58, 27-38.
3. Becker, C. M., Els, P. S., 2014. Profiling of rough terrain. *International Journal of Vehicle Design*, 64, 240-261.
4. Becker, C.M., 2008, Profiling of rough terrain, Unpublished MEng Thesis, University of Pretoria, Pretoria, South Africa.
5. Becker, C. M., & Els, P. 2012. Wheel Force Transducer Measurements on a Vehicle in Transit. *Proceedings of the 12th European Regional Conference of the ISTVS*. Pretoria, South Africa.
6. Blundell, M., Harty, D., 2004. *Multi-Body Systems Approach to Vehicle Dynamics*. 1st Edition. SAE.
7. Budynas, R., Nisbett, K., 2010. *Shigley's Mechanical Engineering Design + Connect Access Card to accompany Mechanical Engineering Design*. 9th Edition. McGraw-Hill Science/Engineering/Math.
8. Byoung, S. K., Chang, H. C., Tae, K. L., 2007. A study on radial directional natural frequency and damping ratio in a vehicle tire. *Applied Acoustics*, 68:5, 538-556.
9. Cabrera, J. A., Ortiz, A. Carabias, E., Simon, A., 2004. An Alternative Method to Determine the Magic Tyre Model Parameters Using Genetic Algorithms. *Vehicle System Dynamics*, 42:2, 109-127.
10. Cho, J. R., Choi, J. H., Kim, G. J., Woo, W. S., 2006. Estimation of dry road braking distance considering frictional energy of patterned tires, *Finite Elements in Analysis and Design*, Volume 42 (Issues 14-15), 1248-1257.
11. CORREVIT Optical Sensors are still the choice of race teams | Datron Technology. 2014. *CORREVIT Optical Sensors are still the choice of race teams | Datron Technology*. [ONLINE] Available at:<http://datrontechnology.co.uk/industry/correvit-optical-sensors-are-still-the-choice-of-race-teams/>. [Accessed 13 September 2014].
12. Cosin scientific software: FTire Product Brief. 2014. *cosin scientific software: FTire Product Brief*. [ONLINE] Available at: http://www.cosin.eu/prod_FTire. [Accessed 10 January 2014].
13. Distributions., , Distributions for assigning random values. 2014. *Distributions for assigning random values*. [ONLINE] Available at: http://resources.esri.com/help/9.3/ArcGISDesktop/com/Gp_ToolRef/process_simulations_sensitivity_analysis_and_error_analysis_modeling/distributions_for_assigning_random_values.htm [Accessed 21 August 2014].
14. FKA, Driving innovations. 2013. . [ONLINE] Available at: <http://www.fka.de/pdf/tyres-in-motion.pdf>. [Accessed 26 May 2014].
15. Frey, W.F., 2009. Master's thesis: 'Development of a rigid ring tire model and comparison among various tire models for ride comfort simulations', Clemson University, August 2009.
16. Gerotek Test Facilities, GEROTEK. 2013. *GEROTEK*. [ONLINE] Available at:http://www.armscordi.com/SubSites/Gerotek1/Gerotek01_landing.asp. [Accessed 04 September 2013].

17. Gillespie, T. D. 1992. *Fundamentals of Vehicle Dynamics (R114)*. First Edition Edition. Society of Automotive Engineers Inc.
18. Gipser, M., 2002. "ADAMS/FTire – A Tyre Model for Ride & Durability Simulations", Adams User Conference, Tokyo, 2000, [ONLINE] Available at: <http://www.cosin.eu/literature> [Accessed 7 August 2013].
19. Gipser, M., 2007. FTire – the tire simulation model for all applications related to vehicle dynamics. *Vehicle System Dynamics*, 45, 139-151.
20. Gipser, M., Hofmann, G., 2013, "FTire - Flexible Ring Tire Model," München, Germany.
21. Gipser, M., 1999. FTire, A New Fast Tire Model for Ride Comfort Simulations, Esslingen university of Applied Sciences, Germany, [ONLINE] Available at: http://web.mscsoftware.com/support/library/conf/adams/euro/1999/Wednesday_papers/FTire%20%20a%20New%20Fast%20Tire%20Model%20for%20Ride%20Comfort%20.pdf [Accessed 14 February 2014]
22. Guthrie, G., & Els, P. (2014). 3D Computer vision contact patch measurements inside off-road vehicle tyres. *Proceedings of the 12th International Conference of the ISTVS*. Pretoria, South Africa.
23. Hajiahmad, A., Goli, H. Jafari, A., Keyhani, A., Abdolmaleki, H., 2014. Side slip angle prediction model of an off-road tire on different terrains. *Journal of Terramechanics*, 56, 25-35.
24. Hamersma, H.A., 2013. Unpublished MEng Thesis: 'Longitudinal vehicle dynamics control for improved', University of Pretoria, Pretoria, South Africa
25. Kat, C. & Els, P.S., 2012. Validation metric based on relative error, *Mathematical and Computer Modelling of Dynamical Systems: Methods, Tools and Applications in Engineering and Related Sciences*, 18:5, 487-520
26. Kim, J., 2009. Identification of lateral tyre force dynamics using an extended Kalman filter from experimental road test data. *Control Engineering Practice*, 17:3, 357-367.
27. Kisilowski, J., Lozia, Z., 1986. "Modelling and simulating the braking process of automotive vehicle on uneven surface", 9th IAVSD Symposium, Linköping, Sweden, *Vehicle System Dynamics*, Vol. 15, 1986, 250-263
28. Lamy, C., Basset, M., 2010. A vision-based approach to wheel camber angle and tyre loaded radius measurement. *Sensors and Actuators A: Physical*, 161:1-2, 134-142.
29. Land Rover, (2006). "Land Rover Defender 110 Workshop Manual", Land Rover.
30. MATLAB - The Language of Technical Computing - MathWorks United Kingdom. 2013. *MATLAB - The Language of Technical Computing - MathWorks United Kingdom*. [ONLINE] Available at: <http://www.mathworks.com/products/matlab/>. [Accessed 29 February 2013].
31. Meriam, J. L., Kraige, L. G., 2009. *Engineering Mechanics: Dynamics, Student Value Edition*. 6 Edition. Wiley.
32. Michelin Americas Truck Tires XZL™ Page. 2013. *Michelin Americas Truck Tires XZL™ Page*. [ONLINE] Available at: <http://www.michelintruck.com/michelintruck/tires-retreads/tireInfo.do?tread=XZL>. [Accessed 11 November 2013].
33. MSC Adams. 2013. [ONLINE] Available at: <http://www.mscsoftware.com/product/adams>. [Accessed 13 July 2013].



34. MTS, 2013. Flat-Trac Tyre Test Systems. [ONLINE] Available at: https://www.mts.com/ucm/groups/public/documents/library/dev_002227.pdf. [Accessed 6 August 2014].
35. Nakajima, Y, 2003. Analytical model of longitudinal tire traction in snow. *Journal of Terramechanics*, 40:1, 63:82.
36. Oosten, J., 2011, How to get tire model parameters, MSC Software Office, Munich, Germany on November 2001.
37. Optimum, Comparing Tires. 2014. . [ONLINE] Available at: <http://www.optimumg.com/docs/TireComparison.pdf>. [Accessed 30 November 2014].
38. Pacejka, H. 2012. *Tire and Vehicle Dynamics, Third Edition*. 3 Edition. Butterworth-Heinemann.
39. Polytec, PSV – 400 Scanning Laser Vibrometer. 2014. [ONLINE] Available at: http://www.polytec.com/fileadmin/user_uploads/Products/Vibrometers/PSV-400/Documents/OM_DS_PSV-400_2011_05_E.pdf. [Accessed 19 May 2014].
40. RACELOGIC - VBOX | Vehicle Speed & Distance Measurement. 2014. *RACELOGIC - VBOX / Vehicle Speed & Distance Measurement*. [ONLINE] Available at: <https://www.vboxautomotive.co.uk/index.php/en/>. [Accessed 12 February 2014].
41. Rill, G., 2006. Vehicle Dynamics, Lecture notes, Fachhochschule Regensburg, viewed 10 August 2013, from <https://hps.hs-regensburg.de/~rig39165/>
42. SAE International Automotive. 2014. *SAE International Automotive*. [ONLINE] Available at: <http://www.sae.org/automotive/>. [Accessed 12 April 2014].
43. Stallmann, M. J., Els, P. S., Becker, C. M. 2014. a. Parameterization and modelling of large off-road tyres for ride analyses: Part 1 – Obtaining parameterization data. *Journal of Terramechanics*, Volume 55, 73-84.
44. Stallmann, M. J., Els, P. S., 2014. b. Parameterization and modelling of large off-road tyres for ride analyses: Part 2 – Parameterization and validation of tyre models. *Journal of Terramechanics*, Volume 55, 85-94.
45. TNO - Mobility & Logistics. 2014. *TNO - Mobility & Logistics*. [ONLINE] Available at: https://www.tno.nl/content.cfm?context=thema&content=innovatiegebied&laag1=896&laag2=913&item_id=913. [Accessed 27 September 2013].
46. Unrau, H. J. & Zamow, J., 1997. TYDEX-Format Description and Reference Manual, Release 1.3, SAE International, 2013, SAE standard: Tire Performance Technology, (SAE J 2047 SAE International, Troy, Michigan
47. Uys, P., Els, P., Thoresson, M., Voigt, K., & Combrinck, W. 2006. Experimental determination of moments of inertia for an off-road vehicle in a regular engineering laboratory. *International Journal of Mechanical Engineering Education*, 34 (4), pp. 291-314.
48. Zebala, J., Ciepka, P, Reza, A., Janczur, R., 2007. Influence of rubber compound and tread pattern of retreaded tyres on vehicle active safety. *Forensic Science International*, 167:2-3, 173-180.
49. Zegelaar, P.W.A., 1998. The dynamic response of tyres to brake torque variations and road unevenness, PhD Thesis, Delft University of Technology, Delft, The Netherlands

A. Appendix – Measurement and simulation results

Vertical tests

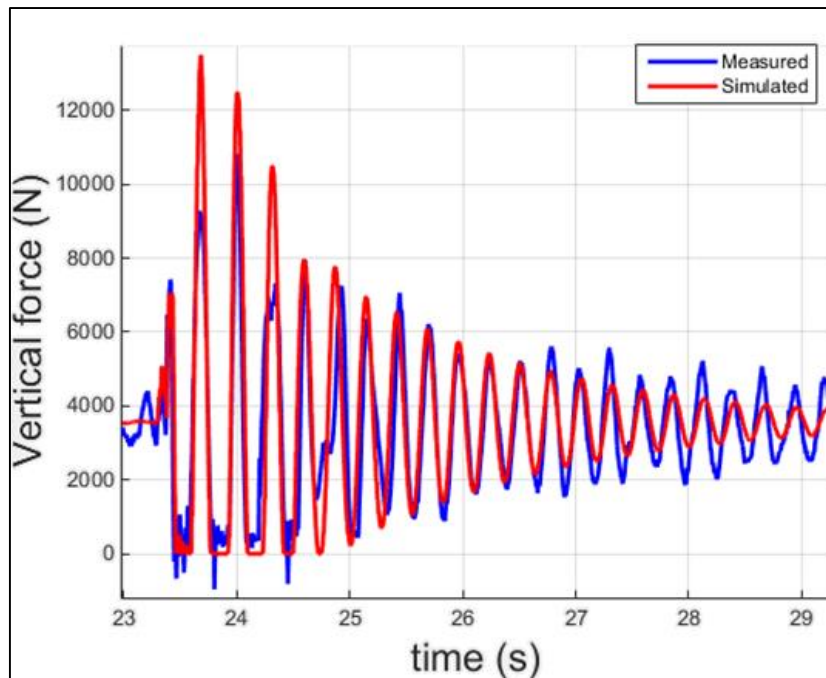


Figure A-1: 50x50mm cleat (LC0) at 6 m/s and 2 bar inflation pressure

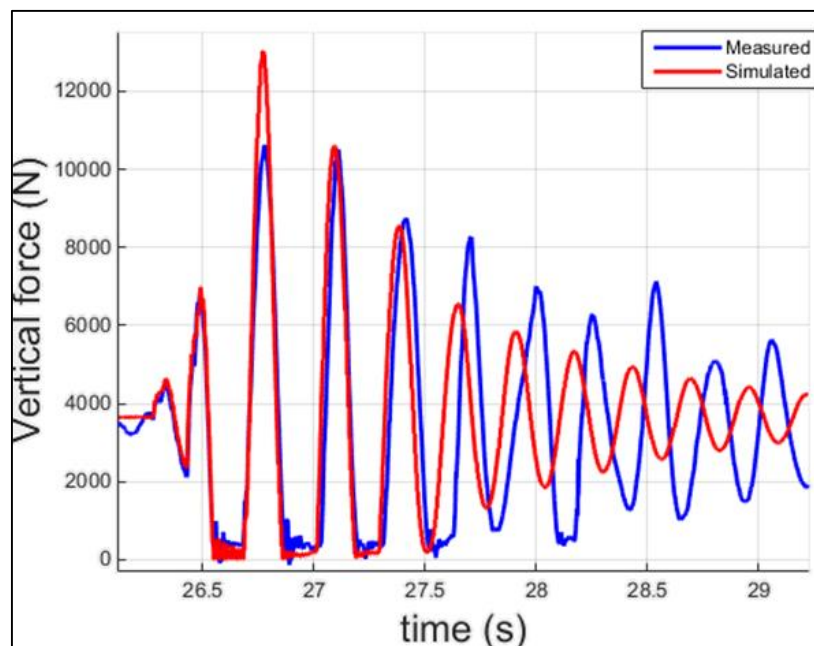


Figure A-2: 50x50mm cleat (LC0) at 3.5 m/s and 2 bar inflation pressure

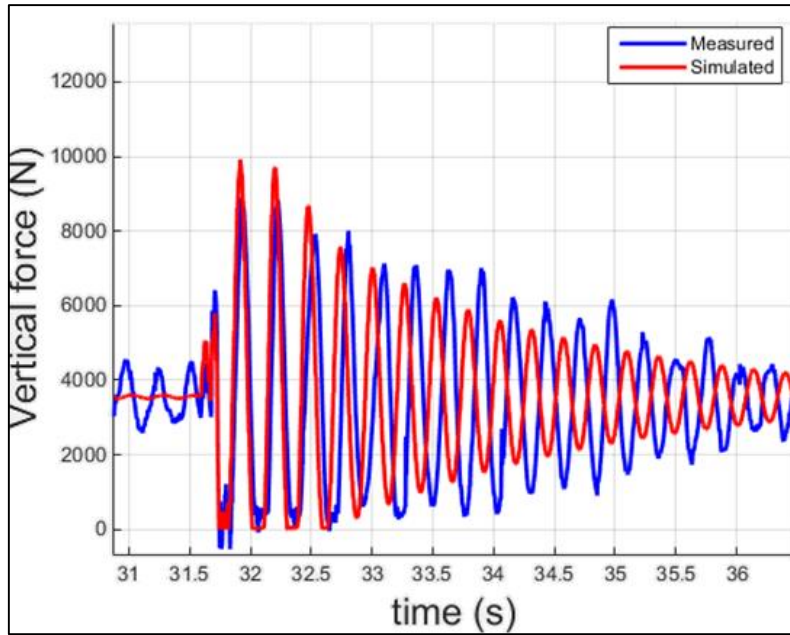


Figure A-3: 32x32mm cleat (LC0) at 6 m/s and 2 bar inflation pressure

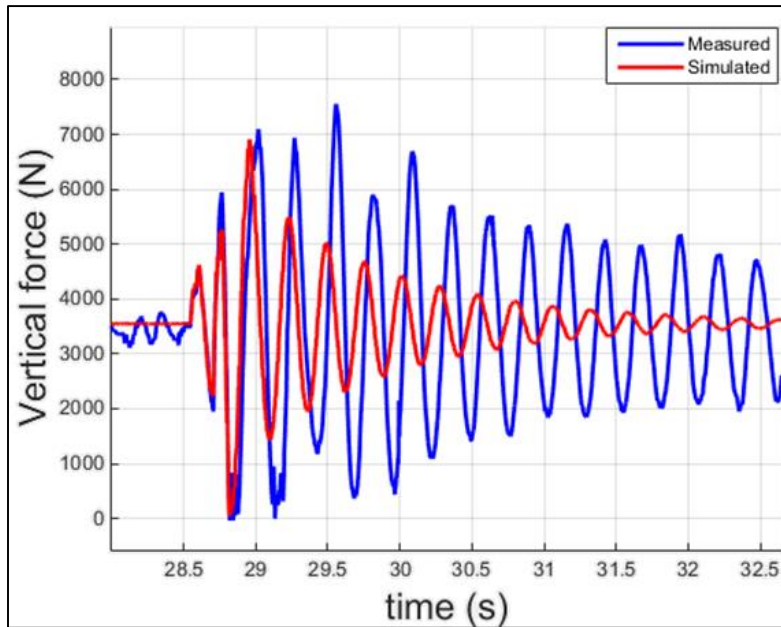


Figure A-4: 32x32mm cleat (LC0) at 3.5 m/s and 2 bar inflation pressure

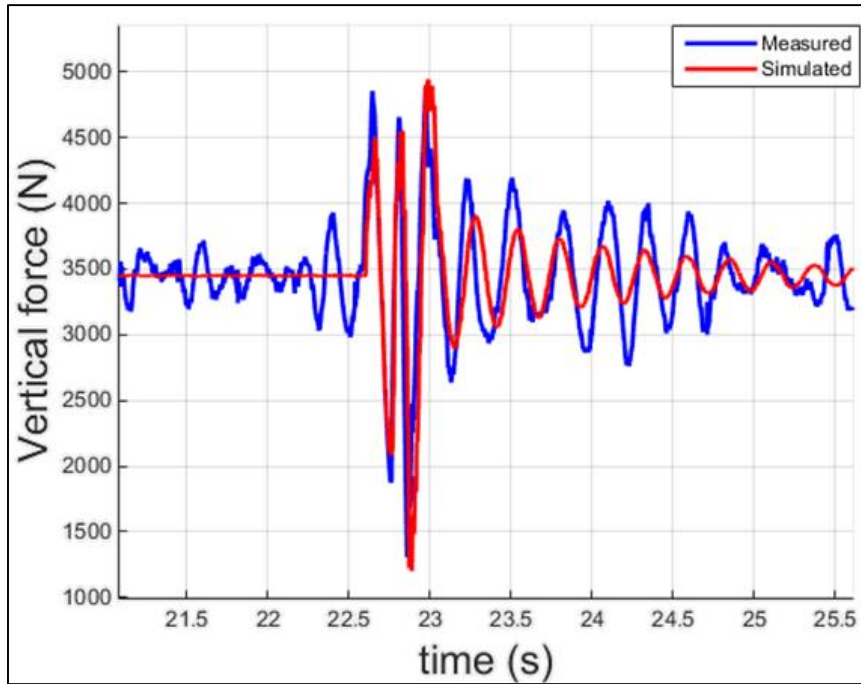


Figure A-5: 25x25mm cleat (LC0) at 6 m/s and 2 bar inflation pressure

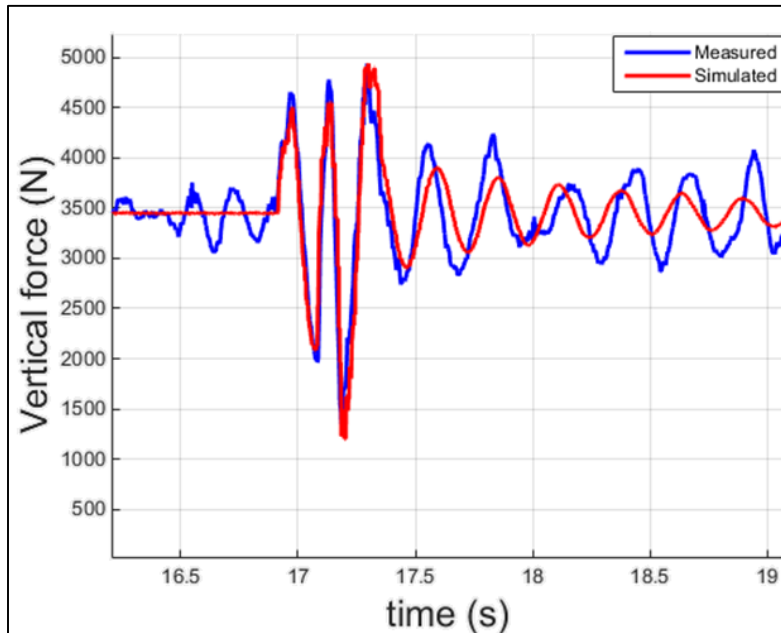


Figure A-6: 25x25mm cleat (LC0) at 3.5 m/s and 2 bar inflation pressure

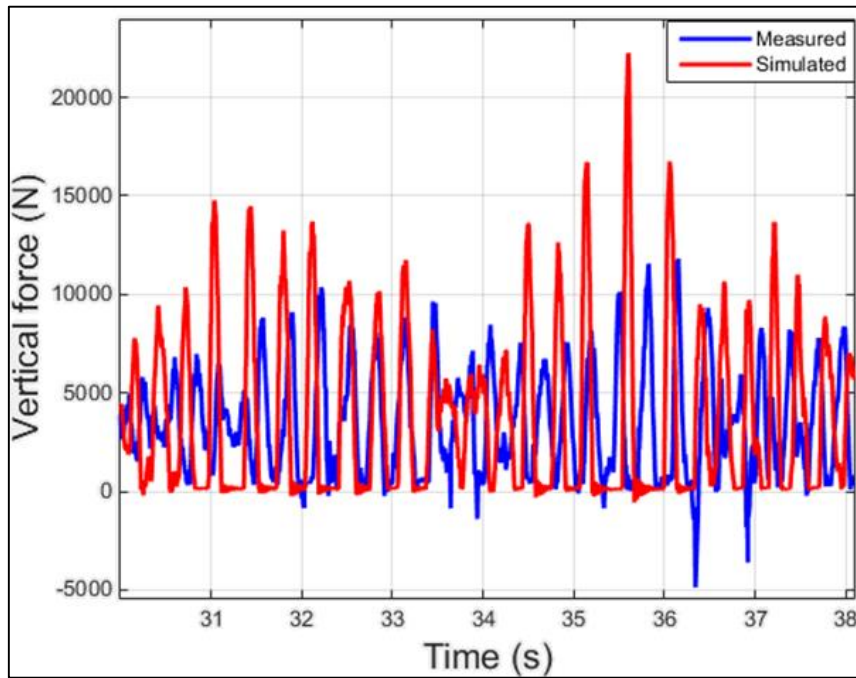


Figure A-7: Belgian paving track (LC0) at 6 m/s and 2 bar inflation pressure

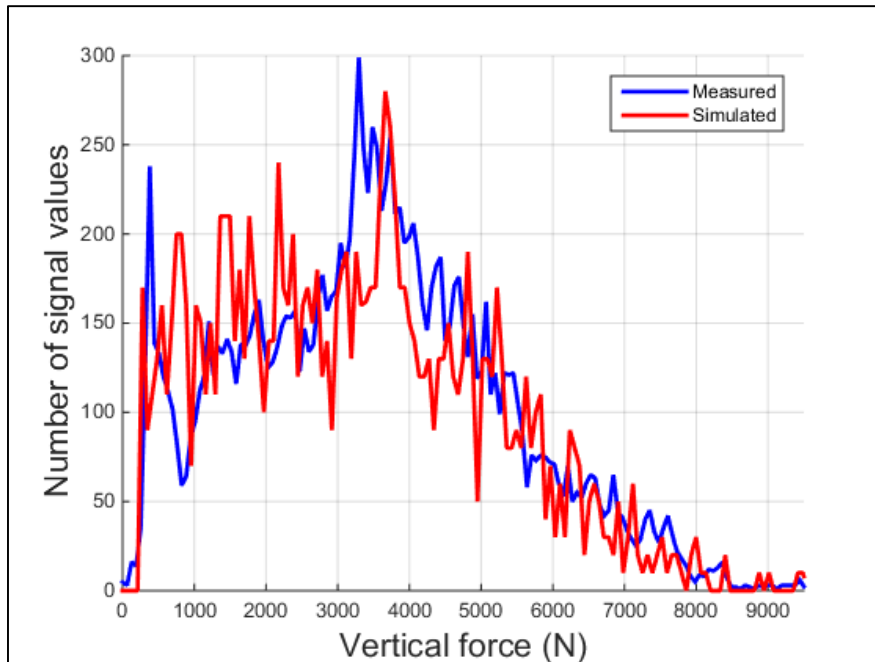


Figure A-8: Belgian paving track (LC0) at 6 m/s and 2 bar inflation pressure validation

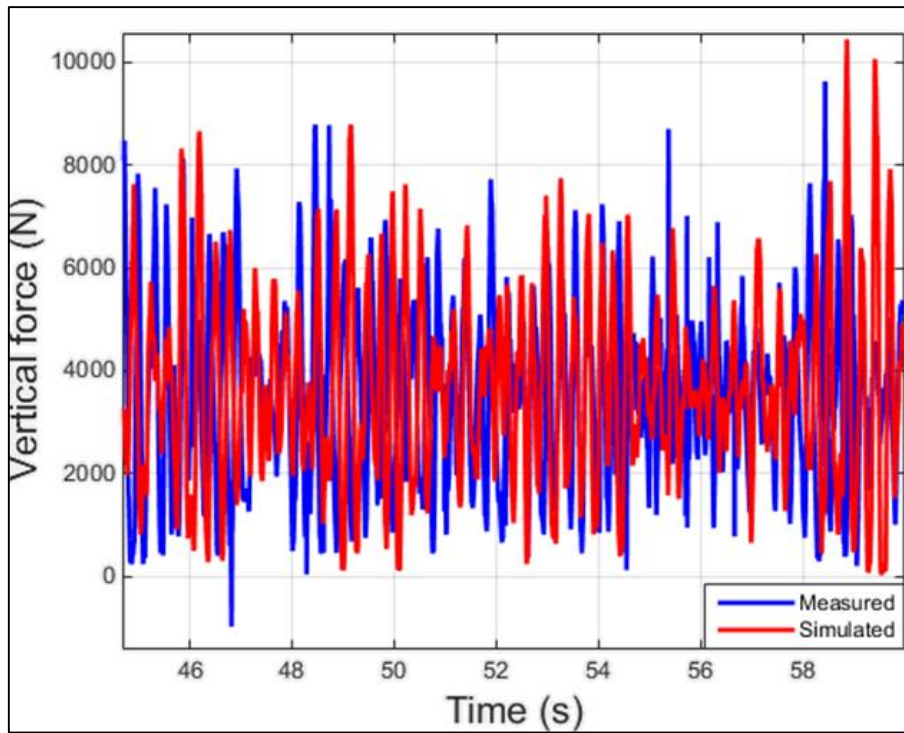


Figure A-9: Belgian paving track (LC0) at 3.5 m/s and 2 bar inflation pressure

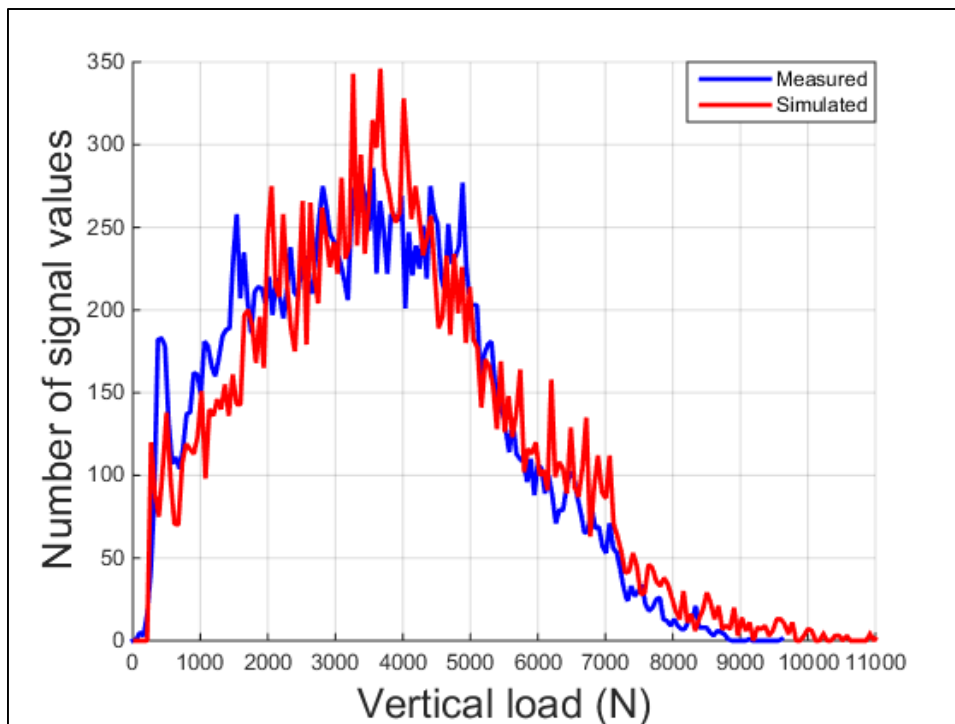


Figure A-10: Belgian paving track (LC0) at 3.5 m/s and 2 bar inflation pressure validation

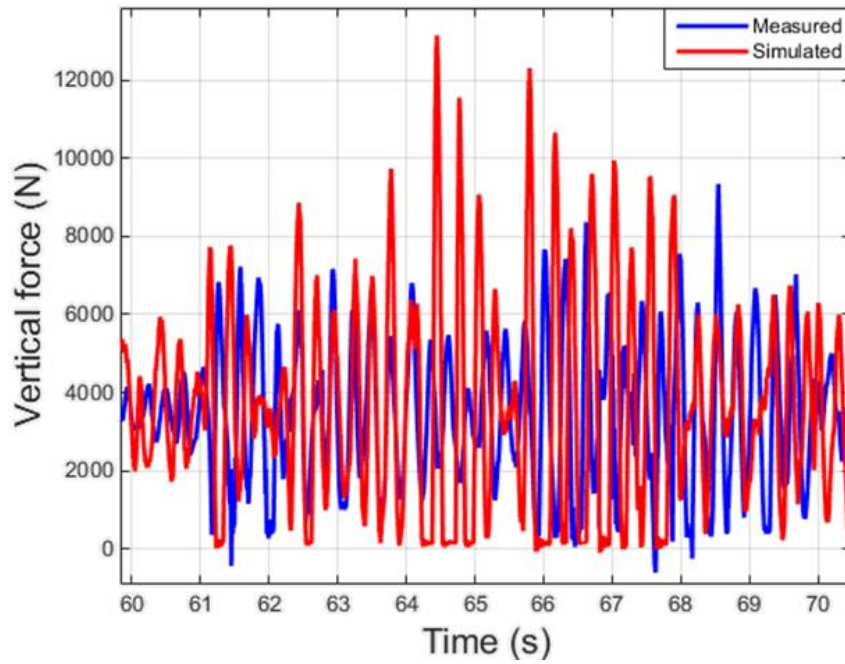


Figure A-11: Fatigue track (LC0) at 6 m/s and 2 bar inflation pressure

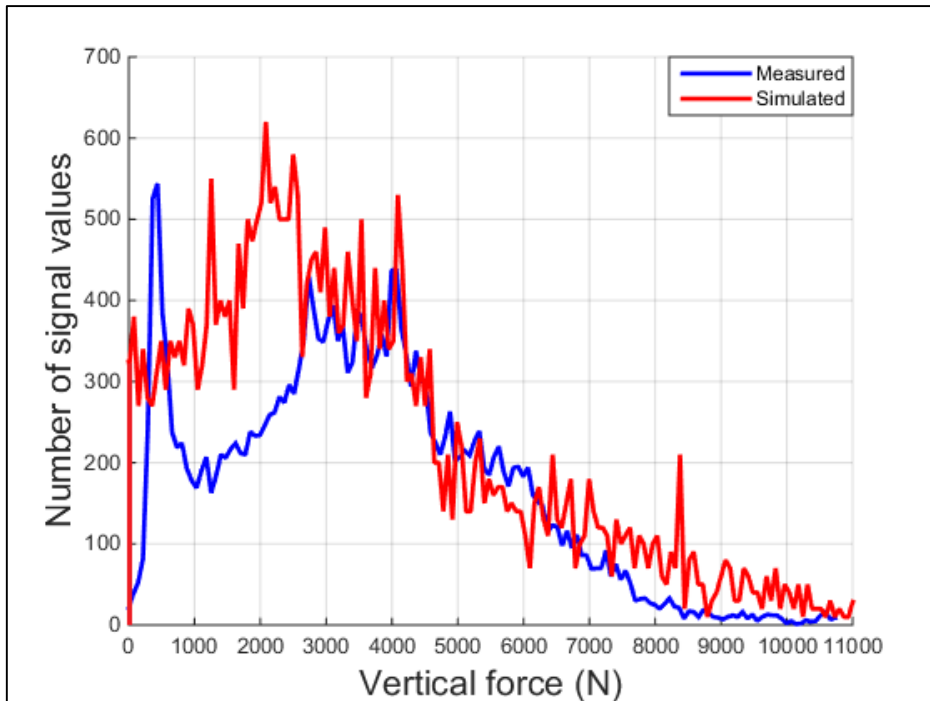


Figure A-12: Fatigue track (LC0) at 6 m/s and 2 bar inflation pressure validation

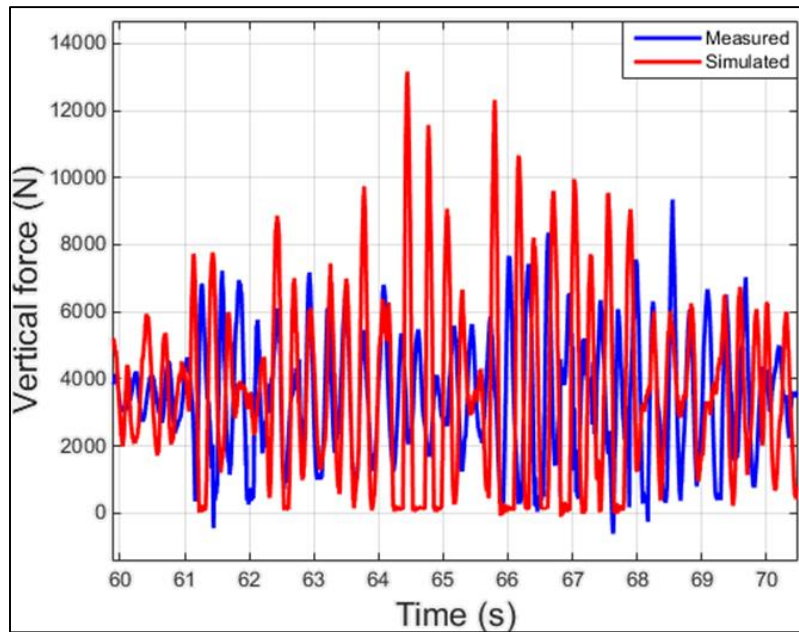


Figure A-13: Fatigue track (LC0) at 3.5 m/s and 2 bar inflation pressure

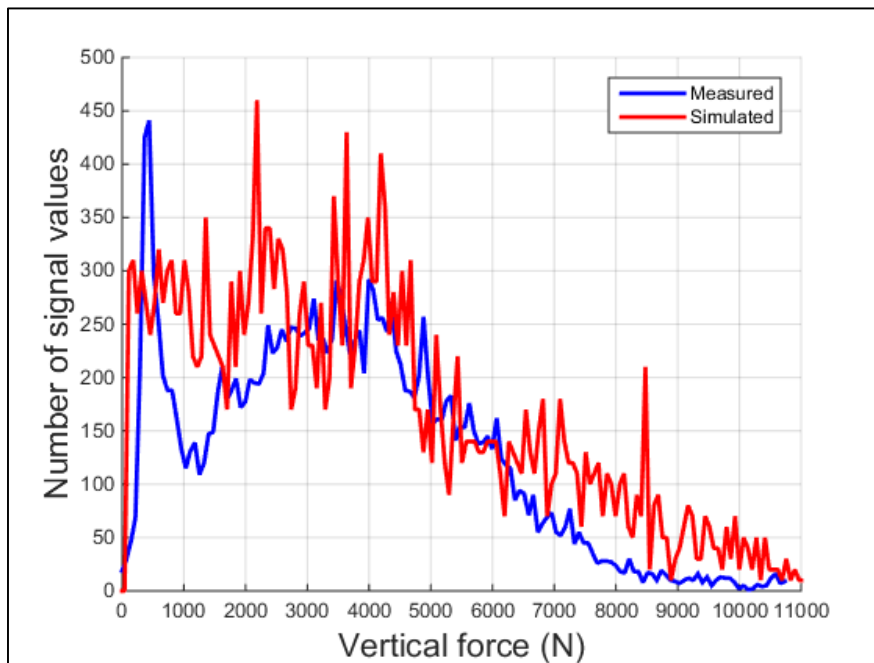


Figure A-14: Fatigue track (LC0) at 3.5 m/s and 2 bar inflation pressure validation

Traction tests

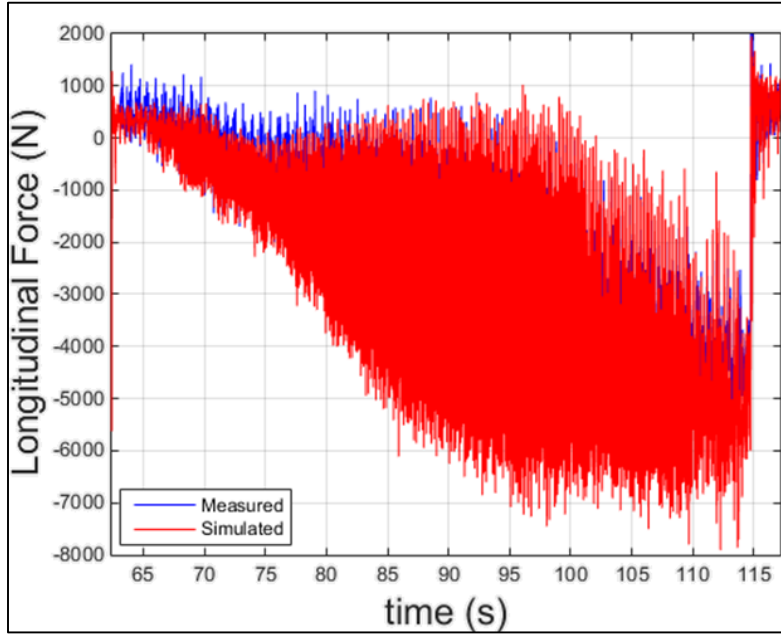


Figure A-15: Longitudinal force (LC3) at 2 bar inflation pressure

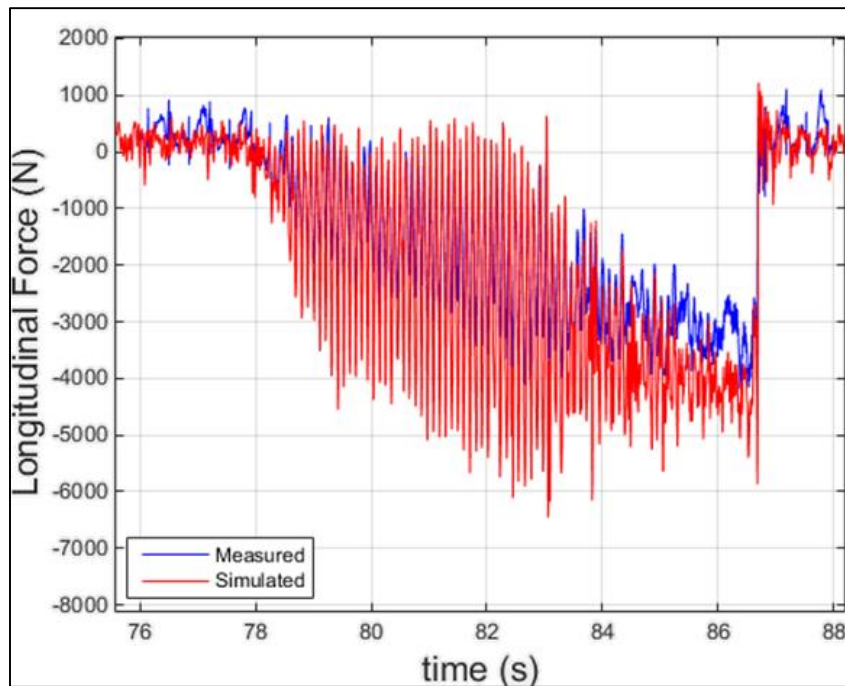


Figure A-16: Longitudinal force (LC1) at 2 bar inflation pressure

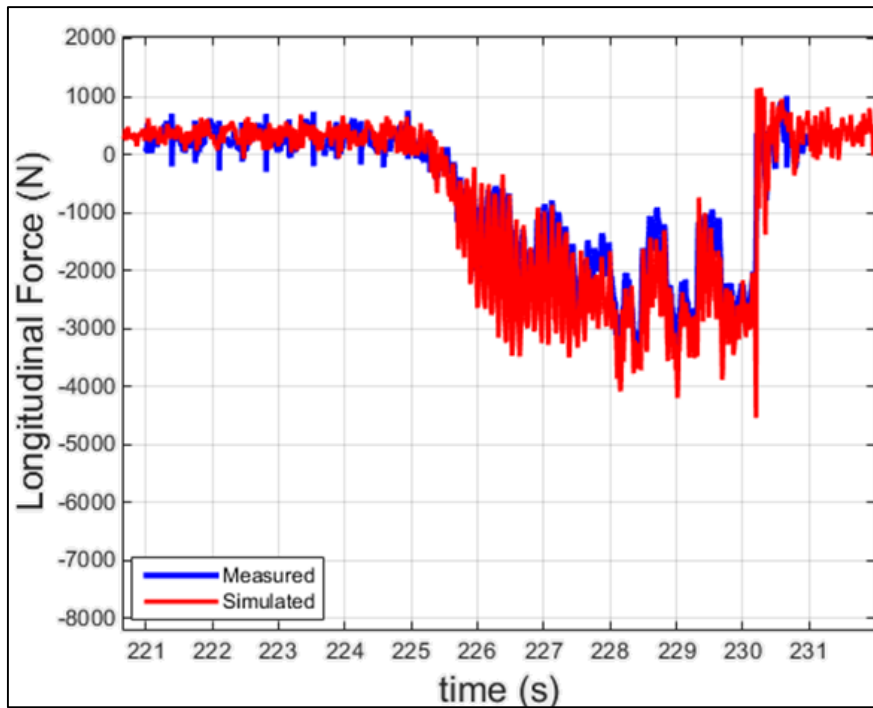


Figure A-17: Longitudinal force (LC0) at 2 bar inflation pressure

Handling tests

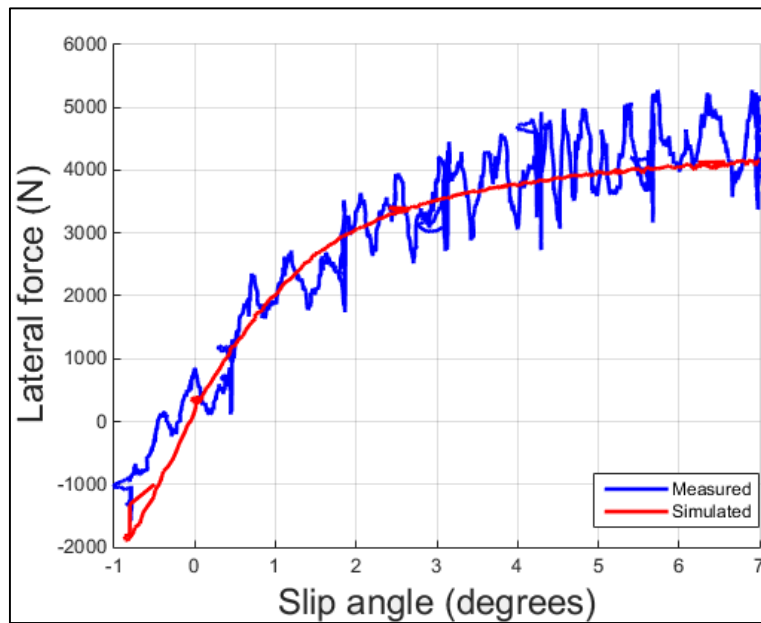


Figure A-18: Lateral force vs. slip angle (LC1) at 0° camber angle and 2 bar inflation pressure

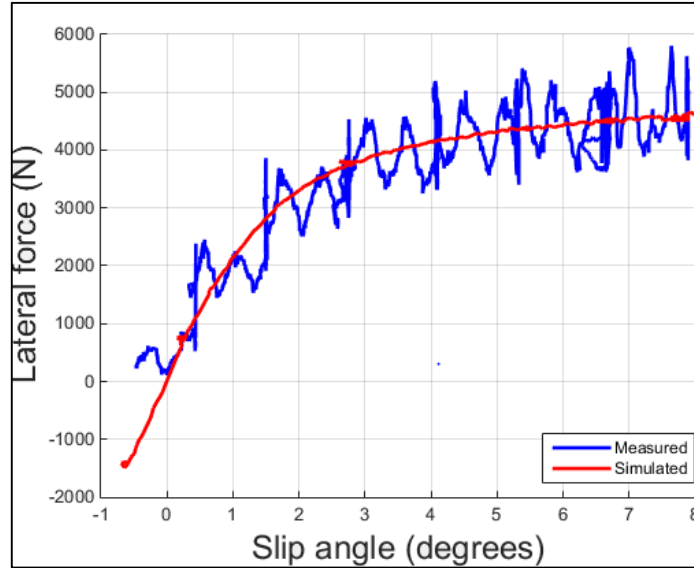


Figure A-19: Lateral force vs. slip angle (LC1) at 2° camber angle and 2 bar inflation pressure

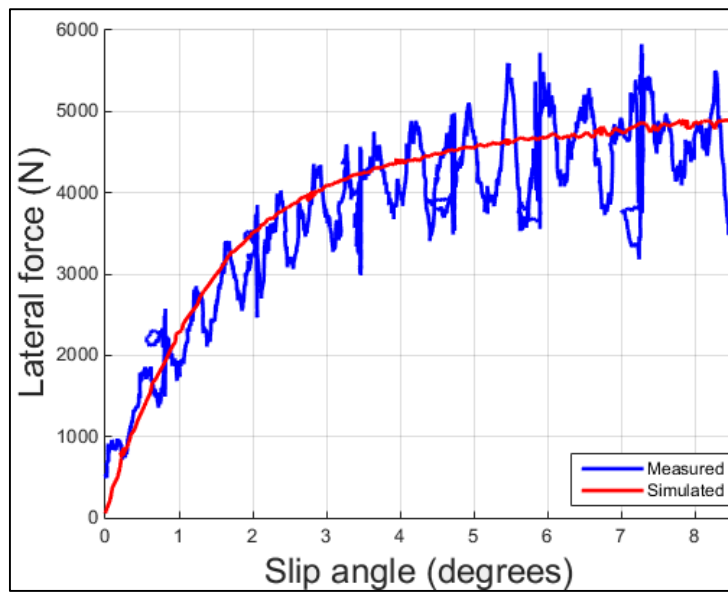


Figure A-20: Lateral force vs. slip angle (LC1) at -2° camber angle and 2 bar inflation pressure

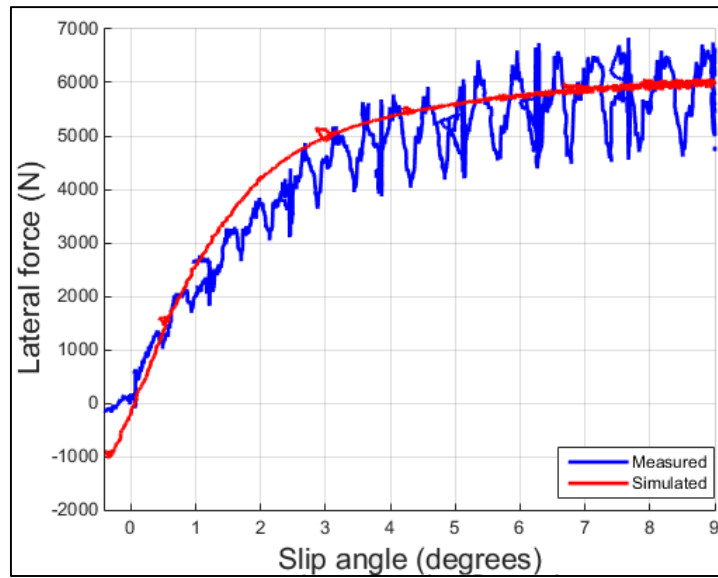


Figure A-21: Lateral force vs. slip angle (LC3) at 0° camber angle and 2 bar inflation pressure

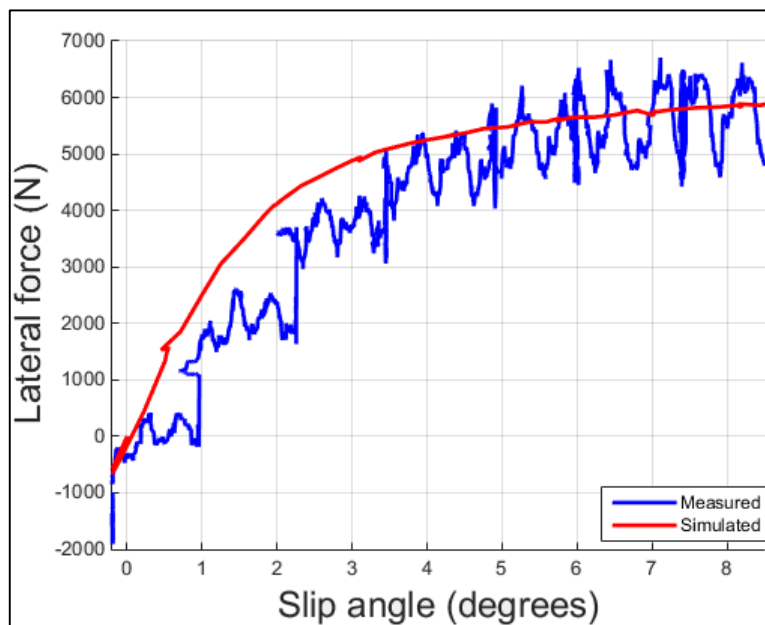


Figure A-22: Lateral force vs. slip angle (LC3) at 2° camber angle and 2 bar inflation pressure

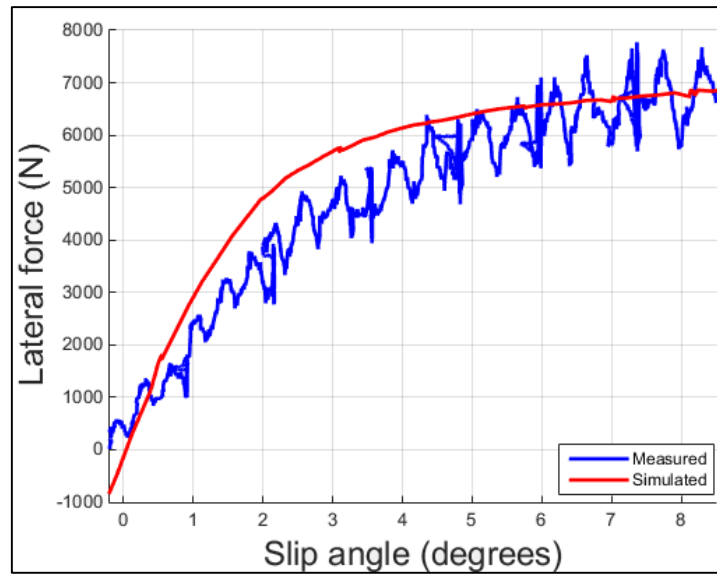


Figure A-23: Lateral force vs. slip angle (LC3) at -2° camber angle and 2 bar inflation pressure